Department of Physics and Astronomy
University of Heidelberg

Optimizing cleaning in radio interferometric imaging by the use of multi-scale clean

Bachelor Thesis in Physics by

Nico Krieger

at the
Max-Planck-Institute of Astronomy in Heidelberg
under the supervision of
Fabian Walter

ABSTRACT

In this bachelor thesis I present the basic theory of imaging in interferometric radio astronomy and show the application in imaging data of The HI Nearby Galaxy Survey (THINGS). All analyses is done using the software packages `CASA` plus IDL and GIPSY for additional analyses. The main part of this thesis deals with multi-scale cleaning and the comparison with its progenitor, the Högbom `clean` algorithm using a subset of 3 galaxies of THINGS. Various tests demonstrate that the capabilities of multi-scale clean clearly exceed those of the 'traditional' `clean`, as e.g. demonstrated by very deep cleaning of the galaxy NGC5055.

ABSTRACT

In dieser Bachelorarbeit lege ich die grundlegenden Prinzipien der Bildgebung der interferometrischen Radioastronomie dar und verwende sie zur Darstellung von Daten der HI Nearby Galaxy Survey (THINGS). Diese wird mit den Programmen `CASA`, sowie IDL und GIPSY für weitergehende Auswertungen durchgeführt. Der Hauptteil der Arbeit betrifft den Vergleich von multi-scale clean mit seinem Vorläufer, Högboms `clean` Algorithmus anhand dreier Galaxien von THINGS. Diverse Tests zeigen, dass die Fähigkeiten des multi-scale cleans die des traditionellen `clean`s deutlich übersteigen, wie beispielsweise ein sehr tiefer clean der Galaxie NGC5055 zeigt.

Contents

1 Introduction

For thousands of years, mankind wondered about the sky and stars without the chance of gaining real insight of the underlying effect. In the 1920s galaxies were discovered to be far away accumulations of stars like our own milky way and later detections showed them to contain large amounts of gas, mainly hydrogen. On form in which hydrogen can appear is in its neutral atomic form, called HI. Detections are possible due to the so-called 21 cm line that offers the chance of observing exciting processes like star formation from gas clouds, dynamics and structure of the interstellar medium (ISM) and even dark matter distributions. However, the astronomical facilities of 1920s and later, equipped single-dish telescopes were not able to gather the needed high-resolution data. The first radio interferometer was launched in 1946 and originated a new era in radio astronomy. Todays observatories allow detailed measurements of flux distributions which can be converted to HI gas masses and densities that are the basis of all further analyses.
The practical work is not as easy as the summary seems because there are several difficulties in reduction and analysis. Radio interferometry can only lead to useful results when a process of deconvolution is done that bases on modeles of the observed region. Differing modeles can cause significantly deviating results and the duty of this thesis is to find out the properties of a new method called multi-scale clean.

Section 2 characterises the fundamentals of measuring the 21 cm line of neutral hydrogen, followed by a short description of The Nearby Galaxy Survey (THINGS) in section 3 whereof the data comes. The theory of interferometric imaging is outlined in section 4 together with the mathematics of converting measured flux densities to some further quantities. Data reduction and analysis is perfomed mainly with the software package `CASA` whose functions are described in section 5. The results are presented in section 6 and 7 whereof the latter contains an uncommented set of the basic information attained during the three months I spend on this thesis. Regrettably, the university sets a strict and short period for bachelor theses that prevented the cleaning method found to be the best (section 6.6) from being applied to the whole data set.

2 The HI line of neutral hydrogen

In the Big Bang nucleosynthesis the by far most produced element was hydrogen. Still today, 13.8 billion years later (Planck Collaboration, 2013), little of it was converted into other chemical elements by stars. In astronomy three forms of hydrogen are of importance: neutral, atomic hydrogen (HI), ionized hydrogen (HII) and hydrogen molecules (H_2). Due to the low temperatures in the interstellar space, HI exists mostly in the electronical groundstate $1^2S_{1/2}$. This means the single electron in the first shell with spin 1/2 has angular momentum 0. The interaction of the spins of nucleus and electron add up to the hyperfine structure which has only two states for this case: Parallel or anti-parallel alignment of the spins with quantuum number $F = 0$ and $F = 1$. A transition between these two states is possible, although 'permitted' by atomic physics, in which the emitted electromagnetic wave has a frequency of 1.420 405 751 786 (30) GHz. In terms of wave lenght this corresponds to 21.106 cm and the common name '21 cm line'. Because of the very low energetic difference of the states of $5.87 \cdot 10^{-9}$ eV and the type of transition, a magnetic transition, the transition probability is extremly low, corresponding to approx. 11 million years. Therefore, in most astronomical cases 21 cm emission can be refered to as optical thin, which means that an electromagnetic wave is only slightly damped. Excitation is caused by rare collisions in the thin (1 - 1000 atoms/m^3) hydrogen clouds. The immense quantity of hydrogen in the universe outnumbers said low probabilities causing the 21 cm line to be an easily detectable line.

2.1 Line broadening

So far the spectral line is assumed to be infinetely sharp in the form of a Dirac δ-function. Three effects broaden the line to a lorentzian profile:

- The long lifetime of 11 million years of the excited state corresponds to a uncertainty in the energic difference according to Heisenberg's uncertainty relation $\Delta E \Delta t \geq \frac{\hbar}{2}$. The observable result is a line 21 cm line with a *natural linewidth* of $1.5 \cdot 10^{-47}$ cm.
- *Collisional broadening* reduces the lifetime by collisions between atoms causing further broadening.
- The biggest influence on linewidth is caused by the *Doppler effect*. If observer and source have a relative velocity, the line gets shifted towards lower frequencies (red shift) when moving away from each other or higher frequencies (blue shift) when approaching. Galaxies move relative to the observer on earth, but also rotate allowing us to gain kinematic information. The light of the part of the galaxy turning towards earth is therefore received at slightly higher frequencies than the opposite which is observed at lower frequencies.

To get all necessary information the line is observed across a frequency range wide enough to contain the fastest and slowest (relative to earth) atoms. As contineous detection is impossible the frequency gets bined into so-called *channels*. To translate measured frequencies into moving velocities of the emitting sources different definitions are used.

2.2 Velocity definitions

Due to the Doppler effect and the characteristic as a spectral line it is possible to measure the radial velocity of hydrogen. In most cases one of two approximations for $v \ll c$ of the exact relativistic formula is used.

- Relativistic velocity: $v_{rel} = c \, \frac{1-\left(\frac{\nu}{\nu_{rest}}\right)^2}{1+\left(\frac{\nu}{\nu_{rest}}\right)^2}$
- Radio velocity: $v_{radio} = c \, \frac{\nu_0-\nu}{\nu_0}$
- Optical velocity: $v_{optical} = c \, \frac{\lambda-\lambda_0}{\lambda_0} = cz = c \, \frac{\nu_0-\nu}{\nu}$

λ: wave length, ν: frequency
The index 0 refers to the rest frame of the emitting atom, whereas no index stands for the detected quantity.
c: speed of light, z: redshift

These different approximations are obviously not identical, but merge for small velocities ($\nu \approx \nu_0$) and are often a source of confusion. As an attempt of simplification I will implicitely use the optical definition from now on whenever a velocity is mentioned.

2.3 HI detection

For a circular telescope with diameter D a theoretical resolution[1] of $58.4° \cdot \frac{\lambda}{D}$ can be achieved. Given a wave length of 21 cm one would need a single dish telescope of 14.7 km to resolve a small-scale structures of 3" inside a galaxy. It is needless to say that telescopes this large are impossible to build. A practical solution is an array of smaller telescopes that are connected to each-other to work as one large tool. The resolution is given by $\frac{\lambda}{D}$ whereas D now represents the distance between two single telescopes, called a baseline.

[1] In radio astronomy resolution is understood as a synonym of FWHM. Using the physical definition would only change the prefactor to 145.3°

3 The HI Nearby Galaxy Survey (THINGS)

The HI Nearby Galaxy Survey (Walter et al., 2008) is a survey of HI emission among 34 galaxies aiming at a high spectral (1.3 - 5.2 km/s) and spatial (~ 6") resolution. It was obtained using the NRAO Very Large Array (VLA) in B, C and D configuration. Providing objects at distances between 2 and 15 Mpc, linear resolutions of 100 to 500 pc are reached. Enough to study the interstellar medium (ISM) in detail for a variety of star formation rates, total HI masses, absolute luminosities and metalicity. I will use an intermediate product of their work: Calibrated, continuum-substracted visibilty files (see chapter 4.2) that contain the combined information of the measurements in all configurations. As a bachelor thesis is only a short term project I cannot work on every object of THINGS, but limit my analysis on a subset of three galaxies, namely NGC2403, NGC3804, NGC5055.

4 Theory of interferometric imaging

As the data sets I will work with in section 6 are already reduced (calibrated, flagged for bad visibilities, continuum substracted), the theory will focus on imaging.

4.1 Interferometry

Interferomtry setups can be described easily for the minimum number of two antennas and then generalized towards more complex setups, such as the VLA.

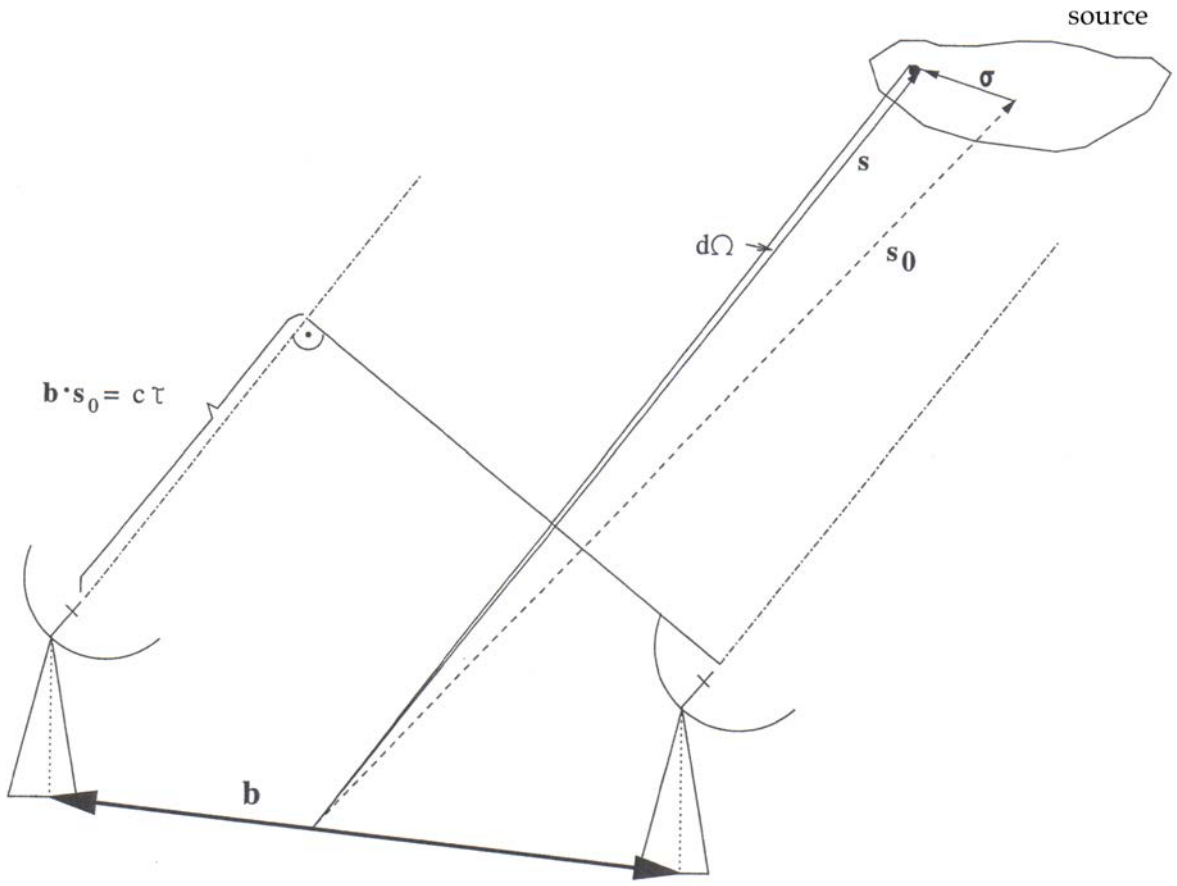

Figure 1: Sketch of a simple interferometric layout with two antennas. (Image taken from Ott (1999))

Figure 1 shows the basic principle of an interferometer: Two antennas that are separated by the distance b, the so-called *baseline*. The dishes point towards the source s illustrated by the unit vector $\vec{s}$ and receive a signal at slightly different times denoted by the *geometrical delay*

$$\tau = \frac{\vec{b} \cdot \vec{s}}{c} \tag{4.1}$$

After correlating the signals and filtering out the high frequency part the result is:

$$r \propto \cos(2\pi\nu\tau) \tag{4.2}$$

So far, a monochromatic point source is assumed. For astrophysical sources with extend the radio brightness $I(\vec{s})$ (intensity) in the direction of $\vec{s}$ at frequency ν is introduced. The power received in bandwidth $\Delta\nu$ from a solid angle element $d\Omega$ is then given by $A(\vec{s})I(\vec{s})\Delta\nu d\Omega$ with $A(\vec{s})$ being the effective collecting area in direction $\vec{s}$. When taking the correlator into account the result using 4.1 and 4.2 is

$$r = \int_S dr = \int_S 2\pi A(\vec{s})I(\vec{s})\Delta\nu \cos\left(\frac{\vec{b}\cdot\vec{s}}{c}\right) d\Omega \tag{4.3}$$

The S specifying the integral's domain stands for the whole surface of the celestial sphere, but in practice the primary beam (section 4.5) and the dimension of the source restrict the field of view.
The center of the field of view is refered to as *phase tracking center* or *phase reference position* $\vec{s_0}$, so that any point of the source can be mapped by $\vec{s} = \vec{s_0} + \vec{\sigma}$. $\vec{\sigma}$ has to lie inside the primary beam to receive radiation as the telescopes are fixed towards $\vec{s_0}$.

4.2 Visibility: Definition

The *visibility* $\mathcal{V}$ is "a measure of the coherence. [...] It can be regarded as an unnormalized measure of the coherence of the electric field, modified to some extend by the characteristics of the interferometer." (Thompson, 1999)
It is defined as

$$\mathcal{V} = |\mathcal{V}|\ e^{i\Phi_\mathcal{V}} = \int_S \mathcal{A}(\vec{\sigma})I(\vec{\sigma})e^{-2\pi\nu\vec{b}\cdot\vec{\sigma}/c}\, d\Omega \tag{4.4}$$

where the normalized antenna reception pattern $\mathcal{A}(\vec{\sigma}) = A(\vec{\sigma})/A(\vec{s_0})$ is used. It is the basis of all further analysis and is related to the correlator output r by

$$r = A(\vec{s_0})\Delta\nu\,|\mathcal{V}|\cos\left(\frac{2\pi\nu\vec{b}\cdot\vec{s_0}}{c} - \Phi_\mathcal{V}\right) \tag{4.5}$$

Via a local oscillator, it is possible to determine amplitude and phase of the visibility, but most correlators are able to provide real and imaginary part directly. To receive the desired quantity $I(\vec{\sigma})$, the definition 4.2 that is nothing else than a fourier transform of $\mathcal{A}(\vec{\sigma})I(\vec{\sigma})$, must be inverted.

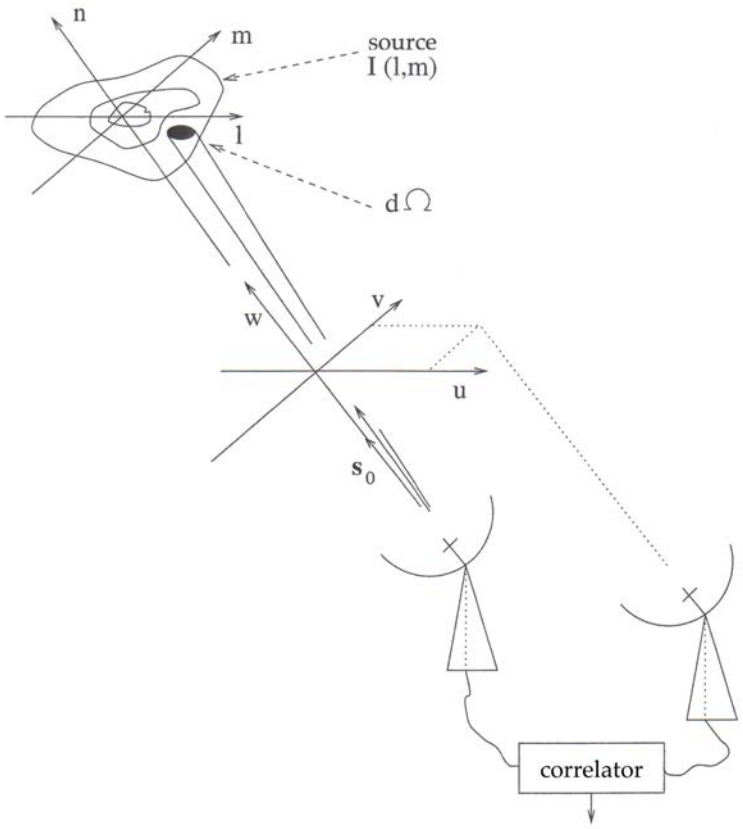

Figure 2: Coordinates systems used in interferometry. u points east, v to the east and w to the phase tracking center. (Image taken from Ott (1999))

4.3 Coordinate systems

To perform the inverse transform, two coordinate systems for image space and the corresponding fourier space are introduced:

- image space: coordinates l, m, n
- fourier space: coordinates u, v, w

The u, v, w system can be understood as the projected baselines as seen from the source. u is defined to point north, v to the east (along right ascension α) and w towards the source. This means the visibility is the intensity distribution on the u, v plane. The image coordinates l, m are measured in a tangent plane to the celestial sphere and therefore are direction cosines with respect to the u, v axes. n keeps the direction of w, but measures the image coordinate.
The product $\vec{b} \cdot \vec{\sigma}$ in the visibility definition (4.2) can now be expressed in terms of the new coordinates.

$$\frac{\nu}{c}\ \vec{b} \cdot \vec{\sigma} = \lambda\ \vec{b} \cdot \vec{\sigma} = ul + vm + wn \tag{4.6}$$

$$\frac{\nu}{c}\ \vec{b} \cdot \vec{\sigma} = w \tag{4.7}$$

$$d\Omega = \frac{dl\ dm}{n} = \frac{dl\ dm}{\sqrt{1 - l^2 - m^2}} \tag{4.8}$$

The appearance of $\frac{\nu}{c} = \lambda$ in the exponent suggests that u, v, w coordinates are measured in terms of wavelength λ.
The reduction of the resulting relation between $\mathcal{V}(u, v, w)$ and $\mathcal{A}(l, m, n)I(l, m, n)$ to a two-dimensional fourier transform can be done under two conditions (Thompson, 1999):

- small objects for which $\left|\frac{\Delta\nu}{c}\vec{b} \cdot (\vec{s} - \vec{s_0})\right| \ll 1$ and $|w(l^2 + m^2)| \ll 1$ holds:

$$\mathcal{V}(u, v) = \int_{-\infty}^{\infty}\int_{-\infty}^{\infty} \mathcal{A}(l, m)I(l, m)e^{-2\pi i(ul+vm)} dl\ dm \tag{4.9}$$

- larger objects:

$$\mathcal{V}(u, v) = \int_{-\infty}^{\infty}\int_{-\infty}^{\infty} \mathcal{A}(l, m)I(l, m)e^{-2\pi i(ul+vm+w(\sqrt{1-l^2-m^2}-1))} \frac{dl\ dm}{\sqrt{1 - l^2 - m^2}} \tag{4.10}$$

To get the intensity in image coordinates l, m modified with the antenna reception, only the fourier inverse has to be applied. For objects small enough to fall below the constraints above, the inverse transformation reads:

$$\mathcal{A}(l, m)I(l, m) = \int_{-\infty}^{\infty}\int_{-\infty}^{\infty} \mathcal{V}(u, v)e^{2\pi i(ul+vm)} dl\ dm \tag{4.11}$$

$$= \hat{\mathbf{F}}^{-1}[\mathcal{V}] \tag{4.12}$$

$\hat{\mathbf{F}}^{-1}$ stands for the inverse fourier transormation in mathematical short notation.

4.4 Visibilty: Fourier inversion and the effects of an incompletely sampled u,v plane

A visibility data set consists of many points in the u, v plane each measured with amplitude and phase. The fourier transformation converts this collection into its spectrum whereas each point is transformed to a wave pattern that looks like stripes in the images (figure 4. The image of an astrophysical object is then build up by superposing thousands of waves as shown by figure 3.
As in other physical cases, quantities in the two spaces connected by a fourier transform correspond to each other. The position of a visibility point determines the wave in the image plane such that angle Ψ and length $|\mathcal{V}|$ of the position vector define the direction of the wave vector k and frequency. Amplitude and phase $\Phi_\mathcal{V}$ in the u, v plane transform to amplitude and the waves offset from the origin. Figure 4 shows this behaviour for a selection of locations and visibilities to gain an intuitive understanding of visiblities.
Due to the position - frequency relation, it is necessary having visibility measures over the whole u, v plane to recover structures of all size in the image plane. Hence, the number of baselines should be maximized by using more than just two telescopes. In *aperture synthesis*, n antennas provide $\frac{n(n-1)}{2}$ baselines to cover some more u, v points. An optimuum is achieved by using non-redundant setups that do not cover a baseline several times, but only once.
The by far largest contribution on covering the plane is caused by the unevitable rotation of the earth. While other observation techniques require much effort to correct for this effect, synthesis interferometry would have a poor resolution without. As earth rotation constantly changes the u, v positions of the telescopes, it provids a better u, v coverage. But there are two fundamental reasons left that prevent total coverage. The baselines have lower and upper limits as two telescopes cannot be placed side by side with an infinitesimal small distance and even with telescopes on earth and in space the longest baseline is still finite. A so-called *short spacing correction* can be applied by combination of interferometric and single dish data to reduce the problem of missing short baselines. Figure 5 shows the u, v plane for a THINGS measurement of NGC2403 with the high density towards the origin and the curved tracks due to earth rotation.

As derived in section 4.4 the intensity distribution can be recovered from the measured visibilties by applying an inverse fourier transform $\mathcal{A}(l, m)I(l, m) = \hat{\mathbf{F}}^{-1}[\mathcal{V}]$. The antenna reception $\mathcal{A}$ is also called *primary beam* and can be eliminated by a simple division as described in section 4.10. The further procession introduces a *sampling function* that accomodates for the incompletely sampled u, v plane. The easiest possible sampling function gives covered u, v points the weight 1 and sets the rest of the plane to 0.

$$S(u, v) = \sum_{k=1}^{M} \delta(u - u_k, v - v_k) \tag{4.13}$$

The index k labels M measured visibilities at the position u_k, v_k. δ is the Dirac delta distribution, defined as

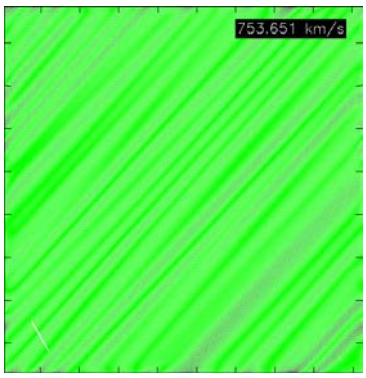

(a) Cross correlations (baselines) of antenna 14 and 19 in scan 3 (VLA B configuration) result in this dirty image.

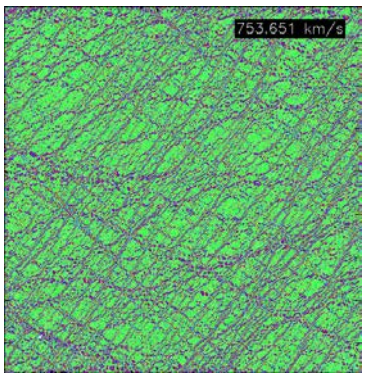

(b) The baselines between antenna 14 and 19 of measurements in B, C and D configuration are taken into account.

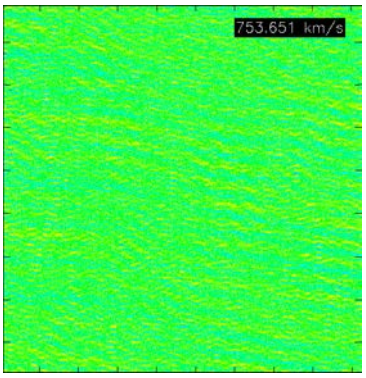

(c) Cross-correlations and auto-correlations of antenna 1 with antenna 1 to 10 complicate the structure.

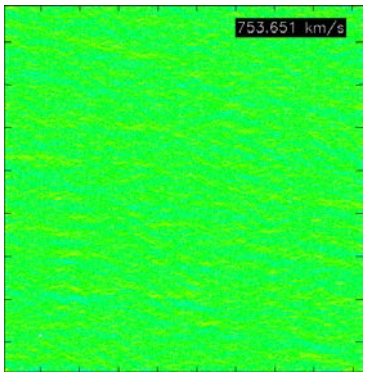

(d) In this dirty image all baselines involving antenna 1 were used.

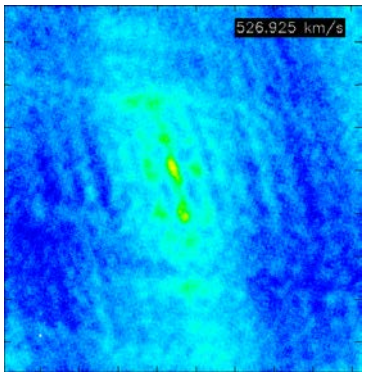

(e) More baselines are included: All baselines involving antenna 1 to 10.

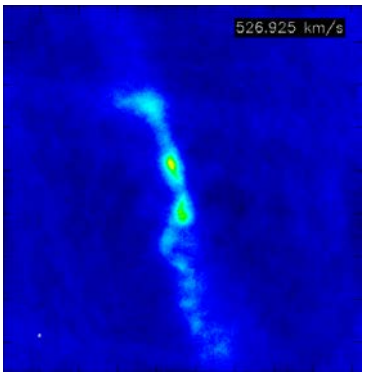

(f) If all baselines are included the galaxy becomes clearly visible.

Figure 3: The plots show from 3a to 3f how the image is composed of superpositions of waves. If only one baseline in one measurement is considered (3a), the wave structure clearly shows up. The measurement in B configuration took six hours, so more than one visibility was recorded and the image consists of more than one single wave. Figure 3b was produced using the baselines between antenna 14 and 19 in all three configurations. Adding more baselines forms a more complex structure in the images, but it needs all baselines involving antenna 1 to 10 to form a recognizable galaxy shape. The last image 3f shows the dirty image when using all recorded visibilities.

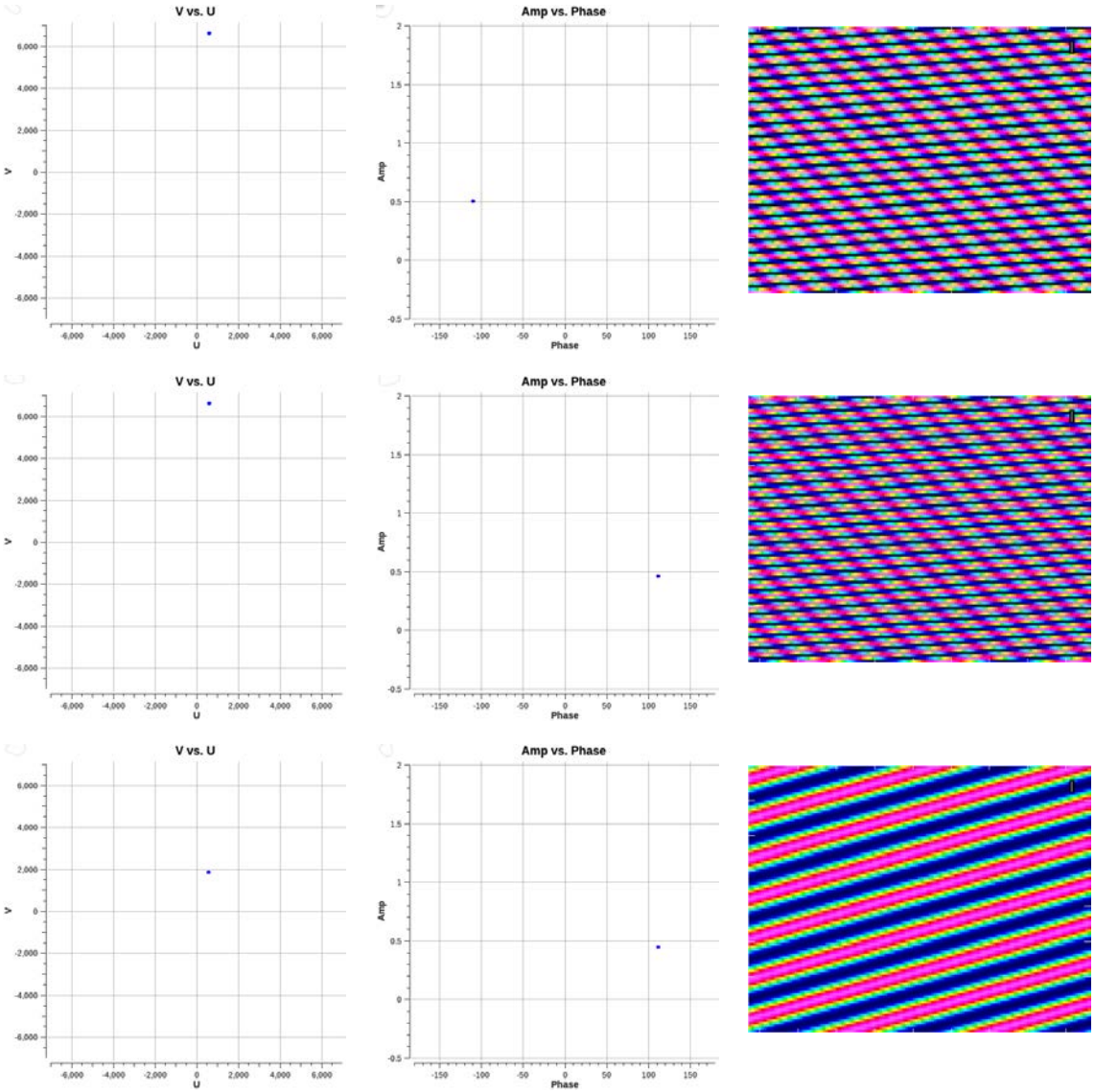

Figure 4: Every pair of pictures shows a visibility point and its fourier inverse in the l, m plane. Going from top to bottom only one quantity is changed per image illustrating the effect of location (angle and radius), amplitude and phase of visibilities.

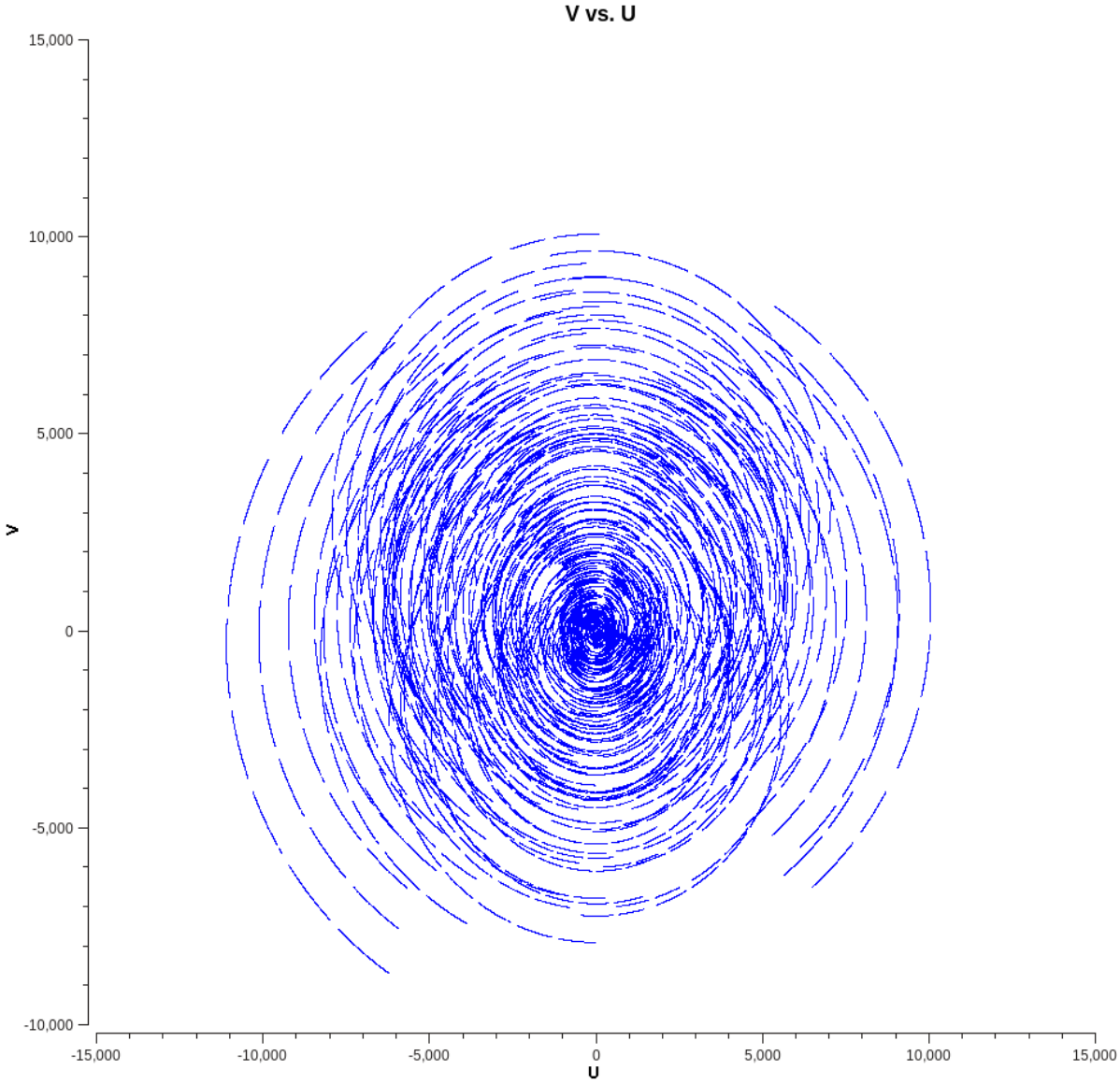

Figure 5: Sampling of the u, v plane for the THINGS observation of NGC2403 where each point represents one visibilty. As intensity is a real quantity, the visibility must be hermitian with $\mathcal{V}(-u, -v) = \mathcal{V}^*(u, v)$ resulting in a sampling function that is symmetrical to the origin.

$$\delta(u-u_k, v-v_k) = \begin{cases} 1 & \text{if } u = u_k \text{ and } v = v_k \\ 0 & \text{else} \end{cases} \tag{4.14}$$

The image obtained using this sampling function is called the principal solution I. The true values of the uncovered areas of the u, v plane are not known and therefore all functions with different assumptions of these points offer correct solutions, too. Section 4.6 discusses the possibilities of modifying the sampling function.
The mathematical expression of gaining a first so-called dirty I^D image then is:

$$\begin{aligned} I^D(l,m) =& \hat{\mathbf{F}}^{-1}[S(u,v)\mathcal{V}(u,v)] && (4.15)\\ =& \hat{\mathbf{F}}^{-1}[S] * \hat{\mathbf{F}}^{-1}[\mathcal{V}] && (4.16)\\ =& B * I && (4.17) \end{aligned}$$

According to the Convolution Theorem (Bracewell, 1978) the fourier transform of a multiplication of functions is equal to the convolution of the fourier transformed functions. Therefore the calculation can be simplified to the dirty image I^D being the concolution of dirty beam B (section 4.5) and true sky brightness I (Cornwell, 2008).

4.5 Primary beam, dirty beam and clean beam

The primary beam is the beam of a single telescope, therefore the fourier transform of the aperture. Its size is given by the FWHM and is $30'$ for the 25 m telescopes that make up the VLA.
The dirty beam B is the reaction of the interferometer, i.e. all telescopes together, to a hypothetical centered point source and therefore determines the achievable resolution.

$$B = I^D(\textit{point source}) = \hat{\mathbf{F}}^{-1}[S] * \delta(0,0) = \hat{\mathbf{F}}^{-1}[S]$$

A typical size for the dirty beam is around $15''$ as can be seen in Figure 6b.
Its shape is not gaussian as one would want it to be, nor are all the values positive. In fact, the total spatial integral over the dirty beam is zero. This is due to the incompletely sampled UV plane and the ability of fourier transforms to generate alternating functions with negative values. Because the large primary beam is sampled by the smaller dirty beam, the convolution of dirty beam and true image is the dirty image. As a result of the vanishing integral over the dirty beam, the sum over the dirty image is also zero. Of course the true flux from an astronomical source is not zero and negative fluxes are physically impossible. To correct these effects a cleaning procedure is necessary as described in section 4.8.1 and 4.8.3. Cleaning removes the structure outside the main maximum that is caused by missing short baselines. These so called sidelobes are not present in the clean beam which is a gaussian-like curve fitted to the main maximum of the dirty beam. In theory, a perfectly sampled UV plane would result in a gaussian

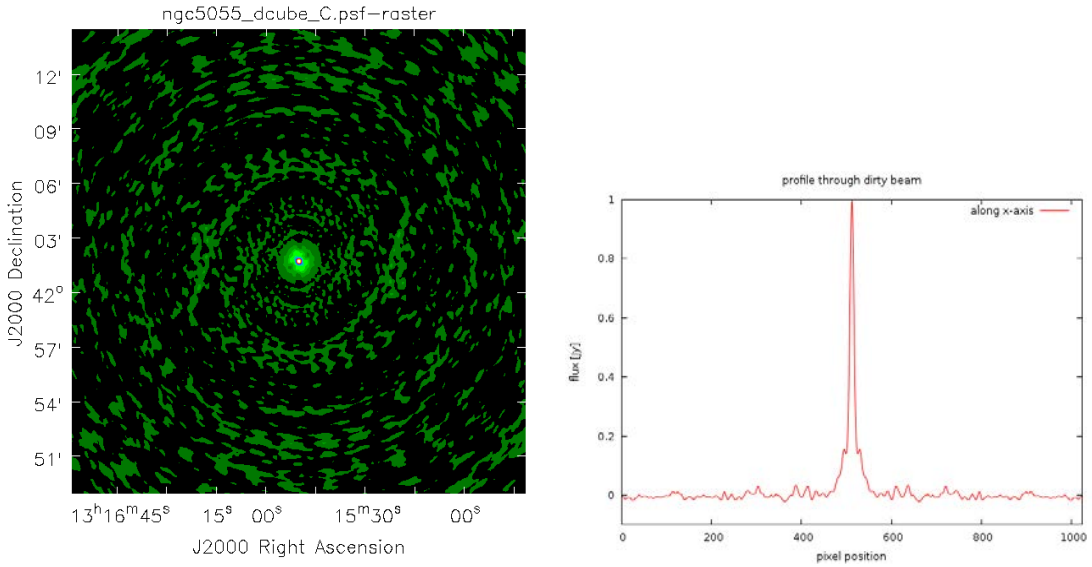

(a) Image (b) Profile

Figure 6: Image (6a) and profile (6b) of the dirty beam of NGC5055 measured by the VLA in C configuration along the x-axis (right ascension). One pixel corresponds to 1.5″.

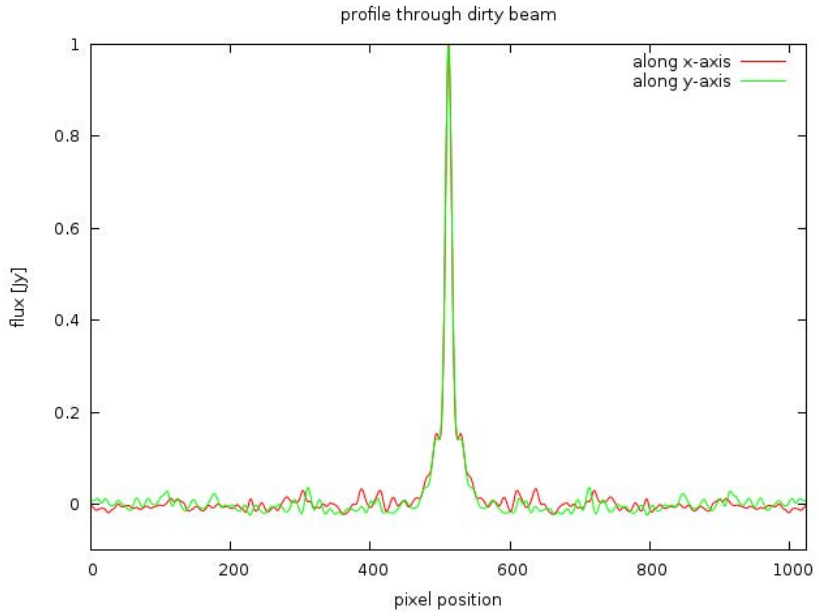

Figure 7: The dirty beam is not spherical symmetric. The sidelobes differ in two profiles along the x- (right ascension) and y-axis (declination).

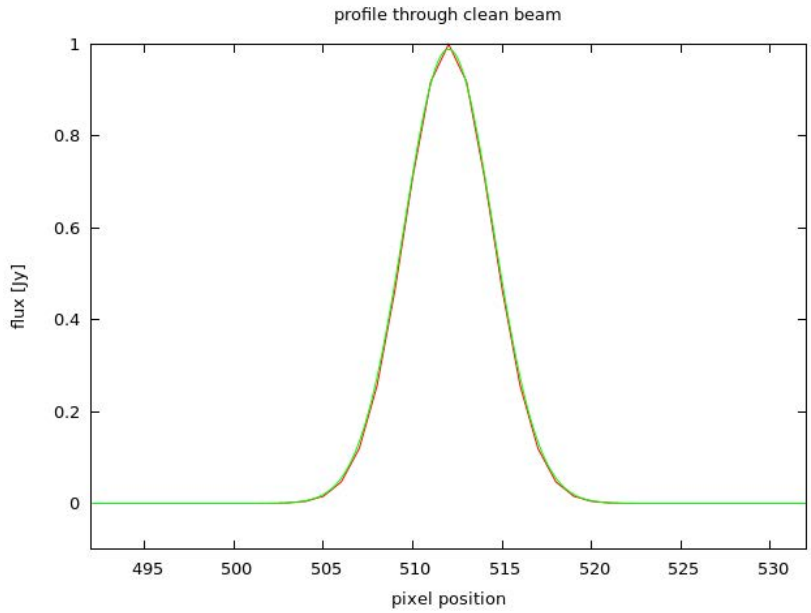

Figure 8: A profile through the radial symmetric clean beam that is used by `CASA` (red). The green curve is a gaussian fit. As can be seen, the difference is quite minor and basically due to the discrete pixel pattern.

beam which is why the clean beam gets a shape close to a gaussian bell curve as can be seen in figure 8.
In case of the THINGS data sets, the dirty beam has a complex shape as can be seen in Figure 9.
It emerges from combining three visibilties from three different antenna configurations to one single file per galaxy. Below the main maximum two ridges per side can be seen that are due to the broader main maximum of the dirty beams in VLA's C and D configuration.

4.6 Weighting

The easiest possible sampling function S is the sum of Dirac delta functions for each covered dot in the u, v plane. To gain more control over the shape of the synthesized beam, a more complex ansatz is needed: a weighted sampling function $\mathcal{V}^W$.

$$\mathcal{V}^W = \sum_{k=1}^{M} R_k T_k D_k \delta(u - u_k, v - v_k) \mathcal{V}(u_k, v_k) \tag{4.18}$$

R_k, T_k and D_k are three weighting functions described below.

Reliabilty function R_k: The reliabilty function weights the visibility data points according to given system parameters, such as integration time, temperatur and bandwidth. These

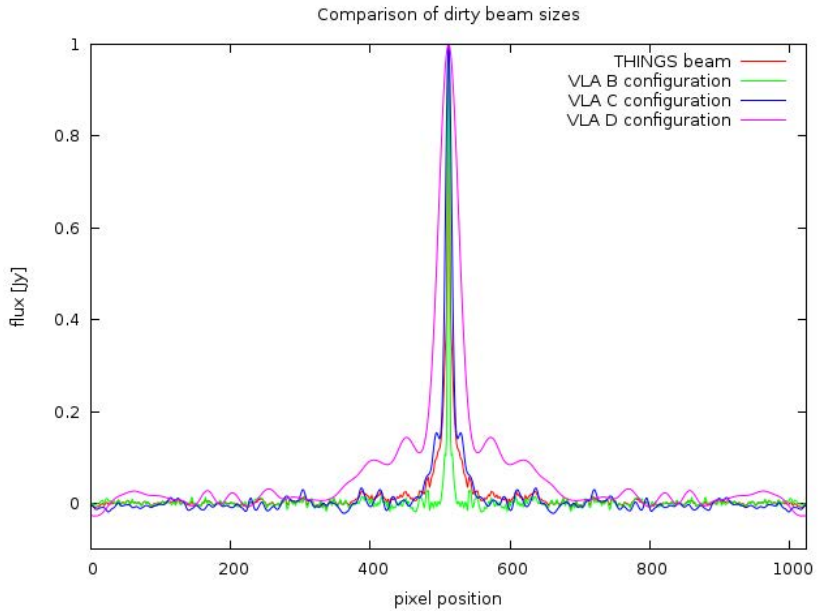

Figure 9: The VLA dirty beams differ noticeably. By combining data of B, C and D configuration, the THINGS dirty beam gets a very complex structure.

cannot be changed during imaging but codetermine the properties of the restored images.

Tapering function T_k: As tapering functions gaussians of circular shape are often used. The purpose is to downweight data in the outskirts of the covered UV plane. This is needed because the limited length of baselines apply some kind of cut-off in the coverage of the UV plane that is fourier transformed to a $sinc(x)$. *sinc* or $sin(x)/x$ looks like a damped *cos* function and therefore has strong sidelobes. By tapering, some information in the image gets lost leading to a lower resolution.

Density weighting function D_k: With the density weighting function it is possible to correct for varying density in the UV coverage. The exstablished possibilities of D_k are:

natural weighting $D_k = 1$
: All data points are weighted equally resulting in the best signal-to-noise ratio possible. As can be seen in section 4.4, the density is higher towards the (u, v) origin, hence emphasizing the shorter spacings that produce a broad dirty beam and lower resolution.

uniform weighting $D_k = \frac{1}{N_s(k)}$
: This weighting scheme depends on the density of data points $N_s(k)$ around point k with a radius s or a box with size s, depending on the programm. Here, each grid cell on the UV plane has the same weight, independent of its position. As the external visibilties get strengthened, the resolution increases at the expense of increasing the noise in the longer baselines.

super-uniform weighting
: In some special cases uniform weighting is not enough, so the parameter s is increased to reduce the effect of poorly sampled cells.

robust weighting
: Briggs (1995) describes a compromise between natural and uniform weighting that is capable of combining the advantages of both weightings but keeping out part of the disadvantages. A so called robustness parameter[2] adjusts the algorithm to work as in natural weighting, uniform weighting or interpolating in between. Unfortunately is is necessary to empirically determine the value for an optimum between signal-to-noise ratio and resolution.

4.7 Data cubes

Every data set consists of spatial information given as right ascension (RA) and declination (DEC), but also contains measurements for multiple frequency channels. To illustrate the data all channels are placed consecutively in a *cube* with two spatial and one frequency or velocity axes. With `CASA` (section 5) cubes can be viewed as films jumping from one channel to the next. Diagramms along other directions can be calculated as well, but interpretation must be done carefully as spatial and frequency axes are mixed together.

4.8 Deconvolution

Now that the different beams and the influence of the sampling function is defined, the final step can be made: Deconvolution. The result of section 4.4 was $I^D = B * I$ meaning that the true sky brightness I is convolved with the dirty beam B in the dirty image I^D. The task of finding I from the dirty image I^D is only possible by assuming a suitable model. The easiest model, a collection of point sources, is used in Högbom's `clean` algorithm that is described in the following section. Multi-scale clean expands it with emission on larger scales as detailed in section 4.8.3.

4.8.1 The `clean` algorithm

As already mentioned in section 4.5 the dirty images are not useable to measure the flux and are blurred due to the strong sidelobes as an effect of the incompletely sampled u, v plane. The theoretically perfect beam is known, as well as the dirty beam, so it is possible to reduce the effects and recover an improved image.
Högbom (1974) describes a suprisingly easy algorithm that works very well in most cases. The `clean` algorithm bases on a model of point sources that make up the true image. Extended emission is not condsidered firsthand, but emerges by many point sources next to each other. The following three iteration steps are performed on the dirty image

[2]The Briggs robustness parameter ranges from -2 (uniform) to +2 (natural). However, `CASA` uses a range of -5 to +5.

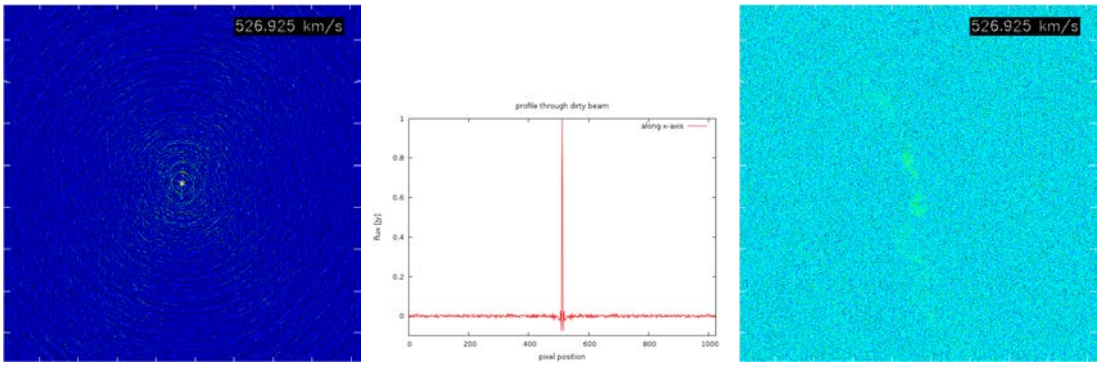

robust = -2.0 (uniform)

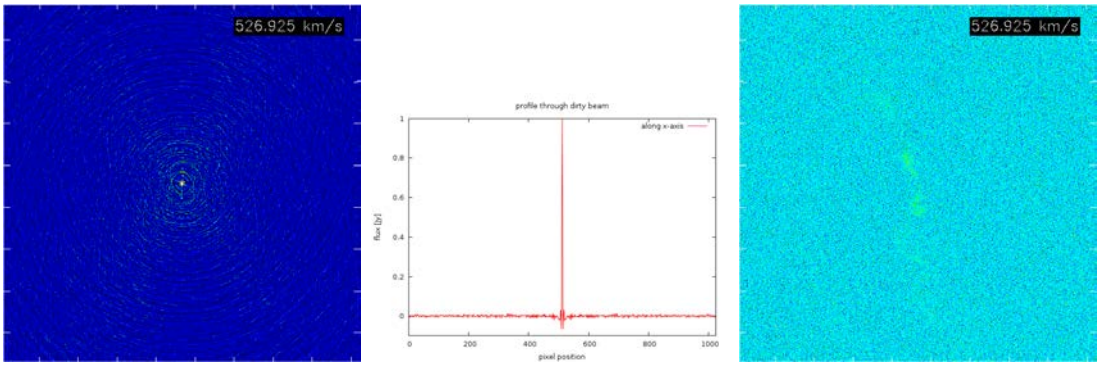

robust = -1.0

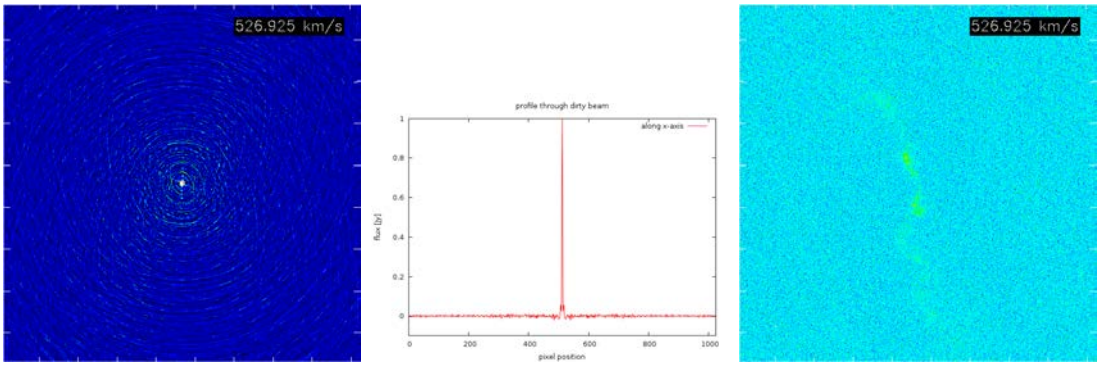

robust = 0.0

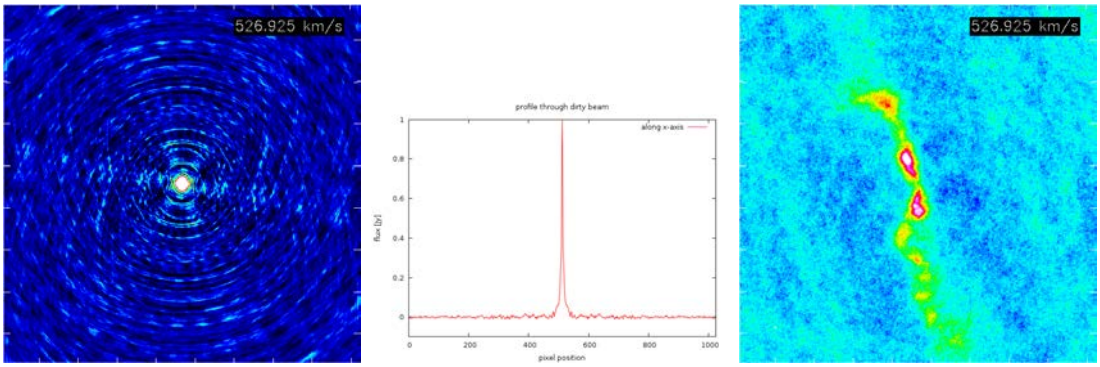

robust = +1.0

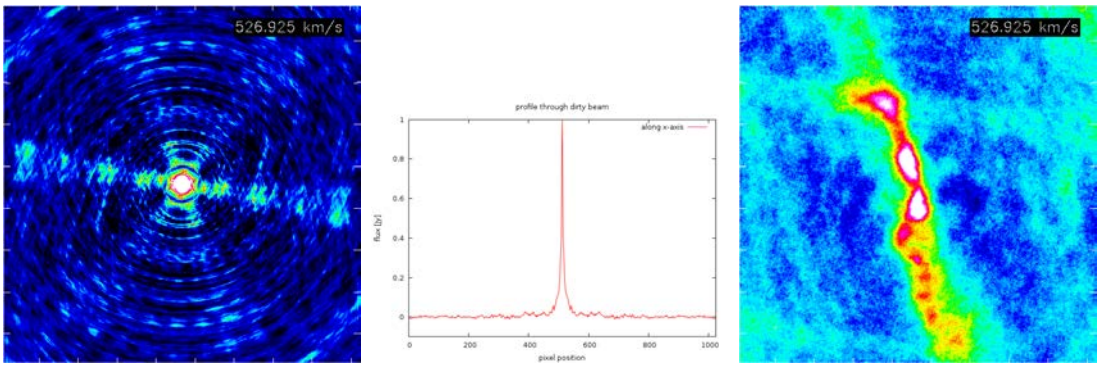

robust = +2.0

Figure 10: Different weighting parameters have great influence on the dirty beam. Here, the beams of a measurement of NGC5055 are shown. From left to right, the dirty beam (-5mJy to 8mJy), its profil and the dirty image (-10mJy to 50mJy) is displayed. Robust parameters over +2 and below -2 show no difference in the image. Therefore only the interesting range between -2 and +2 is printed.

for the first iteration and afterwards on the image resulting in step 3 until a stopping criterion is reached.

1. locate the pixel with maximum flux in the image
2. write the flux value multiplied with a loop gain factor and the location in a `clean` table
3. substract the dirty beam scaled by the loop gain factor at the logged position

It is unnecessary and with todays computational possiblities almost impossible to `clean` the whole image. Because the loop gain is typically around 0.1, every pixel that contains real emission is `clean`ed more than once. This approach asures that that no point gets `clean`ed to too low values since the sidelobes affect the surrounding as well and not only the maximum. To prevent `clean` from digging into the noise and perform unnecessary operations, it is convenient to define a stopping criterion in terms of noise level, "such as stop at 2.5σ". Another possibility is to stop after a specified number of iterations. To further reduce the computational effort, the established programms allow the user to set `clean` windows or masks that specify where emission is expected.
To recover an usable image after stopping the above iteration, three steps are necessary.

4. fit a gaussian or gaussian-like function, the `clean` beam, to the dirty beam
5. colve every `clean` component from the `clean` table with the `clean` beam and add them together as a model image
6. add the model image to the residual image which is the last image of step 3 to obtain the `clean`ed image

The restored image includes the `clean`ed emission and also the noise. Problems that arise by adding both together are discussed in section 4.9.
The evolution of the dirty/resiudal image and the model image are shown in Figure 11.

4.8.2 Descendants of `clean`

The original Högbom `clean`[3] algorithm was enhanced by Clark (1980) and Schwab (1984) to improve the computational speed. Both algorithms use major and minor cycles whereas a minor cycle is basically the same as in the original procedure. Differing from Högboms version and the Cotton-Schwab algorithm, Clark clean only considers a central region of the dirty beam and cuts off the rest. This proceeding approximates the `clean` components, but with fewer computation time needed. In a minor cycle, not all, but only the highest residuals down to a threshold depending on the sidelobes of the dirty beam are considered. A major cycles then calculates a new residual image from the cumulated

[3]To distinguish between different clean algorythms, I will use different fonts from now on. Typewriter font stands for the original Högbom `clean`, whereas "clean" denotes other cleaning algorithms or the procedure in general.

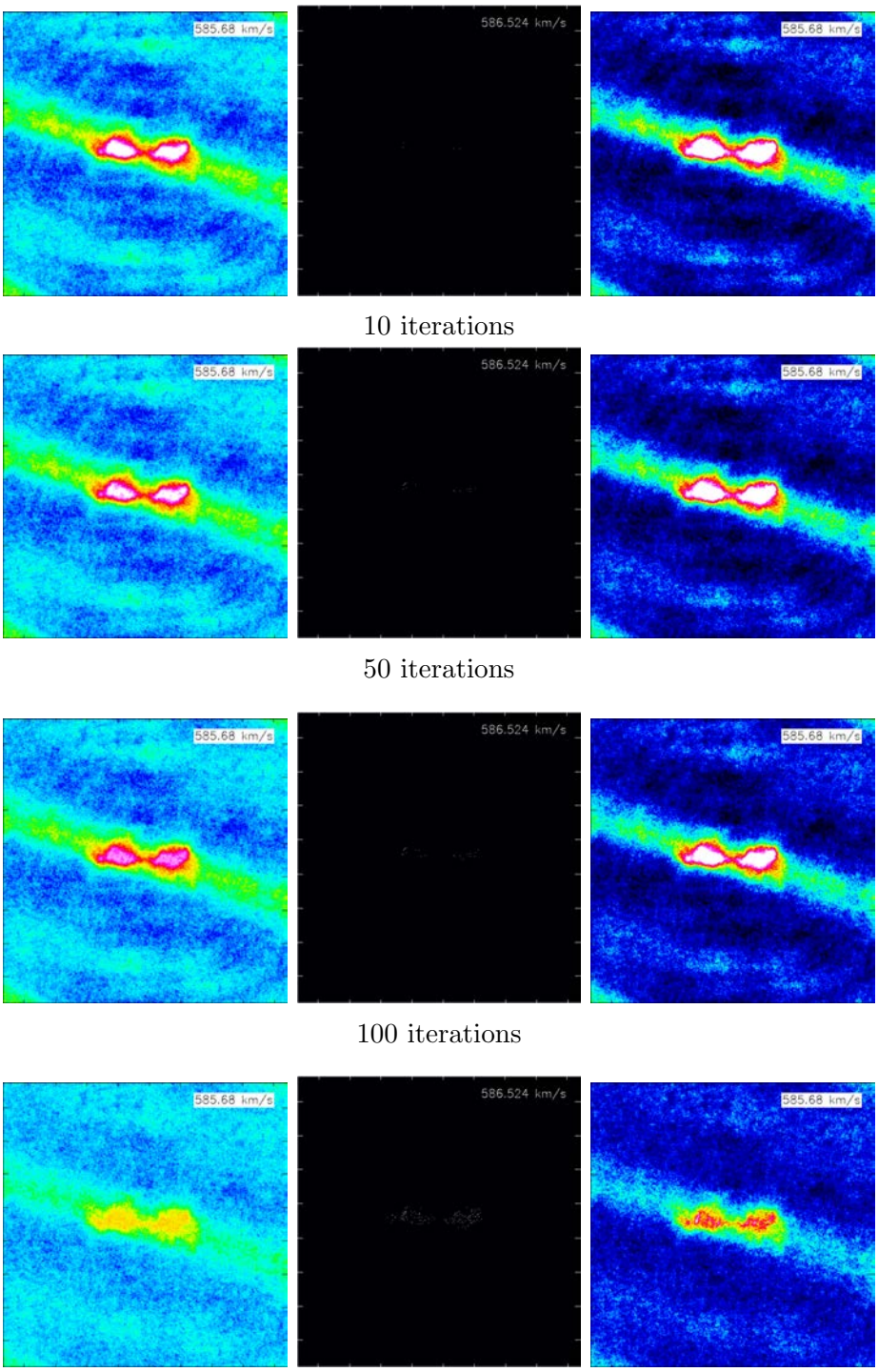

Figure 11: The evolution of `clean` when increasing the number of iterations from 10 (almost no cleaning) to 50000 (cleaned down to a threshold of 0.6mJy). From left to right are displayed: residual image, model image and the sum of both (restored image).

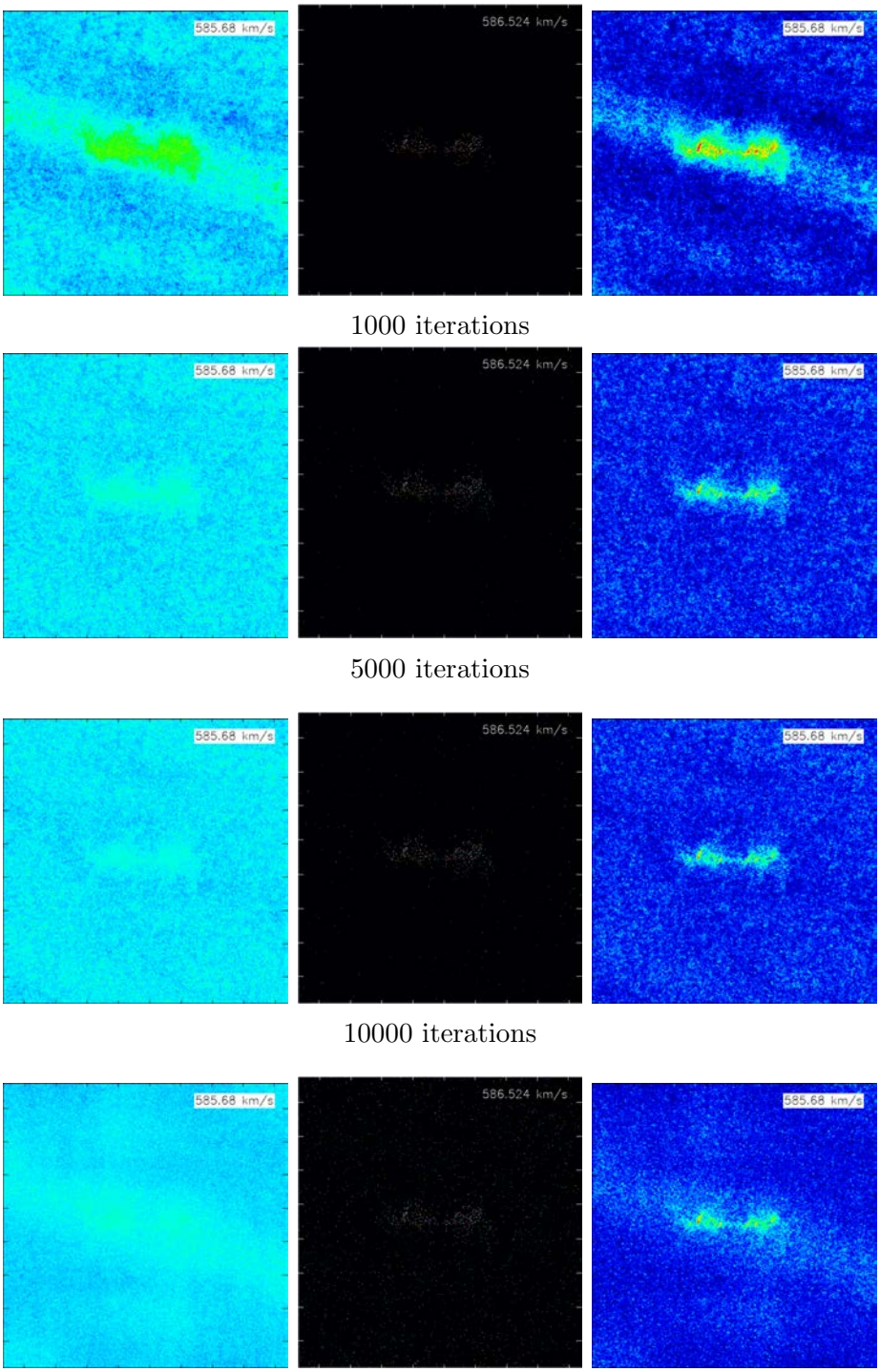

Figure 11: The rainbow color map runs from -2 to 6 mJy/beam for residual images, 0 to 0.4 mJy/pixel for the models and -5 to 8 mJy/beam in the restored image.

`clean` table. Clark and Cotton-Schwab algorithm differ in the way how this is done. Whereas Clark `clean` uses the dirty image and a single pair of fast fourier transforms (FFT), Cotton and Schwab designed their algorithm to work on the visibility data to avoid aliasing[4] due to inevitable gridding[5]. Errors made by the approximations in minor cycles can be corrected in subsequent cycles.

4.8.3 Multi-scale cleaning

Altough `clean` models all emission by point sources, it works surprisingly well on extended sources. However, its performance can be approved by assuming a more complex model: Emission can appear on larger scales, as well as it can be emitted by point sources. Different algorithms, such as Multi-Resolution `clean`, Multi-scale Maximum Entropy or Adaptive Scale Pixels, expand the original `clean` to work with extended emission. Those methods have improved the results but have problems such as a fixed scale order or high computional requirements.
A relativly new member of the multi-scale family is the Cornwell (2008) Multi-scale `clean` (msclean). It is based on Högbom `clean` with an multi-scale extension that searches the best scale size in each iteration. The scales are defined by a single dimensionless parameter α that indicates the size in terms of pixels. A model for one "single emission" is formed by the product of clean list entry I_q (position and strength) and clean component $m(r, \alpha_q)$, just as in `clean`. The index q denotes the different scales over which must be summed to get the total model I^M. In general the clean component m can be a function of image coordinates x, y and scale α_q but some constraints must be satisfied: The model should be physical plausible which rules out all functions with negative values. Rotating the image does not change the physical properties, hence m must have radial symmetry, so $m(x, y)$ can be simplified to $m(r)$ with $r = \sqrt{x^2 + y^2}$. And finally, the clean component should not extend over all space, but must be truncated to allow support constraints (see section 4.12). The solution is a prolate spheroidal wave function $\Psi(r)$ multiplied with a tapered, truncated and scale dependend parabola.

$$m(r, \alpha) = \Psi(r) \left(1 - \left(\frac{r}{\alpha_q} \right)^2 \right) \tag{4.19}$$

Figure 12 shows the clean component $m(r, \alpha_q)$. For $\alpha = 0$ the result is identical to a `clean` beam, whereas greater values produces a curve that is similar to broader gaussians. Now, msclean follows the same sequences as `clean`, looking for the peak residual the perform the substraction. Instead of merely scanning the pixel positions, it also searches the in principle non-discrete axis α_q. To speed up the search, only some user-defined scales are concidered. Mathematically, the choise of α_q is ill-defined, but it appears to be

[4] Aliasing is the effect of sky brightness lying outside the field of view being aliased or folded back into the primary beam

[5] Gridding is an element of FFT algorithms and therefore necessary. Calculating the FT directly is so slow that it is impossible to pursue scientific goals.

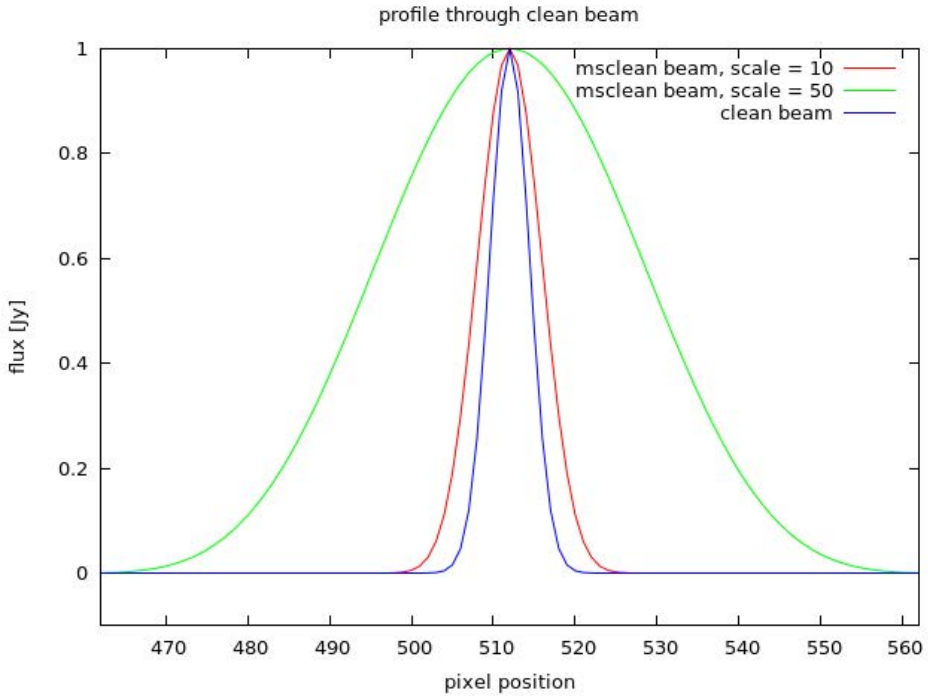

Figure 12: The shapes of `clean` beam and msclean components are very similar to suitably scaled Gaussians. The scale size α corresponds approximately to half of the total width.

not too important. Of corse $\alpha = 0$ must be included to represent point sources and the largest scale should be approximately the size of the largest expected structure. To cover to scales in between, Cornwell recommends a geometric progression. The advantage of msclean is to search for the best scale and can therefore fall back to merely point sources as in `clean` if the given scales are chosen in a wrong way. A fine coverage of the space between zero and the largest scale wastes computational time as only a subset of the given scales is used. On the other hand, a coarse set of scales can cause poorer converge. The scale decision algorithm calculates a residual images for all given α_q and evaluates which has the maximum adjusted residual, i.e. for which scale the substraction has the greatest effect. This scale is used afterwards in the actual substraction that is recorded in the residual image and msclean table.
Now, a bright point source with little extended emission around it would be modeled by a larger scale resulting in a residual image with an almost uncleaned point source surrounded by a negative bowl[6]. In principle this can be corrected in subsequent iterations, but it is better to avoid the problem right from the start. To do so, a small scale bias must be introduced that reduces the a priori greater effect of larger scales. Cornwell calculates this factor as $S(\alpha_q) = 1 - scb * \alpha_q/\alpha_{max}$, where scb can be adjusted to, as an example, give more weight on larger scales when modelling a structure with few point sources.
As in `clean`, the modeled component is scaled by the loop gain as is the substracted beam. If only point sources are considered, the beam to substract is just the dirty beam that is the interferometer response to such a source. In the case of $\alpha \neq 0$, the dirty beam is convolved with the clean component $m(r, \alpha_q)$ and therefore broadend to behave like the interferometer response to extended emission. Since the scale sizes are defined as some fixed values, it is possible to pre-calculate the convolutions and reduce the computional effort to scaling, shifting and substracting. Nevertheless, msclean must evaluate multiple residual images instead of only one in `clean`, but this is compensated as a larger beam removes considerably more flux and therefore needs less iterations. Instead of calculating the residual images consecutively, msclean works on one image for each scale to parallelise the computation. At the end of an iteration, all images are updated with the beam of the scale found.
The remaining tasks are identical to `clean`: Stop the iteration when a residual threshold or a maximum number of iterations is reached. Restoring the image is done by convolving msclean table and clean beam to get the model image and adding the residuals.
The main tasks of msclean are summarized in the following chart.

1. calculate the beam to substract $B * m(r, \alpha_q)$, the small scale bias $S(\alpha_q)$ and the scale-convolved starting residual images $I^R * m(r, \alpha_q)$

start iteration

2. locate the pixel with maximum flux in the residual image for each scale
3. apply small scale bias and choose scale with maximum cleaning effect

[6]This is what multi-resolution clean does.

4. write the gain-scaled flux value, location and scale in the msclean table I^M
5. substract the precomputed beam scaled by the loop gain factor from all residual images

end iteration when residual threshold or maximum number of iteration reached

6. convolve model with clean beam $B_C * I^M$ to obtain model image
7. get restored image by adding residual image

4.9 Residual scaling (Rescaling)

As described above, the resulting image after cleaning or mscleaning is the sum of a model image and the residuals that remain after cleaning. Whereas the residual image contains flux measured in Jansky per dirty beam, the model image was restored using the clean beam and therefore offers flux in Jansky per clean beam. Those beams differ significantly, otherwise cleaning wouldn't be necessary. The result of these different units is an overestimated residual in the combined map due to the large dirty beam compared to the smaller clean beam. The clean beam is considered the correct one, so the residual have to be scaled down to provide correct fluxes in the assembled image. A scale ratio ϵ by which the residuals need to be divided can be introduced by $\epsilon = \Omega_{dirty}/\Omega_{clean}$ where Ω stands for the respective beam size. Ω_{clean} is determined as in formula 4.31 from the FWHM. The dirty beam does not have a simple gaussian shape which is why its size needs to be measured by hand. To do so the flux Ω_{dirty} inside a centered sqare on the dirty beam image is measured for various side lengths. When plotted against growing square size, ϵ decreases to reach an asymptotic value allowing us to define a single factor for rescaling that is applicable for flux measurements inside an area above a certain threshold (square size).
This procedure is only feasible in areas that contain real emission because it should scale the inevitably leftovers of cleaning but reduces real noise as well. Altogether rescaling enables correct flux measurements at the price of erroneous noise properties. To get both quantities correctly, usually two data cubes are produced: A "normal", not rescaled one for analyses that depend on noise and a second rescaled cube to obtain flux.
An example for the effect of rescaling is shown in figure 13 where the upper half of the image shows a normal restored image of NGC5055 that is added to a rescaled image in the lower half.

4.10 Primary beam correction

The last step in image processing is to correct for the varying sensitivity of the antennas over the field of view. This can be done by simply dividing the image by the primary beam. Applying the correction in earlier steps leads to wrong results.

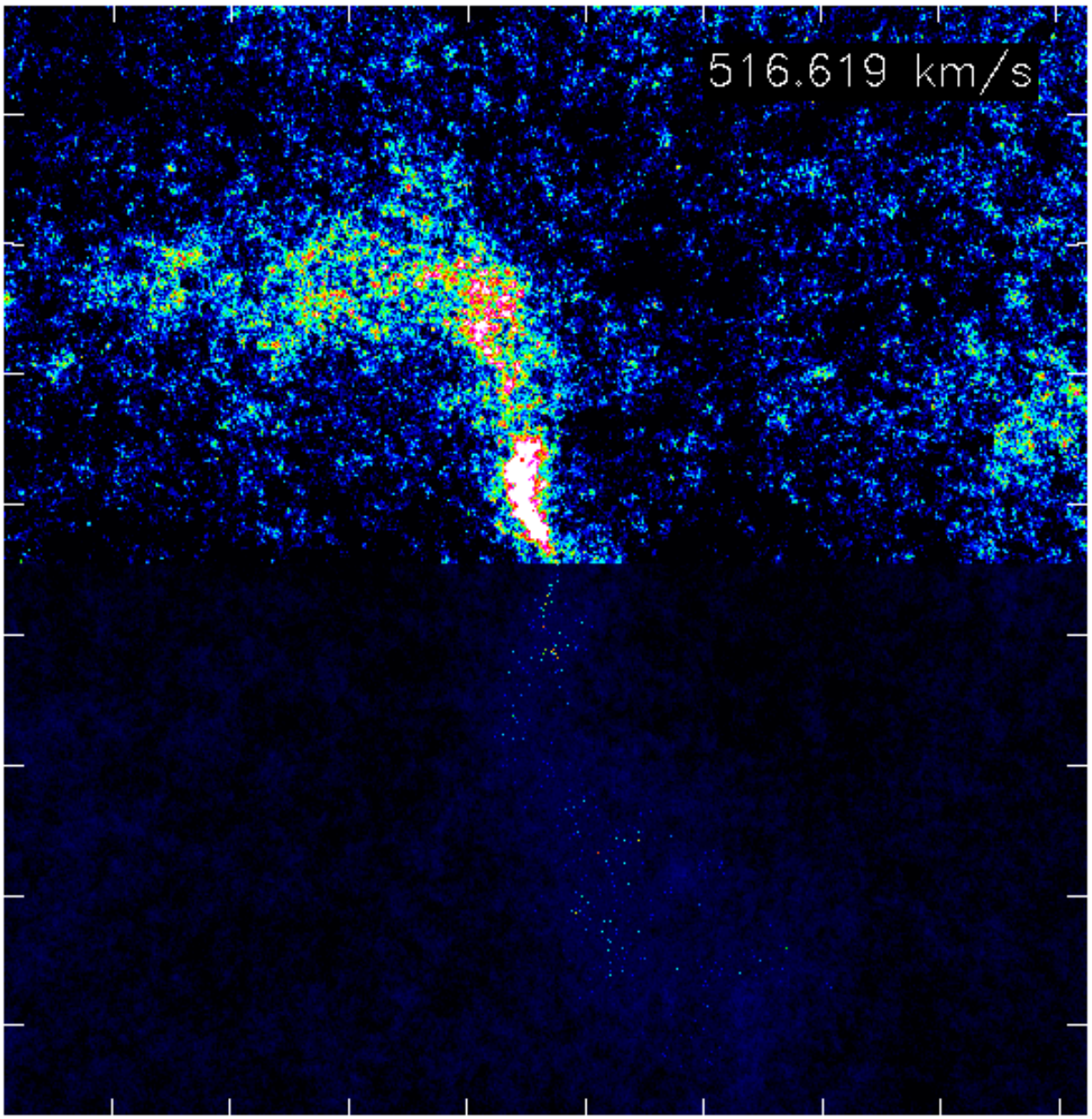

Figure 13: NGC5055 at a velocity of 517 km/s. The upper half shows a normal (unrescaled) image, whereas the lower half contains the respective part of the rescaled image. The color range for the whole image goes from -0.05 to 2 mJy/beam.

4.11 Moment maps

Beside channel maps, so-called moment maps can be produced that represent different features depending on the number. Generally, the n-th moment is defined as an integral over intensity $I(v)$ depending on velocity v.

$$M_n = \int I(v) v^n dv \tag{4.20}$$

- moment 0

$$M_0 = \int I(v) dv \tag{4.21}$$

  For $n = 0$ M becomes the velocity integral over the HI maps which is the summation of all channels into one map. It displays the total distribution of HI in the galaxy given in Jy km/s.

- moment 1

$$M_1 = \langle v \rangle = \frac{\int I(v) v dv}{\int I(v) dv} \tag{4.22}$$

  The first moment shows the normalised velocity distribution $\langle v \rangle$ in km/s.

- moment 2

$$M_2 = \sigma = \sqrt{\frac{\int I(v)(v - M_1)^2 dv}{\int I(v) dv}} \tag{4.23}$$

  The second moment is a normalised map of the velocity dispersion σ in km/s.

4.12 Masking

As mentioned in section 4.8.1 `clean` can work with windows or masks that limit the region where emission is expexted. Setting windows aims at reducing the computational effort of searching the highest residual and cleaning noise unnecessarily. As a successor of `clean`, msclean can handle masks, too, but needs some additions to ensure correct cleaning. If emission is expected only inside a mask, the algorithm must assure that the clean beam of any scale does not reach outside that region. Therefore, msclean can find point sources everywhere inside the mask, but for broader emission a scale-dependend second mask must be introduced during calculation. Hence, masks should not be set too tight around emission to receive good cleaning results. In addition, masks should always be computate from natural weighted cubes as robust weighting strenghtens the noise that can lead to mask defined by noise instead of real emission.

4.13 Flux

The physical quantity of interest when working with radio data is the flux. As the cleaned maps contain only the flux per beam, it is necessary to know the beam area before calculating flux.

4.13.1 Beam area

The beam area is defined as the volume below the two-dimensional gauss-like beam. Therfore it can be derived from the standard deviation σ.

$$\text{beam area} = \int_{-\infty}^{\infty}\int_{-\infty}^{\infty} \exp\left(-\frac{x^2}{2\sigma_x^2} - \frac{y^2}{2\sigma_y^2}\right) \mathrm{d}x\mathrm{d}y \tag{4.24}$$

$$= \int_{-\infty}^{\infty} \exp\left(-\frac{x^2}{2\sigma_x^2}\right) dx \int_{-\infty}^{\infty} \exp\left(-\frac{y^2}{2\sigma_y^2}\right) dy \tag{4.25}$$

$$= \sqrt{\pi}\sqrt{2\sigma_x} \cdot \sqrt{\pi}\sqrt{2\sigma_y} \tag{4.26}$$

$$= 2\pi\sigma_x\sigma_y \tag{4.27}$$

The relation between σ and full width at half maximum (FWHM) is:

$$\frac{1}{2} = \exp\left(-\frac{\mathrm{FWHM}^2}{2\sigma^2}\right) \tag{4.28}$$

$$\ln 2 = \frac{\mathrm{FWHM}^2}{2\sigma^2} \tag{4.29}$$

$$\sigma = \frac{\mathrm{FWHM}}{2\sqrt{2\ln 2}} \tag{4.30}$$

Using this result in 4.27 the beam area can be expressed in terms of FWHM.

$$\text{beam area} = \frac{\pi}{4\ln 2}\ \mathrm{FWHM}_x\mathrm{FWHM}_y \tag{4.31}$$

$$= 1.13309\ \mathrm{FWHM}_x\mathrm{FWHM}_y \tag{4.32}$$

Note that the beam area is measured in $''^2$ because the FWHM is given in arcseconds, although it is derived from an integral over the beam.

Now that the beam area is known, the flux density S can be calculated. This is done by applying a mask to ensure that only real emission is measured and followed by calculating the sum for every channel, so the noise does not have to be concidered anymore. The images contain the flux per beam in Jy/beam for each pixel why it is necessary to know how many beams fit in the masked region. This is calculated from pixelsize (in $''$) and the beam area (4.31) as $\frac{(\text{pixel size})^2}{\text{beam area}}$. The entire formula reads:

$$S = \frac{1\text{Jy}}{beam} \cdot \frac{\text{pixel size}^2}{1.13309\ \text{FWHM}_x\text{FWHM}_y} \tag{4.33}$$

So far, only the flux density (in Jy) is known, but multiplying it with the width of one channel (in km/s) results in the flux F [Jy km/s]. Often the long term flux density is shortened to flux. Due to the simple conversion between them, this causes no problems and can immediately be distinguished by the used unit (Jy with or without km/s).

4.14 Column density

When looking at the sky, a telescope can only see a planar projection of the real, three dimensional properties. Such is Column density the number of atoms along the line of sight projected onto a plane. The conversion of flux density S to column density N_{HI} makes use of the Rayleigh-Jeans law that approximates Planck's law for black body radiation at low frequencies ν:

$$S = \frac{2kT_B}{\lambda^2}\,\Omega \tag{4.34}$$

The flux density S is related to radiation temperature T using Boltzmann's constant k, wave length λ and the observed solid angle element Ω. Astronomical objects of hydrogen are almost always optical thin, meaning the optical depth $\tau = \int_0^L \alpha(\nu)dx$ is $\tau \ll 1$. The integration is performed over an infinitesimal part dx of the path length L between source and observer that has the absorption coefficient $\alpha(\nu)$. In this case, true temperature T and radiation temperature T_B are related by $T_B = \tau(\nu) \cdot T$ and the number of atoms along the line of sight corresponds to T_B. For low velocities of the moving gas an approximation can be made that leads to formula 4.35 for optical thin HI (Walter et al., 2008).

$$T_B = 6.07 \cdot 10^5 \frac{S}{\text{FWHM}_{major}\text{FWHM}_{minor}} \tag{4.35}$$

The result is T_B in Kelvin when flux density and FWHM of the beam is inserted in Jy/beam and $''$, respectively.
The relation of T_B to column density N_{HI} is given by (Walter et al., 2008)

$$N_{HI} = 1.822 \cdot 10^{18} \sum_i T_{B,i}\Delta v \tag{4.36}$$

When the velocity integrated surface brightness $T_{B,i}\Delta v$ (over channel i) is entered in K km/s, column density N_{HI} has the unit cm^{-2}.

4.15 Surface density

Surface densities Σ_{HI} are another product that can be calculated from fluxes. It describes the gas mass inside an area projected the projected plane in units of solar mass $M_\odot$ per square parsec. (Leroy et al., 2008) calculates Σ_{HI} from the intensity I and inclination i as

$$\Sigma_{HI} = 0.020 \cos(i) \cdot I(\mathrm{K\,km/s}) \tag{4.37}$$

The prefactor 0.020 accounts for the presence of helium.
Using the relation between intensity and flux of formula 4.35, the numerical result is:

$$\Sigma_{HI} = 13755.7 \frac{\cos(i)}{\text{pixel size}^2} F(\mathrm{Jy/beam\,km/s}) \tag{4.38}$$

5 The Imaging process with CASA, IDL and GIPSY

The *C*ommon *A*stronomy *S*oftware *A*pplications package CASA[7] was developed for reducing data obtained by VLA and ALMA. It consists of image reduction tasks written in C++ that can be accessed via python scripts or an interface. Additional tools, such as an image viewer, should enable the user to perform all necessary steps in CASA. For the analyzing procedure in this thesis, another tool is still needed: IDL[8]. The *I*nteractive *D*ata *L*anguage provides possibilties to build masks that CASA is missing yet. Due to it's young age, CASA is missing additional functions, such as elliptical integrations to obtain radial profils of galaxies. A programm with a simple built-in task for this is the *G*roningen *I*mage *P*rocessing *Sy*stem[9] (GIPSY).

This analysis was carried out using the versions 4.0.1 and 4.1.0 of CASA, IDL 8.2.1 and Gispy 3.6. As CASA is being developed actively, it is very likely for the mentioned tasks to have changed since this thesis was written.

5.1 Importing visibility data

The already calibrated data sets of THINGS were produced using AIPS[10] that outputs .fits[11] files. CASA however, introduced a new format called *M*easurement *S*et into which the u, v data has to be imported with the task importuvfits(). From time to time CASA crashes during cleaning because of bugs or incorrect parameters and corrupts the measurement set. To ensure correct results, a new .MS file is created from the original .fits file for most of the sub-tasks, such as cleaning and mscleaning.

```
importuvfits(fitsfile = 'galaxy.fits',
             vis      = 'galaxy.MS'
            )
```

The parameter *vis* is used whenever a measurement set must be named.

5.2 Dirty image

The first impression of the selected galaxy can then be gained when looking at he dirty cube. As CASA does not feature a seperate task for simple deconvolution without cleaning, the task clean() must be used. The complete task with some fundametnal parameters for a galaxy called gal looks like the following.

```
clean(vis           = 'gal.MS',
      imagename     = 'dcube/gal_dirty_cube',
```

[7] http://casa.nrao.edu/
[8] http://www.exelisvis.com/IDL
[9] http://www.atnf.csiro.au/computing/software/gipsy/
[10] *A*stronomical *I*mage *P*rocessing *S*ystem, aips.nrao.edu/
[11] fits stands for *F*lexible *I*mage *T*ransport *S*ystem

```
      mode          = 'channel',
      interpolation = 'nearest',
      nchan         = 50,
      start         = 10,
      width         = 1,
      weighting     = 'natural',
      imsize        = 1024,
      cell          = '1.5arcsec',
      niter         = 0
     )
```

Important in this example is the keyword `niter` that is set to zero to perform no cleaning iteration, but only the fourier inversion to get the dirty image. `clean()` does not only produce a single restored image (`.image`), but also files that contain residual (`.residual`), model (`.model`), dirty beam (`.psf`), clean beam (`.flux`) and the optionally used masked (`.mask`). To keep all these files ordered a subdiretory 'dcube' is used in the task. `mode = 'channel'` tells `CASA` to expect the range to clean (`nchan`, `start`) in terms of channel numbers. The first 10 channels (0 to 9)[12] contain only noise that does not yield information, but requires computing time. Gridding of u, v data is set by `interpolation` and `width` allows averaging over channels. The image parameters are defined by `imsize` and `cell` to be a square of 1024 pixels with 1.5 arcsec/pixel.

5.3 Half-cleaned image

Depending on the individual measurement it is not possible to use the dirty image for the masking process as sidelobes can pile up to annihilate real emission. In this case, the mask would not inlcude a significant part of the flux leading to wrong results. Using a so-called half-cleaned image solves the problem. When cleaned down to a level of five times the noise, a large enough part of the sidelobes are removed to show where real emission can be found. `CASA` comes along with a `Viewer` that is capable of performing easy task, such as measuring the noise inside a box in a part the image that contains no emission. If the dirty image contains a noise level of 0.5 mJy, the task for half-cleaning looks like the following:

```
clean(vis           = 'galaxy.MS',
      imagename     = 'half_cleaned/galaxy_half_cleaned',
      mode          = 'channel',
      interpolation = 'nearest',
      start         = 10,
      nchan         = 50,
      width         = 1,
      threshold     = '2.5mJy',
      niter         = 100000
```

[12] `CASA` uses python indexes that usually start from zero.

```
    weighting     = 'natural',
    outframe      = 'BARY',
    veltype       = 'optical',
    imsize        = 1024,
    cell          = '1.5arcsec',
   )
```

Setting the parameters `outframe` (bary-centric) and `veltype` (optical velocity) helps avoiding inconstistence with other data. `niter` allows up to 100.000 iterations in every channel before stopping the task.

5.4 Masking with IDL

`CASA`'s clean algorithm can use boxes to limit the search for residuals, but only easy shape, such as rectangulars, circles and ellipses are supported. The mask should follow the emission smoothly and therefore another program must be used for masking. IDL has many possiblities to handle images, but cannot read `.image` files. The `CASA` task `exportfits()` allows to export the half-cleaned image as a `.fits` file.

```
exportfits(imagename = 'half_cleaned/galaxy_half_cleaned.image',
               fitsimage = 'half_cleaned/galaxy_half_cleaned.fits',
          )
```

In IDL the mask is produced via a script[13] with various options of controling the mask's shape.

```
sig_thresh = 2.5
nchan      = 3

growxy   40.
growz    1.
lox      270.
hix      750.
loy      250.
hiy      750.
loz      100000.
hiz      100000.
```

The most important parameter is `sig_thresh` that specifies the masking threshold in terms of the noise level σ. Pixels with flux values above this threshold are included in the initial mask, if this constraint is satisfied in a certain number `nchan` of consecutive

[13] Annahi Caldu (MPIA) provided this script since a three months bachelor thesis is too short to learn programming in IDL and working on a scientific task. Further scripts used in this masking script date back to Andreas Schruba (now NRAO).

channels. To prevent a frayed mask, the half-cleaned cube is smoothed, then pixels containing emission are identified and set to one in a preliminary mask that is otherwise containing zeros. The last step is growing the relevant areas in xy- (right ascension, declination) and z-direction (frequency). An additional constraint can be set by the `hi_` and `low_` parameters that define an outer boundary (in pixel coordinates) of the possible mask.
IDL writes a `.fits` image containing the mask that needs to be imported as `.image` using `CASA`'s image tool. Image data (right ascension, declination, polarisation, frequency) can be stored in different orders that `CASA` fails to reorder of necessary. Instead the user has to care for it with gratuitous scripts.

5.5 Cleaning

The `clean()` task in `CASA` provides many options to select data and manipulate the deconvolution process. The parameters used in section 6 are shown in the following example.

```
clean(vis           = 'galaxy.MS',
      imagename     = 'clean/galaxy_cleaned',
      mask          = 'masks/galaxy_mask.image',
      mode          = 'channel',
      interpolation = 'nearest',
      start         = 10,
      nchan         = 50,
      width         = 1,
      threshold     = '1.0mJy',
      niter         = 100000,
      weighting     = 'natural',
      imagermode    = '',
      psfmode       = 'hogbom',
      gain          = 0.1
      outframe      = 'BARY',
      veltype       = 'optical',
      imsize        = 1024,
      cell          = '1.5arcsec',
      pbcor         = False,
     )
```

In addition to the parameters explained before `imagermode` and `psfmode` are changed from their defaults to use the original Högbom `clean`. Primary beam correction (`pbcor`) will be done in another task at the end to obtain both images, corrected and uncorrected.

Multiscale cleaning is done by setting a list of scales (`multiscale`) and the necessary parameter `smallscalebias` described in section 4.8.3.

```
clean(vis             = 'galaxy.MS',
      imagename       = 'msclean/galaxy_mscleaned',
      mask            = 'masks/galaxy_mask.image',
      mode            = 'channel',
      interpolation   = 'nearest',
      start           = 10,
      nchan           = 50,
      width           = 1,
      threshold       = '1.0mJy',
      niter           = 100000,
      weighting       = 'natural',
      imagermode      = '',
      psfmode         = 'hogbom',
      multiscale      = [0,5,15,45],
      gain            = 0.2,
      smallscalebias = 0.6,
      outframe        = 'BARY',
      veltype         = 'optical',
      imsize          = 1024,
      cell            = '1.5arcsec',
      pbcor           = False
     )
```

Instead of preparing and starting the tasks by hand, various python scripts are used that define all necessary parameters and execute multiple task for different weightings or scale sizes.

5.6 Cleaning without mask

When compution time is not a crucial factor it is better to clean a whole cube without a mask. Outside the galaxy's emission only a few low-valued pixels reach above the threshold that will get cleaned with the effect of less addtionally cleaned flux. The maps will only slightly get better, but when cleaning to very low thresholds with increasing power.
For Clark's algorithm cleaning an unmasked image is no problem. The dirty beam is treated as being zero outside a cut-off and therefore can be handled as extending over all space. `Clean` and the Cotton-Schwab algorithm use a dirty beam to substract that ends at finite pixel positions 0 and 1023 for an `imsize` of 1024. When a residual peak in the lower left corner (0,0) is found, the dirty beam would reach only to the center and `clean`ing would have no effect for a large portion of the relevant part of the image (figure 14).
The largest possible subarea that is cleaned correctly is a centered box with side length of half of the respective side. `CASA` calls this "cleaning only the inner quarter of the image" when `psfmode = 'hogbom'` or `imagermode = 'csclean'` is specified and no mask is

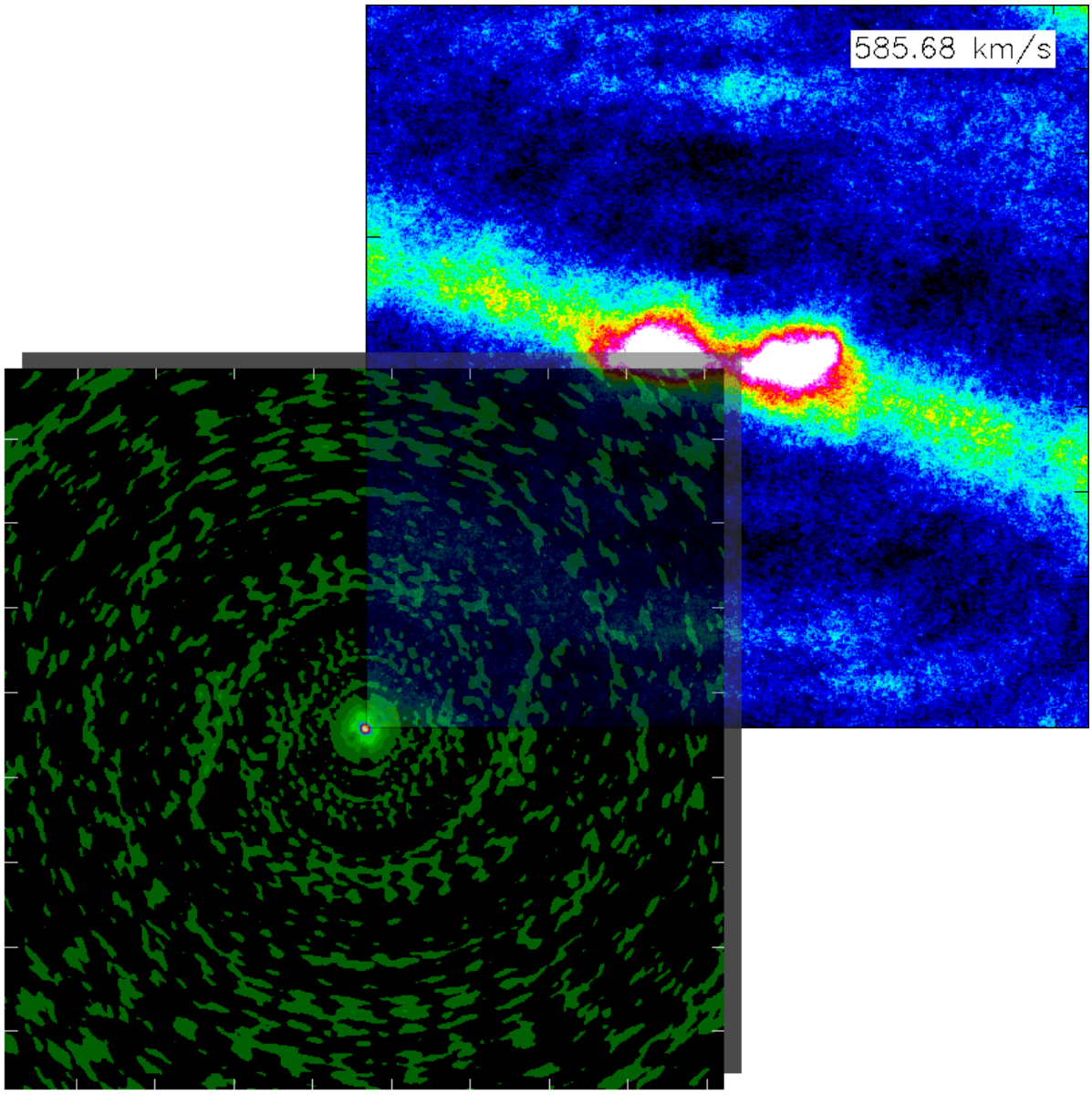

Figure 14: Cleaning a pixel at the lower left edge leaves too many pixels of the relevant central region untouched to receive a good result. The suddenly ending dirty beam imposes sharp edges in the residual image that complicate cleaning. Therefore only the inner quarter of an image gets cleaned where the dirty beam reaches far enough to cover the whole considered area.

used. Now `imsize` needs to be doubled in order to clean to whole area of interest with the disadvantage of an image four times as big as before that also scales up compution time.

5.7 Primary beam correction

Primary beam correction is done seperately by the task `impbcor()`. Beside input and output file name, a `pbimage` is needed that contains the primary beam.

```
impbcor(imagename = 'clean/galaxy_cleaned.image',
        pbimage   = 'clean/galaxy_cleaned.flux',
        outfile   = 'clean/galaxy_pb_corrected.image'
       )
```

5.8 Extracting fluxes

Altough `outframe = 'BARY'` is set to use bary-centric coordinates, positions in the cleaning model are parametrized in *Local Standard of Rest* (LSRK) coordinates. All remaining cubes including the mask use bary-centric reference. The `imstat()` task for image statistics cannot deal with files of different parametrization, which is why the mask needs to be regridded first.

```
imregrid(imagename = 'masks/galaxy_mask.image,
         template  = 'clean/galaxy_cleaned.model',
         output    = 'masks/galaxy_mask_LSRK.image',
        )
```

`imregrid()` is able to extract the desired coordinate system from a template file and regrid the mask to be saved in a new image.
The flux density inside a given mask can be calculated with the `imstat()` task. It logs image statistics for the whole image or a subset defined by a mask, the cubes axes, channels or boxes.

```
imstat(imagename = 'clean/galaxy_cleaned.image',
       axes      = [0,1],
       mask      = 'masks/galaxy_mask.image',
       logfile   = 'log.txt'
      )
```

The `axes` parameter defines over which axis the statistics should be calculated. In the used order of axes, 0 and 1 are right ascension and declination, thus `imstat()` prints statistics for each channel (axis 3).
In case of a `.model` file the correct regridded mask must be used.
Statistics of restored and residual image are measured in units of Jy per pixel as they depend on the dirty beam size. Model images only depend on the known clean beam and `CASA` can directly calculate the flux density when using `imstat()`. To compare all values, formula 4.33 is applied to receive flux densities for restored and residual image.

5.9 Moment maps

The task `immoments` calculates up to 11 moments of images. Integrated spectrum, velocity field and dispersion are the first three among them and can be computed in a single task:

```
immoments(imagename  = 'clean/galaxy_pb_corrected.image',
          moments    = [0,1,2],
          mask       = 'mask/galaxy_cleanmask.image'
          axis       = 'spectral',
          includepix = [0.001, 1.],
          outfile    = 'moments/galaxy_moment'
         )
```

The `axis` keyword specifies the axis to integrate over whereas `mask` and `includepix` allow setting additional contraints. The mask works as in `clean()` and blanks unwanted areas. `[0.001, 1]` stands for the flux range in Jy that is considered in the calculation with all pixels being set to 'blank' when not matching this intervall. The output files are furnished with appendices `.integrated`, `.weighted_coord` and `.weighted_dispersion_coord` according to moment 0, 1 and 2.

5.10 Obtaining radial profiles with GIPSY

Using many different programs has the disadvantage of having to import data to special formats. As GIPSY cannot read `CASA` images, the respective files must be exported to `.fits` and re-imported.

```
exportfits(imagename='moments/galaxy.integrated',
           fitsimage='moments/galaxy.integrated.fits',
          )
```

GIPSY stores image data and header information in two seperate files with extensions `.image .descr`. The import task is named `rfits`:

```
RFITS FITSFILE = moments/galaxy.integrated.fits
      OUTSET   = radial_profiles/galaxy
      FREQ0    = 1420405752.000000
```

For collapsed data sets the frequency does not play a role, but must be given for the task to run. The actual work is done by `ellint`. This task fits ellipses the a given image and calculates several quantities.

```
ELLINT INSET    = radial_profiles/galaxy f
       OPTION   = 1
       RADII    = 0,10,20,30,40,50
       WIDTH    = 10
```

```
PA       = 90
INCL     = 45
SEGMENTS = 0,360
POS      = 0,0
SUBPIX   = 2
MEDIAN   = Y
FILENAME = radial_profiles/galaxy.log
FORMAT   = ffffff.fff
```

The given set `galaxy` still consist of three dimensions as `CASA` collapses all spectral planes into a single one. Therefore, GIPSY must know in which plane the ellipses should be applied by adding `f` (frequency) to the file name. The `OPTION` parameter determines which quantities are calculated: basic information like sum, mean and median (`OPTION=1`), surface brightness (`2`) or surface density (`3`). `RADII` and `WIDTH` define a ring that is inclined by `INCL` degrees and rotated according to the position angle `PA` to fit the galaxy. The ellipse ring constructed this way, it centered at the position `POS`. In contrast to `CASA` and IDL, GIPSY uses pixel coordinates from -512 to 511, so the galaxy's center coincides with the image center (0,0). Not all measurements centered the primary beam perfectly on the galaxy leading to little (up to 20 pixels) offsets in `POS` for some galaxies. The obligatory parameter `SEGMENTS` is not needed for this analysis and thus is set to the whole ring from 0 to 360°. All results are writen to the log file `galaxy.log` using float numbers with three decimals.

6 Data analysis

6.1 Clean algorithms

6.1.1 Imaging behaviour

In theory, the different point source cleaning procedures appear to be quite similar, but the restored images differ significantly as figure 15 shows using the example of NGC5055. Tp reduce computing time and show the effects of sidelobes, only the masked region inside the white line was cleaned.
Högbom's algorithm produces a clearly visible galaxy structure with high intensities (white color) at the inner part. The large negative (blue) bowls at the lower part of the image disturb the noise around NGC5055 and cannot be a physical fact, but are inserted by the algorithm.
The central parts modeled by Clark clean are very similar to that of Högbom, but three strong negative bowls ruin the image. Around the lowest masked region clean actively dug into the image as the values are much lower than in the uncleaned map in figure 15a. The triangular arrangement indicate that this is a remaining effect of the sidelobes that pile up to a hexagonal shape. The bad result of Clark's algorithm originates in the attempt to reduce computing effort by cutting of sidelobes at a certain distance. For dirty beams with weak sidelobes this simplification is valid, but the complex dirty beam of THINGS measurements must be taken completely.
Apparently the best result is given by the procedure of Cotton and Schwab. The negative bowls are completely gone and the noise is uniform on a scale of about 15″ (one scale spacing). In principle Cotton-Schwab clean uses the same line of action as Högbom but performs on visibilty data instead of the image. This means the full dirty beam is used and additionally aliasing can be avoided.
Difference images (fig. 16) show the deviation between Clark/Cotton-Schwab and Högbom. Högbom and Cotton-Schwab only differ in treating the emission: The galaxy's shape is clearly visible above a widely uniform background. Interesting is the dark blue (negative) pattern that appears from sources found by Högbom clean but not by Cotton-Schwab. The circular patterns centered on the dark blue regions is another result of that fact and different domains in which the substractions are performed.
Figure 16b demonstrates that Clark clean totally messes up the image. Not only the negative interferometer pattern deviates heavily from the Högbom result, but also in between areas of anomalous increased flux appear. Therefore, Clark clean cannot be used for analyses of THINGS data.

6.1.2 Convergance behaviour

As well as the imaging succes, the divergence behaviour differs drastically. Högbom clean is conceptionally easy and uses the whole dirty beam in the process leading to a good convergance behaviour on THINGS data. If the cleaning threshold is set to appropriate values, meaning a minimum of $\sim 2.5\sigma$, every clean task converges. Below 2.5σ too many noise spikes have to be cleaned with the result of `clean()` getting stuck in a cycle. The

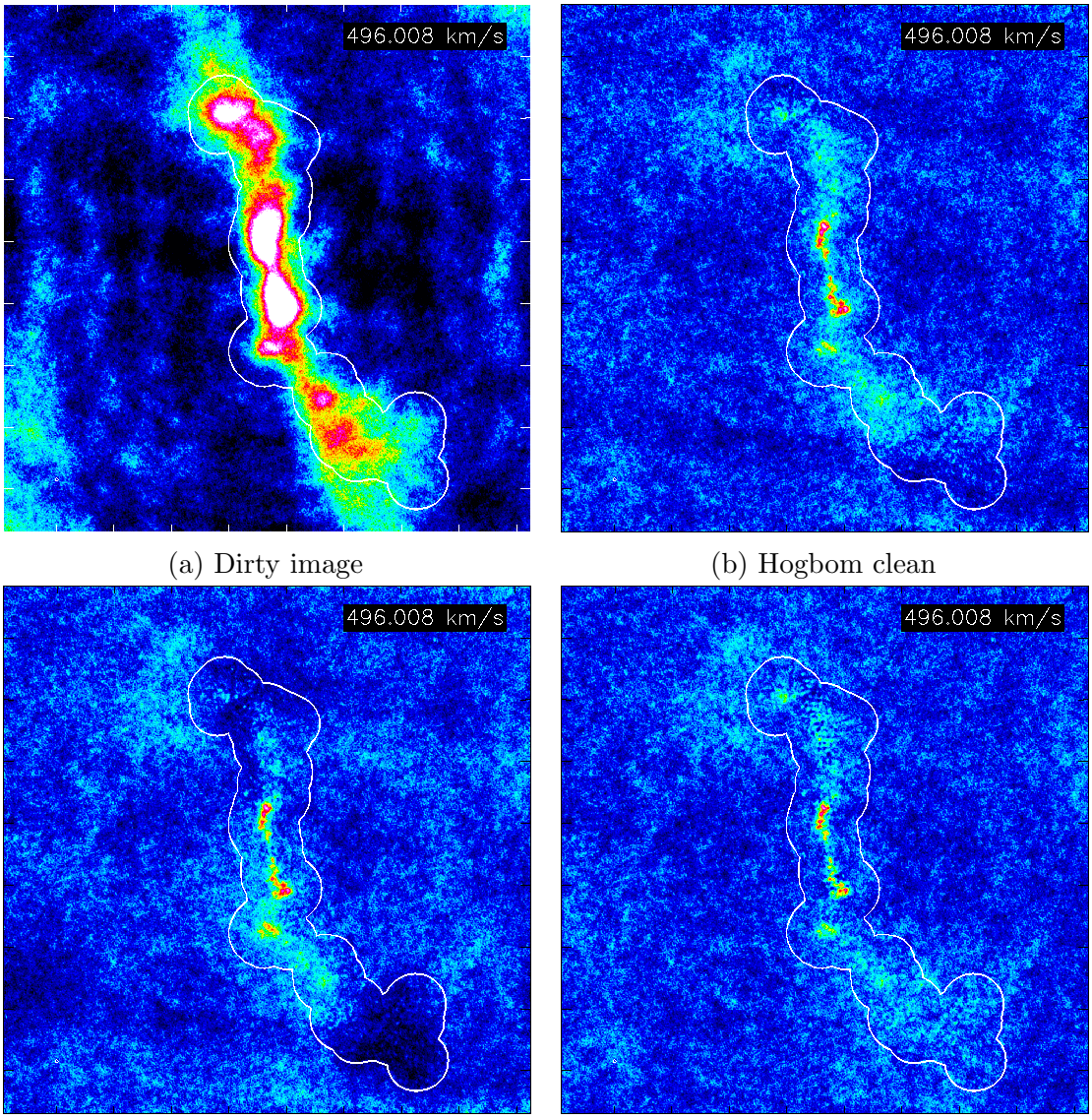

(a) Dirty image

(b) Hogbom clean

(c) Clark clean

(d) Cotton-Schwab clean

Figure 15: These images show a channel of NGC5055 at a velocity of nearly 500 km/s. Högbom and Cotton-Schwab algorithm result in similar maps, whereas Clark clean differs strongly. The color map ranges from -2 (black) to 8 mJy/beam (white).

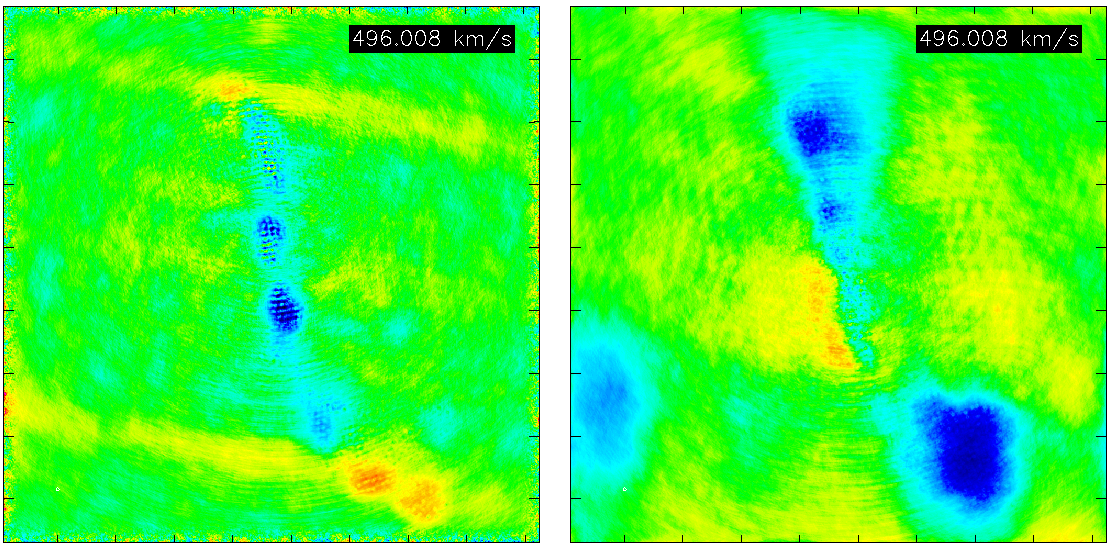

(a) Cotton-Schwab minus Hogbom (b) Clark minus Hogbom

Figure 16: Difference image emphasize the discrepance between the cleaning algorithms. On the left the image of NGC5055 produced by a Högbom clean was substracted from a Clark clean image. The right image shows the difference of Cotton-Schwab and Högbom's algorithm. The color ranges map from -2 (black) to 2 mJy/beam (white).

sidelobes of a substracted beam reduce surounding residuals to fall below the negative value of the threshold. Instead of reaching the threshold, the process jumps between cleaning of negative and positive flux.
Clark clean converges in most cases, but not as often as `clean`. Due to the bad imaging results it cannot be used anyway and convergance does not play a major role.
The poorest characteristics offers the Cotton-Schwab algorithm. Even cleaning with a threshold of 2.5σ is enough to diverge.

6.2 Finding an optimum robust parameter

The different weighting schemes described in section 4.6 have great influence on the resulting dirty beam and image. This variety is needed because of the diverse demands of measurements. Beside natural weighted, all images are produced with robust weighting as it offers a compromise between high signal-to-noise and high resolution. The disadvantage of Brigg's method is the introduction of robust parameter that cannot be determined in advance but must be calculated for every measurement individually.
Figure 17 shows a plot of root mean square (rms) in a region free of emission and beamsize against the robust parameter. The rms of the noise was measured using a rectangular box in CASAviewer. As Beamsize the major axes of the restored (clean) beam can be printed with `CASA`'s image tool (ia.) and the task `ia.restoringbeam`. In this case NGC3184 was used, but other galaxies show the same behaviour of flat signal-to-noise and beam size for high and low robust values. The interesting part is the range between -0.5 and 1, where the beam size grows and noise decreases towards higher robustness. An optimum is achieved around 0 to 0.5, but the choice is not too crucial. When in the following chapters robust weighting is mentioned, a robustness of 0.5 is meant if not stated otherwise. The differences between the three considered galaxies is very little which is why a common parameter can be used.

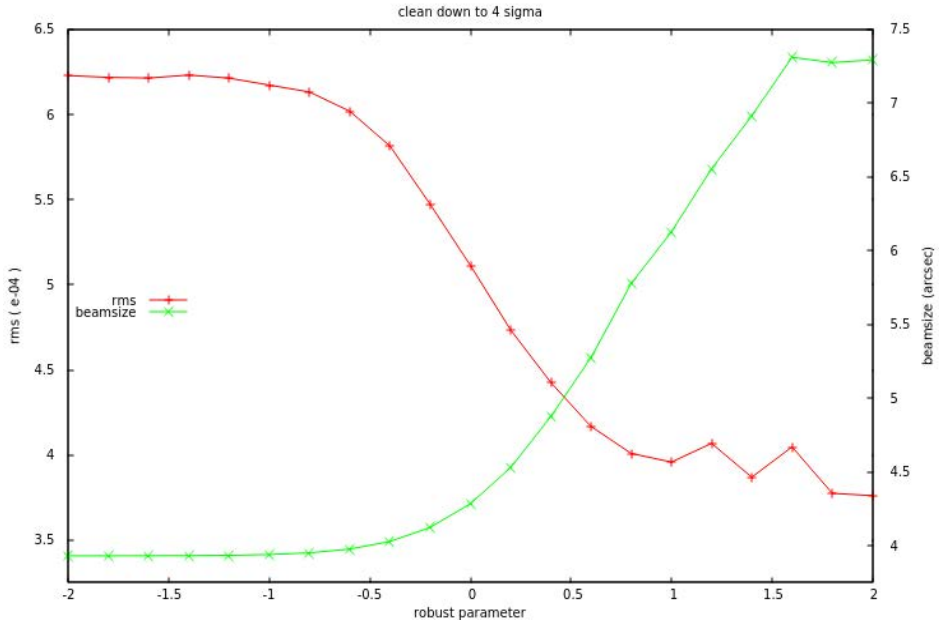

Figure 17: When `cleaning` an image of NGC3184 down to 4σ, the theoretically expected behaviour of noise (rms) and beam size can be observed: A higher robustness parameter leads to lower noise, but a greater beam.

6.3 Scales used in multi-scale clean

In theory, the choice of scales is not crucial when using multi-scale clean. Computation time and convergance, however, depend on the scale. If a larger number of scales is defined, the effort of finding the best one for substracting is increased for every one of the several thousand iterations. Hence, computation time can easily be doubled by choosing a too large set of scales. On the other hand, to few scales represent a coarse model that can lead to poor convergence. Msclean's convergance behaviour is much better than for the point-source clean algorithms. As it is easy to produces non-converging `clean`s by setting improper parameters, all of the multi-scale cleans done during the analysis were converging.
For faster computation the basic distinction between arithmetic and geometric progression and the number of scales needed for good imaging result are done using a mask. The results gained on channel 71 (571.065 km/s) of the THINGS data of NGC3184 can be applied to NGC5055 and NGC2403 as well.
Figure 18 shows the centered galaxy in the model images for arithmetic and geometric progression as well as two sequences in between. All images were cleaned to 2.5σ which is 0.97 mJy using natural weighting or 1.10 mJy for robust and a gain factor of 2.5.
Not only visually, but also in terms of cleaned flux, there is very little difference between detailed and coarse scale selection. The values of table 1 were measured inside the mask that was used for cleaning.

weight	cleaning threshold [mJy]	scale	residual flux [mJy]	model flux [mJy]	image flux [mJy]
natural	0.97	0, 5, 10, ..., 45	0.30	0.75	1.06
natural	0.97	0, 5, 10, 20, 30, 45	0.37	0.75	1.11
natural	0.97	0, 5, 10, 20, 40	0.31	0.75	1.06
natural	0.97	0, 5, 15, 45	0.29	0.75	1.04
robust	1.10	0, 5, 10, ..., 45	0.21	0.68	0.89
robust	1.10	0, 5, 10, 20, 30, 45	0.25	0.68	0.91
robust	1.10	0, 5, 10, 20, 40	0.20	0.68	0.88
robust	1.10	0, 5, 15, 45	0.20	0.68	0.88

Table 1: Residual, modeled and restored flux inside the cleanmask of NGC3184. The modeled flux is independent of the choosen scale that only slightly affects the residuals and therefore the total restored flux of the image.

The modeled flux is suprisingly stable when changing the scales: 0.75 mJy for natural weighting and 0.68 mJy in case of robust weighting. The residuals show little deviation, but remain in agreement to each other except for 0, 5, 10, 20, 30, 45. For both weighting schemes, the residual are significantly higher than in the other cases, although the difference in scale to 0, 5, 10, ..., 45 and 0, 5, 10, 20, 40 is very little. Compared to the arithmetic sequence only some scales in between are missing, but they are not defined in 0, 5, 10, 20, 40 either. To determine the correct source of this effect, further examination

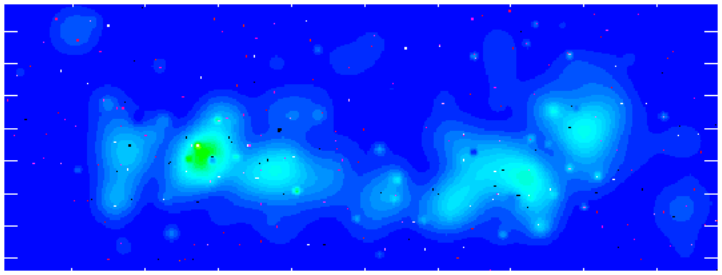

(a) scales: 0, 5, 10, 15, 20, 25, 30, 35, 40, 45 pixels

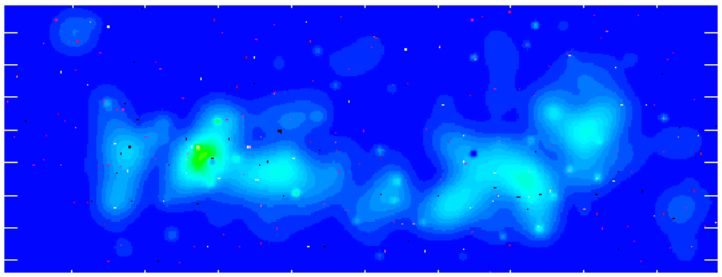

(b) scales: 0, 5, 10, 20, 30, 45 pixels

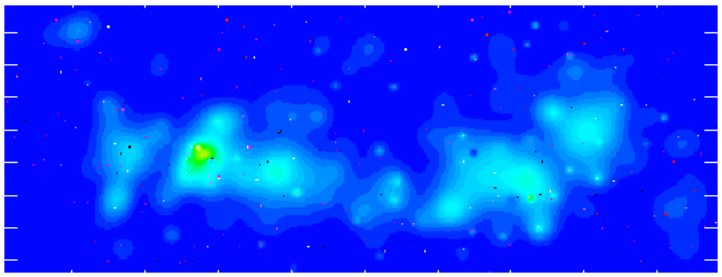

(c) scales: 0, 5, 10, 20, 40, 45 pixels

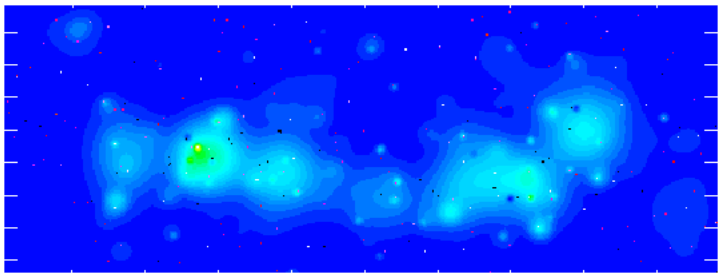

(d) scales: 0, 5, 15, 45 pixels

Figure 18: The emission modeled by msclean does not depend crucially on the choosen scales. The imgaing difference between ten arithmetically arranged scaled and four geometric values is very little. Computation, however, is much faster in the latter case. (Color range from -0.2 to 0.6 mJy/pixel)

would be needed, but this set uses more scales than necessary so it will not be used anyway.
The best option so far is setting the scale parameter to 0, 5, 15, 45. Setting more scales does not improve the image's quality, nor the modeled flux, but consumes considerably more time for imaging.

In theory, the largest scale should be approximately as big as the largest structure in the galaxy, but setting even larger options should not be a problem because clean chooses smaller ones that fit better. From the dirty image a maximum scale of $\sim$50 pixels can be expected as this is roughly the dimension in y-direction (declination). The images in figure 19 show that the theoretical assumption is not fully correct. The small scales such as 0, 2, 4, 8 are not sufficient to model extended emission resulting in an image similar to the ones of Högbom clean. The differences between the other four scale sets are less noticable in the print-out. 0, 3, 9, 27, 75 has a slightly greener background color which stands for higher values of the modeled flux. The reason is the large scale of 75 pixels that is great enough to be used by `CASA` to model noise peaks and the lower noise around. For smaller values like 45 and 64 the wings of the clean beam are too small to cover sufficient portions of the background and only point sources of scale 0 are used to model noise spikes. In image 19d the scale 64 generates a large shape around the galaxy that isn't present in figure 19b and 19c. A maximum scale of 27 pixels (19b) seems to be the best option because it provides the most detailed contours without the vast emission around.
All these images were produced using the default small scale bias of 0.6. With a higher bias towards smaller scales it should be possible to image noise peaks with point sources reducing the background shape without losing the ability to model large structures inside the galaxy. This is a task for further testing that could not be done in a short bachelor thesis.
As before, the flux inside the cleanmask is shown in table 2. In contrast to the number of scales, the fluxes show a strong dependence on the large scale that is used in cleaning. When increasing the largest scale, the residuals drop extremly. The residual images contain mostly noise and some leftover of the cleaning process (see Appendix A). Of corse, a larger scale cleans more flux around the found peaks than a smaller scale leading to higher recovered fluxes and lower residuals. The highest signal (image) to noise (residual) is given for the largest maximum scale of 75, but at the price of background emission in the model images. The visually best option was 0, 3, 9, 27 pixels that now turns out to be not suitable when measuring the flux. Therefore, a scale set of 0, 5, 15 and 45 pixels offers the best compromise and will be used for all further multi-scale cleaning.

The THINGS data sets of NGC3184 and NGC5055 are analysed as images of $1024 \cdot 1024$ pixel with a resolution of $1.5''$ per pixel whereas NGC 2403 uses 2048 pixels and $1.0''$ per pixel. A geometric sequence with factor 3 turned out to be a good choice and is thus used for NGC2403 as well, but expanded with an element of 135 pixels.

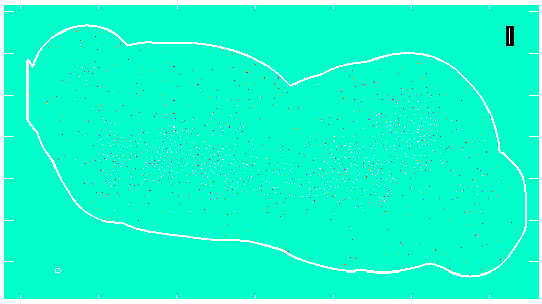

(a) scales: 0, 2, 4, 8 pixels

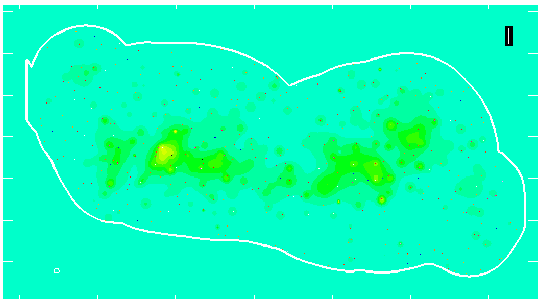

(b) scales: 0, 3, 9, 27 pixels

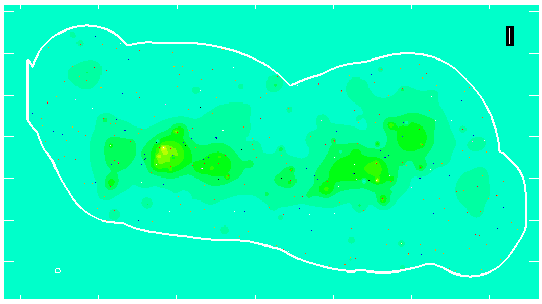

(c) scales: 0, 5, 15 ,45 pixels

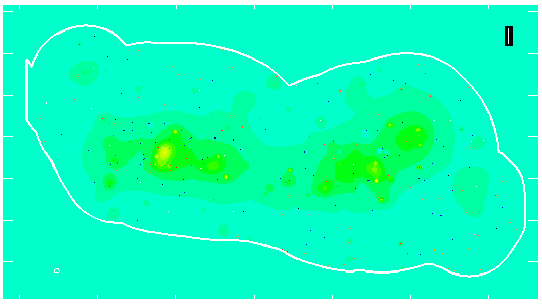

(d) scales: 0, 4, 16, 64 pixels

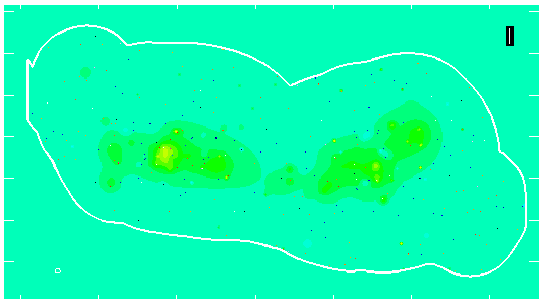

(e) scales: 0, 3, 9, 27, 75 pixels

Figure 19: The small scales of figure 19a are obviously to small to receive an adequate restored image. The large scales like 64 and 75 are too big to image the detailed shape of the emission of NGC3184 and result in large areas of low flux around the galaxy. (Color range from -0.4 to 0.5 mJy/pixel)

weight	cleaning threshold [mJy]	scale	residual flux [mJy]	model flux [mJy]	image flux [mJy]
natural	0.97	0, 2, 4, 8	1.01	0.70	1.71
		0, 3, 9, 27	0.58	0.73	1.32
		0, 5, 15, 45	0.30	0.75	1.06
		0, 4, 16, 64	0.17	0.76	0.93
		0, 3, 9, 27, 75	0.12	0.77	0.89
robust	1.10	0, 2, 4, 8	0.95	0.35	1.30
		0, 3, 9, 27	0.44	0.58	1.02
		0, 5, 15, 45	0.21	0.68	0.89
		0, 4, 16, 64	0.09	0.73	0.89
		0, 3, 9, 27, 75	0.06	0.75	0.80

Table 2: The largest scale determines the residual level with lower values towards greater scales. The modeled flux does not vary that strong, but increases with scale. Large scales cover much of the underlying noise and therefore reduce the residuals.

6.4 Collapsing method for moments maps

`CASA` offers two methods of blanking unwanted pixels while collapsing images to moment maps. Beside a mask, an intervall can be set to ignore certain values. To account only for significant emission and ignoring noise, a threshold of 3σ is set or the mask produced during the clean process is used. Primary beam correction is applied before to receive correct results. Figure 20 shows an overview of the three important moments 0, 1 and 2 for both constraints individually and a combination.
When only the 3σ threshold is used, the other regions amplified by primary beam correction remain part of the final image. As these areas contain mostly noise, the galaxy is superposed by a frame of noise that can be cut out by using the cleanmask. The mask includes not only emission, but few areas of noise, too, because a grow factor enlarges the initial mask that directly follows emission. Hence, the best solution for a maximum of visible details is the application of both constraints to include only significant emission in cleaned areas.

moment 0

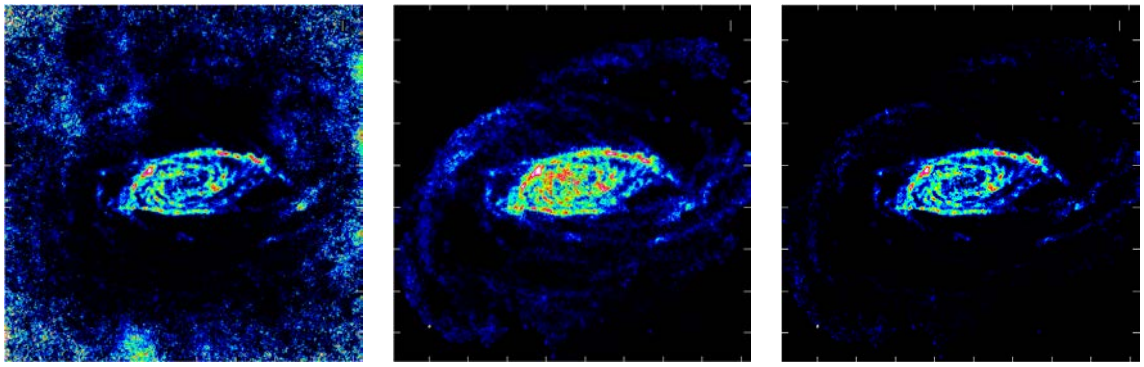

(a) threshold (b) cleanmask (c) cleanmask and threshold

moment 1

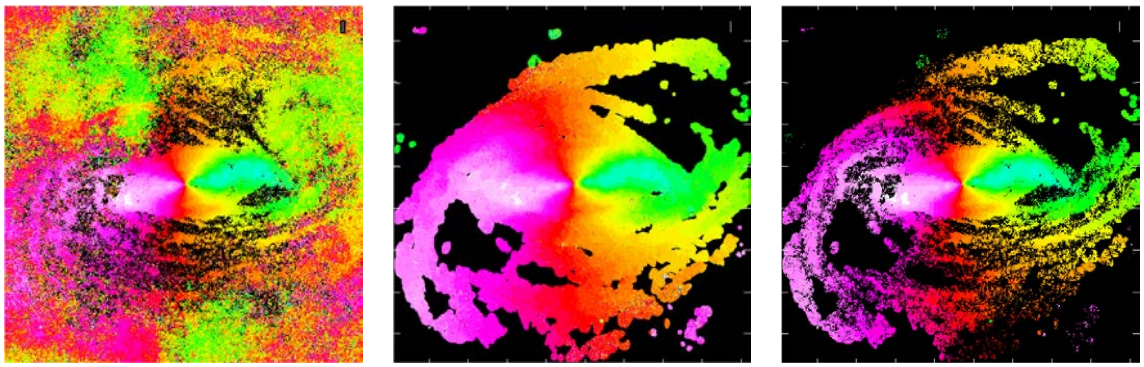

(d) threshold (e) cleanmask (f) cleanmask and threshold

moment 2

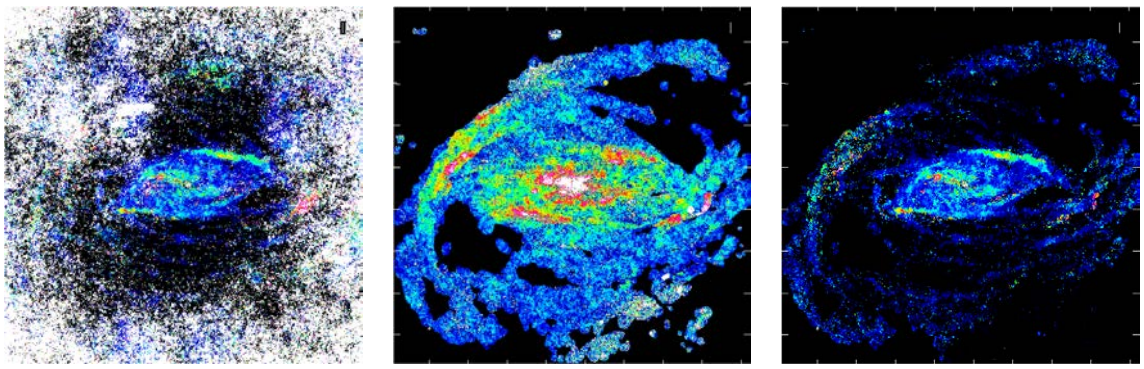

(g) threshold (h) cleanmask (i) cleanmask and threshold

Figure 20: NGC5055, multi-scale clean, natural, color ranges are given by -0.02 to 0.2 Jy/beam km/s (moment 0), 0 to 700 km/s (moment 1) and 0 to 30 km/s (moment 2).

6.5 Comparing `clean` to multi-scale clean

Classical Högbom `clean` and multi-scale clean can be compared in various way emphasizing on the process of imaging or physical properties. The superiority of msclean in imaging with better convergeance behaviour and at least in some cases faster computation was already mentioned. The following section focuses on the scientific characteristics that are affected by cleaning. To be sure that the choosen galaxy does not affect the result, the analyses was carried out for three galaxies whereof one is presented in each section. Regardless of this, the mentioned conclusion apply for all of them and supposably for at least all THINGS galaxies.

6.5.1 Flux density

The first physical quantity that is determined directly from the image is the flux density in Jy/beam. To compare the values that `CASA` outputs, they are converted to flux density in Jy according to formula 4.33.
Table 3 contains the result of various cleans of channel 71 (571.065 km/s) of NGC3184 that allow to identify differing and common characteristics. For both weighting schemes the data set was cleaned down to thresholds of 1.5 to 4.0σ with a noise level of approximately 0.40 mJy measured in a line free channel. Of each output image (residual, model and restored) the flux density measured inside the cleanmask is given in Jansky. For further evaluation, the values of the original THINGS analyses with AIPS clean are given as well.
The first three rows already point out the difficulties that `clean` experiences when using low thresholds: Cleans are not converging and produces wrong flux densities. The other natural `clean`s may be incorrect, too, because of the volatile values. The corresponding images show a strange pattern in the residuals that was caused by clean getting stuck in the blue areas. The respective pixels were cleaned multiple times with negative fluxes over the course of iterations before the threshold was reached.
All multi-scale and the robust Högbom cleans show the expected behaviour of increasing restored flux with increased threshold. The more emission gets cleaned, the less remains in the restored image because of the removed sidelobes of the dirty beam. Similarly, the portion of residual flux in the restored image grows. According to the different beam sizes, modeled flux is declining less than residual flux is rising which is why cleaning to low thresholds is favourable.
Irrespective of cleaning threshold, multi-scale clean cleans more flux resulting in higher model values and less residual. As a consequence, the restored flux is on a lower level if compared to the respective `clean` fluxes. This advantage of high cleaning efficiency can also be seen in the channel maps, such as in figure 22.
Beside absolute values, the distribution of flux is a feature that differentiates between `clean` and multi-scale clean. The deeper the clean, the more obvious the differences get. The ansatz to model extended emission with extended sources in msclean leads to a model that seems to be a better approximation of the real sources. Instead of many point sources on an otherwise empty background, the multi-scale approach find point sources,

natural weighting

method	threshold [mJy]	threshold σ	flux [Jy] residual	flux [Jy] model	flux [Jy] restored	comment
CASA clean	0.6	1.5	1.	0.68	2.07	not converging
	0.8	2.0	1.19	0.68	2.07	not converging
	1.0	2.5	1.19	0.68	2.07	not converging
	1.2	3.0	-0.02	0.78	0.75	
	1.4	3.5	0.36	0.74	1.17	
	1.6	4.0	0.06	0.77	0.84	
CASA msclean	0.6	1.5	0.03	0.78	0.81	
	0.8	2.0	0.12	0.77	0.90	
	1.0	2.5	0.29	0.75	1.08	
	1.2	3.0	0.51	0.73	1.33	
	1.4	3.5	0.71	0.71	1.54	
	1.6	4.0	0.88	0.69	1.73	
THINGS normal	0.97	2.5			1.62	
THINGS rescaled	0.97	2.5			0.73	

robust weighting

method	threshold [mJy]	threshold σ	flux [Jy] residual	flux [Jy] model	flux [Jy] restored	comment
CASA clean	0.6	1.5	0.17	0.69	0.88	
	0.8	2.0	0.23	0.65	0.92	
	1.0	2.5	0.49	0.52	1.09	
	1.2	3.0	0.75	0.38	1.27	
	1.4	3.5	0.89	0.28	1.40	
	1.6	4.0	1.11	0.20	1.50	
CASA msclean	0.6	1.5	0.03	0.76	0.79	
	0.8	2.0	0.07	0.74	0.82	
	1.0	2.5	0.14	0.70	0.86	
	1.2	3.0	0.21	0.66	0.91	
	1.4	3.5	0.28	0.63	0.95	
	1.6	4.0	0.33	0.60	0.99	
THINGS normal	1.1	2.5			1.62	
THINGS rescaled	1.1	2.5			0.73	

Table 3: The flux densities of channel 71 of NGC3184 measured inside the mask that was used for cleaning. The noise σ in a line free channel is approx. 0.40 mJy leading to cleaning thresholds of 0.6 to 1.6 mJy in steps of 0.5σ. The cleaned THINGS data consists merely of restored images that were produced using the given thresholds in AIPS clean.

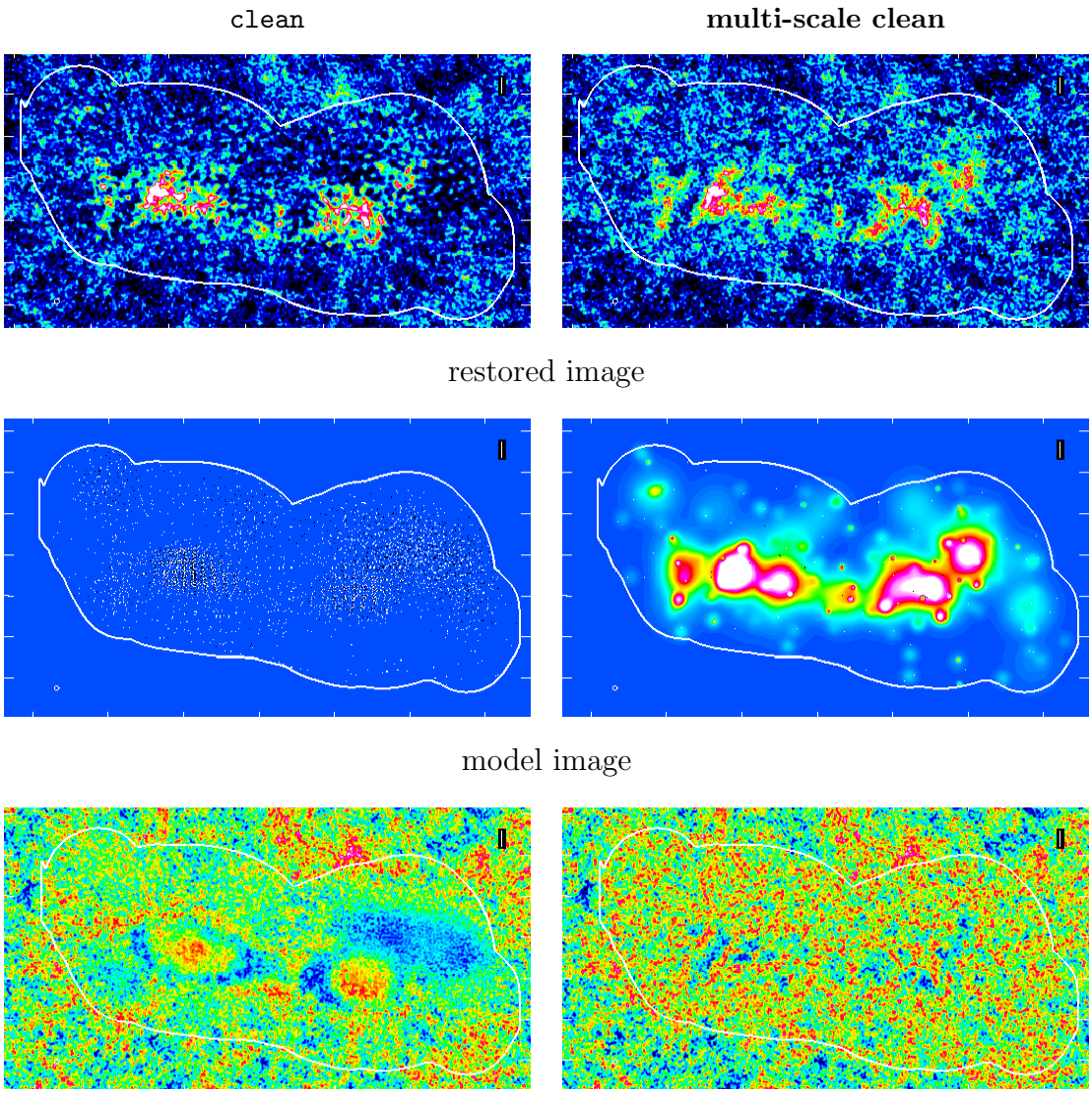

Figure 21: Restored, model and residual image of NGC3184 cleaned with `clean` and multi-scale clean down to a threshold of 1.2 mJy and natural weighting. The colors are coded as -0.5 to 2.5 mJy/beam (restored image), -0.02 to 0.05 mJy/beam (model) and -1.5 to 1.5 mJy/beam (residual).

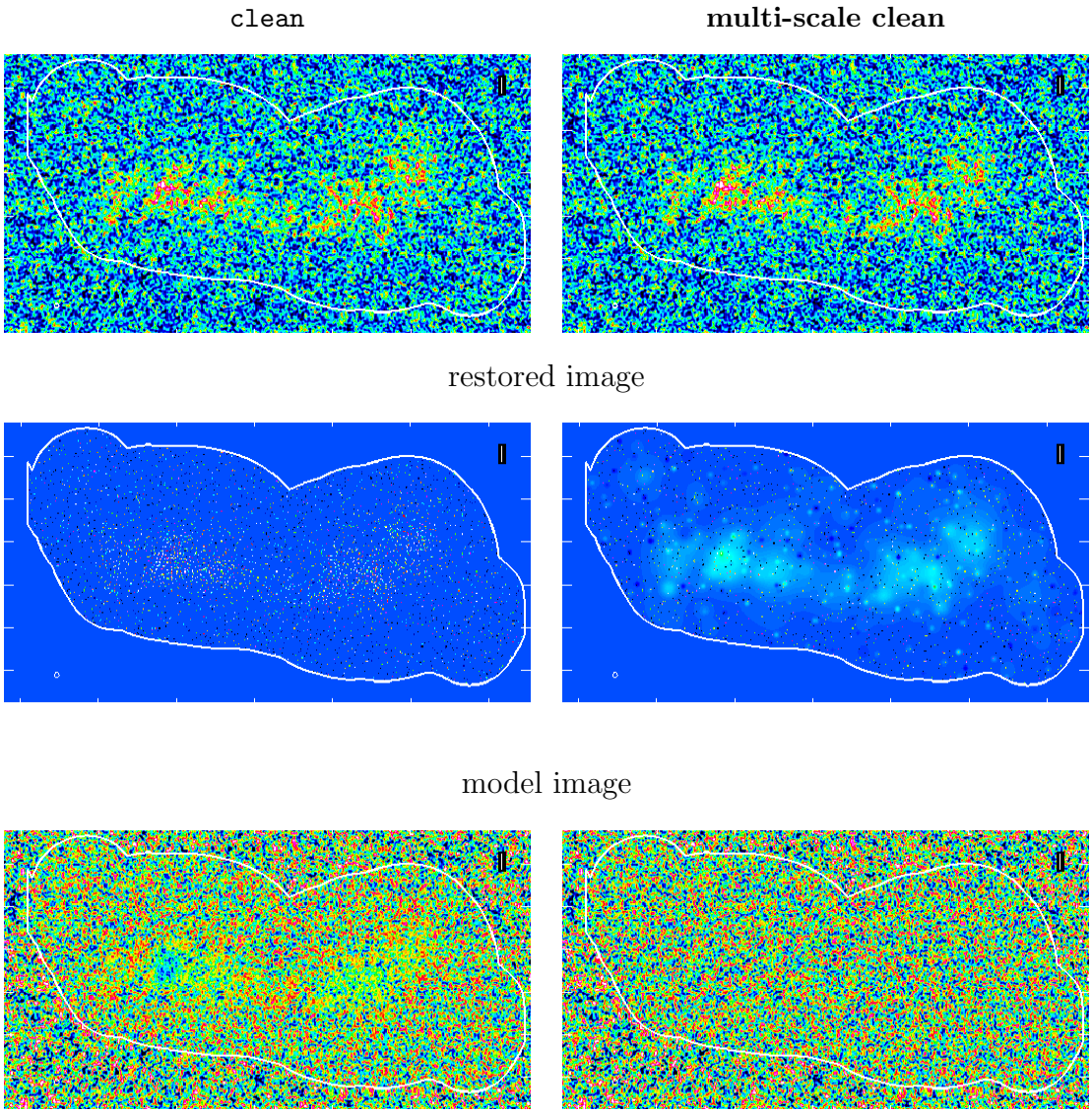

Figure 22: Restored, model and residual image of NGC3184 cleaned with `clean` and multi-scale clean down to a threshold of 1.2 mJy and robust weighting. The colors are coded as -1 to 2 mJy/beam (restored image), -0.2 to 0.5 mJy/beam (model) and -1 to 1 mJy/beam (residual).

too, but on a basis of extended emission throughout the galaxy. In the attempt to model extended emission by point sources, `clean` overshoots the goal and creates a negative hole in areas with much cleaned flux. Msclean, however, leaves homogenous residuals that do not differ significantly from the surrounding noise. Despite the these differences, the restored images appear almost identically, because all emission that was not cleaned or "overcleaned" remains in the residuals and gets added back to the model. So, multi-scale clean provides a similar restored image, but with a physically more plausible ditribution among the components model and residual.

6.5.2 Rescaling

As could be seen in the previous section (6.5.1) for NGC3184, multi-scale clean leads to considerably lower residuals and a higher amount of cleaned flux. Especially for the commonly used threshold of 2.5σ and above, rescaling is nevertheless necessary as residuals can account for a third or more (for natural weighting) of the total restored flux. Only for very deep multi-scale cleans down to 1.5 times the noise level, residual scaling can be neglected as is shown in section 6.6.
The scaling parameter ϵ is determined as described in section 4.9 by measuring the flux inside a square centered on the dirty beam. Since the dirty beam solely depends on the interferometer, but not the used cleaning technique, a common factor can be used for `clean` and msclean assuming identical clean beam sizes. Of corse, both clean beams do not have the same size because in multi-scale cleaning there isn't just one clean beam, but four, one for each used scale of 0, 5, 15 and 45. The mathematically correct solution to this problem is complicated. Should an simple average beam be used or the weighted average according to the distribution of used scales or different approach? Probably, it is oversimplified to use the `clean` scaling factor for msclean as well, but at least for the small scales of 5 and 15 pixel, the differences in beam size are not too great. The consequence is an underestimation of the residuals in rescaled multi-scale clean images.

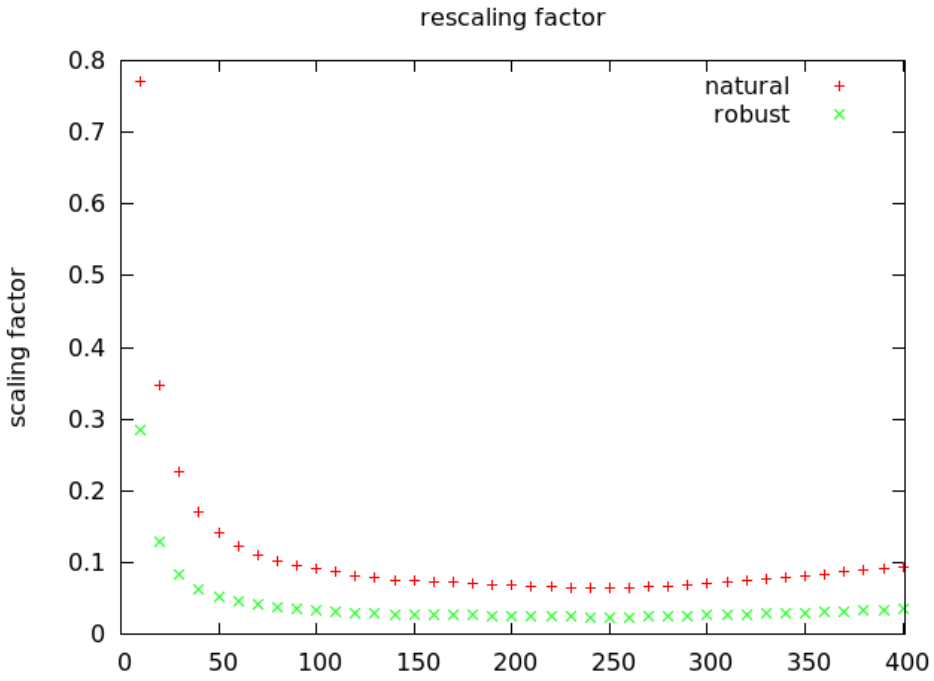

Figure 23: The resclaing factor depends on the size of the square inside which the beam area is measured. For boxes greater than ∼100 pixels the asymptotic values of 0.10 (natural weighting) and 0.045 (robust weighting) are reached.

Figure 23 shows the factor's dependence on the side length of the square for NGC5055. After a steep decline, the factor asymptotically approaches a value of 0.10 (natural weighting) and 0.045 (robust weighting).
In case of a naturally weighted dirty beam, ϵ starts to increases again around 275 pixels side length due to complex shape of the dirty beam. Remind that the integral over the dirty beam is zero, so it must have negative values outside the central peak and its sidelobes. Therefore, dirty beam size reaches a maximum and decreases again when expanding measurement range (square) and as a consequence the scale factor increases. The typical width of a masked and cleaned region of emission is around 100 to 200 pixels which is in the "flat" zone of approximately constant ϵ resulting in correct fluxes.
The normal (unrescaled), not primary beam corrected images of NGC5055 show that the masking was not done perfectly as it does not contain low level emission at the upper and lower end of the galaxy.

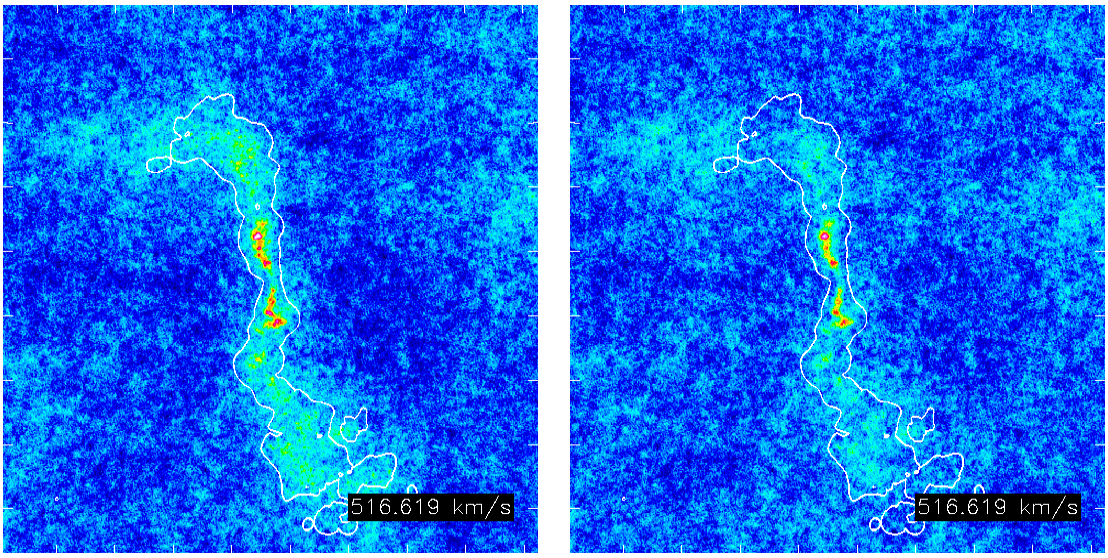

(a) Högbom clean (b) multi-scale clean

Figure 24: The unrescaled (normal) maps of channel 40 of NGC5055 show the qualitativ difference between `clean` and multi-scale clean. Inside the cleanmask that is given by a white contour, the restored images feature differing backgrounds around the emission. The color ranges from -2.5 to 6 mJy/beam.

After scaling the residuals, `clean`'s difficulties in modeling extended emission become clearly visible. Thousands of point sources add up to a sea of emission, but the galaxy's main structure in the center cannot be seen anymore suggesting it is stored in the residual image. Multi-scale clean does not have these problems. The visual main properties remain the same when applying the scaling factor. The cleaned area even fits the noise around leaving little difference between cleaned and uncleaned regions with reservation due to above underestimation.
To be safe in the interpretation a comparison of normal multi-scale clean and rescaled/

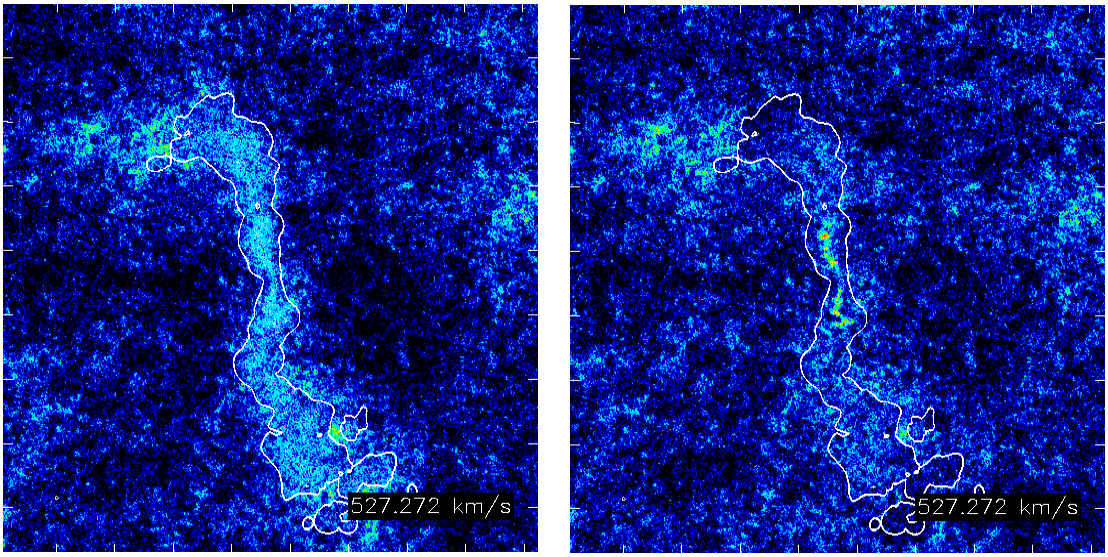

(a) Högbom clean (b) multi-scale clean

Figure 25: After rescaling the different abilities to clean extended emission become clearly visible. For the classical clean algorithm, the rescaled residuals are still significantly higher than in the uncleaned area surrounding the emission. The rescaled multi-scale cleaned image, however, shows no qualitative difference of cleaned areas and noise. Only the restored emission remains above a noise-like background. From black over blue and red to white the color ranges from -0.05 to 0.3 mJy/beam.

unscaled `clean` can be made. Even without rescaling msclean seems to work better in modeling the expexted true brightness distribution with respect to noise properties and distribution of the cleaned flux.
Beside visual differences, a comparison of fluxes of residual, model and restored image is important to decide about the advantages and abilities of msclean. Sadly, a three months bachelor thesis is too short and this task could not be finished in time.

6.5.3 Spectra

The cleaning properties concerning flux density of `clean` and msclean found in section 6.5.1 were shown only for a single channel. Spectra offer the possibility of assuring that those qualities apply to the other spectral channels as well.
The following figures 26, and 27 contain the spectra of NGC2403 made from restored and model image each for natural and robust weighting using a threshold of 2.5σ. The used channel maps were not primary beam corrected, nor residual scaled as this is not necessary for comparison. Besides, the same applies to the published THINGS cubes that are the current reference for these data sets. The THINGS spectra were produced with the same mask that was used in my analysis to work as an additional comparison to test the quality of `clean` and multi-scale clean.
Since the image flux densities are not directly comparable due to different levels of residuals, figure 27 shows the spectra of model fluxes. Rescaled cubes contain residuals on a very low level, hence the measured flux is dominated by the model and the rescaled THINGS cubes are comparable to the model cubes, but keeping in mind that they do not have the same physical meaning.
The natural image spectra in figure 26 confirm the conclusions of section 6.5.1: All cleaning methods follow the same characteristics, but on differing levels. `Clean`'s restored image contains the highest amount of flux because of high residuals. It's model flux is only about 0.1 mJy below that of msclean which lies $\sim$0.3 mJy above the values of THINGS rescaled. This suggest correct modeling of both algorithm with strongly differing residual properties.
In case of robust weighting, `clean` works less efficiently producing less cleaned flux in the model image and therefore lower values in the restored image. The residuals remain at about 3 mJy. Interestingly, this behaviour comes up for all three analysed galaxies. The reason can be found in the fact that robust weighting stresses long baselines compared to natural weighting leading to a lower signal-to-noise ratio. As the cleaning threshold depends on noise `clean` now detects less emission. Multi-scale clean is able to deal better with this problem and modeles only 10% less emission compared to more than 50% less for `clean`.
The eye-catching differences between `CASA clean` and AIPS clean used in THINGS must depend on the differing methods used, Högbom versus Clark, and probably different implementations. In principle, both should result in similar images, but at least for `CASA`'s implementation they do not (see section 6.1.1). Multi-scale clean, however, provides results consistent with previous work by Walter et al. (2008).

The further spectra of NGC3184 and NGC5055 can be found in chapter 7.

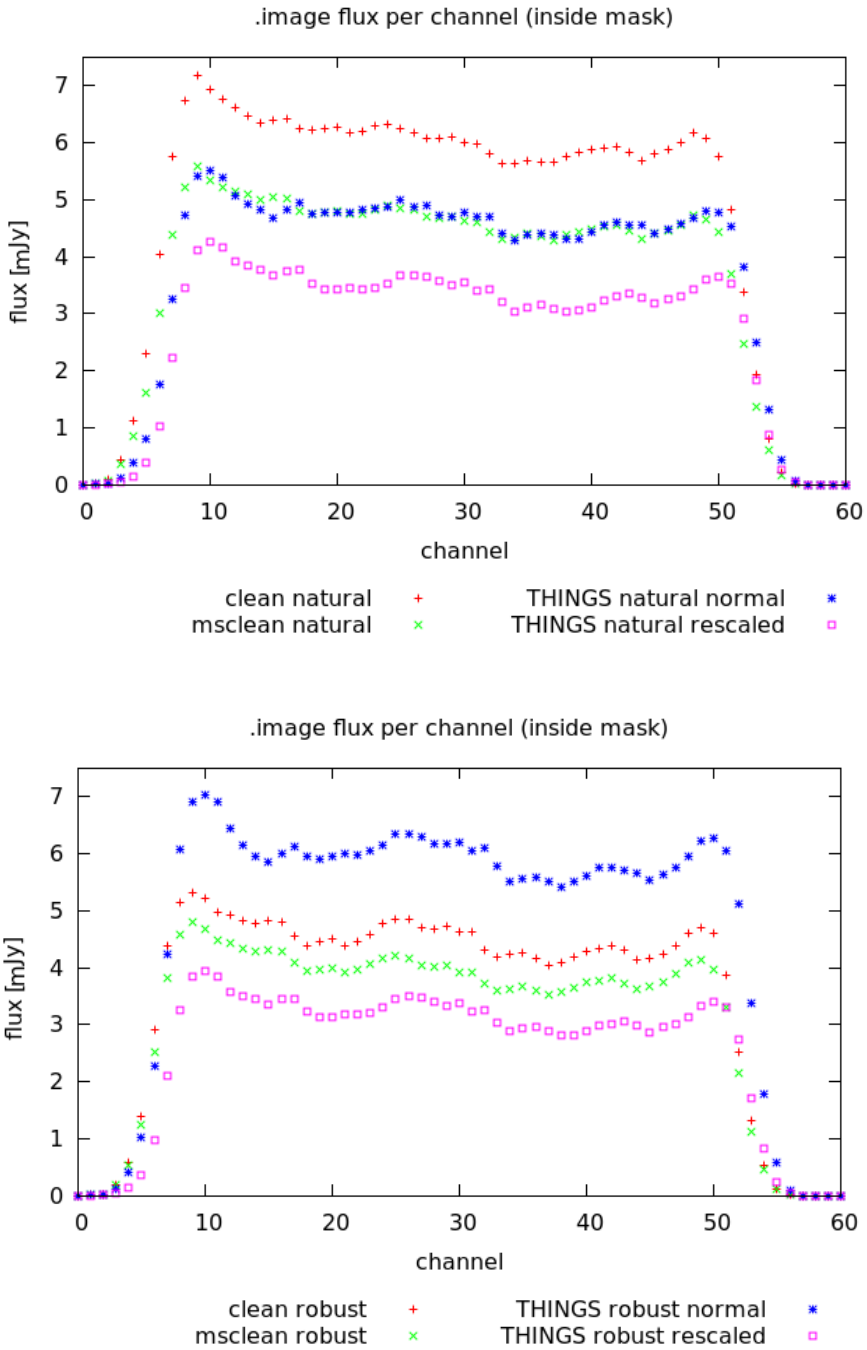

Figure 26: The spectra of NGC2403 made from the restored images show that all cleaning methods detect basically the same structure across the channels, but on different flux levels.

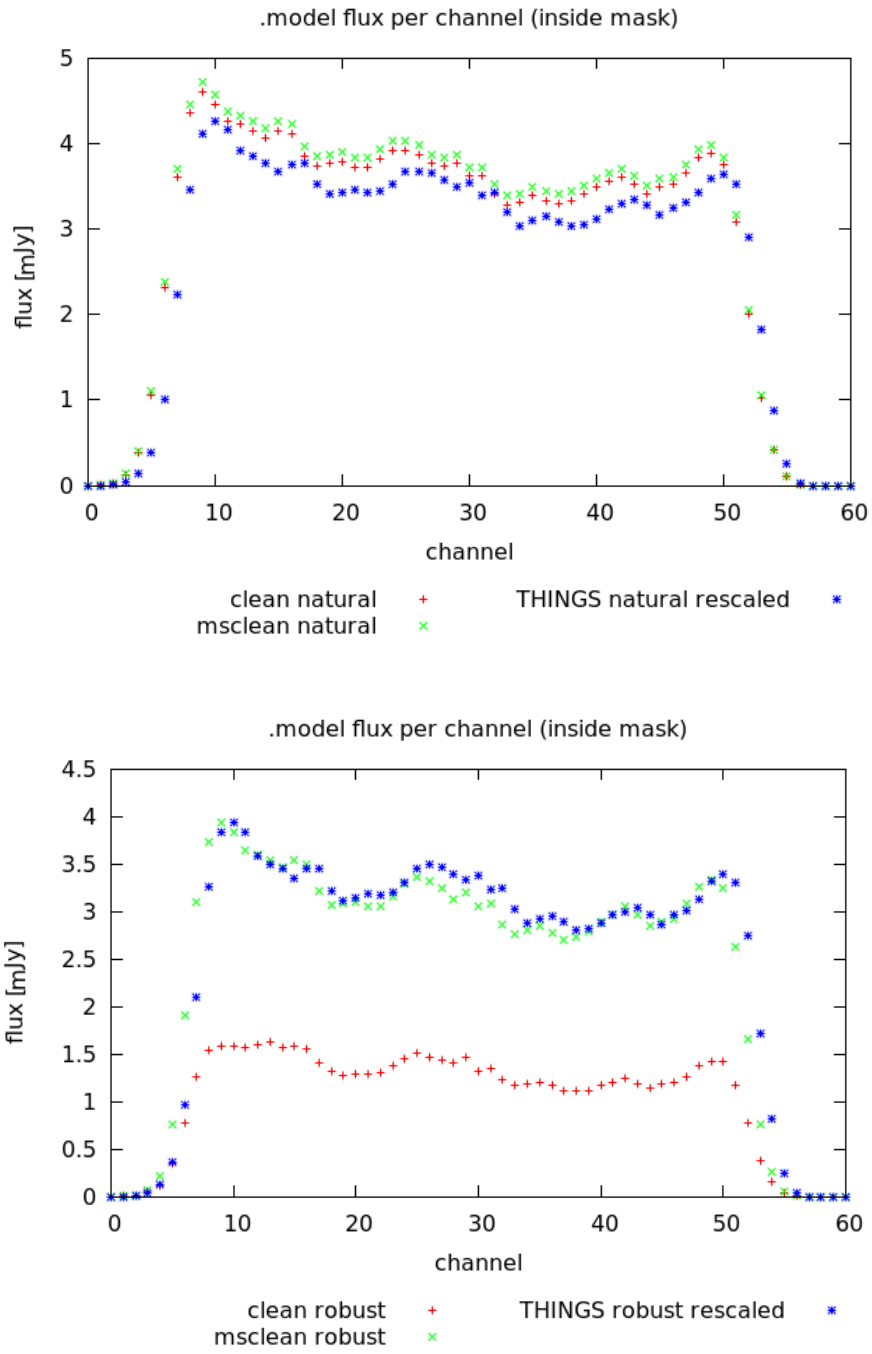

Figure 27: When processing the model images of NGC2403 to spectra strange effects occur. In the case of natural weighting, `clean` and msclean detect the same amount of flux that is slightly above that of THINGS rescaled. Whereas robust weighting causes `clean` to model only about half of the flux that msclean's model contains.

6.5.4 Moment maps

Figure 28 contrasts the three moments 0, 1 and 2 respectively collapsed cube, velocity distribution and velocity dispersion of NGC5055 of `clean` and multi-scale clean.
Independent of the considered moment, a noticeable amount of pixels that are considered in the left images drop out when msclean is used as a consequence of the lower restored fluxes for multi-scale. The same reason is the basis for less high valued pixels (white and red) in the maps of moment 0 and 2 of in the right images. For those moments, this increases the visual contrast making it easier to see the spiral arms in the inner part of the galaxy whereas in the outer areas some faint structures get lost for moment 0. In case of moment 1, the difference is minor and seems to consists merely of blanked pixels in msclean.
Only looking the maps can only be a first qualtative overview about further quantitative analysis that I could not do because of the short working time allowed for a bachelor thesis.
In addition to the printed natural weighted moment maps, the robust maps of NGC5055 can be found in Appendix C and natural msclean data sets of NGC3184 and NGC2403 are provided in section 7 confirming the observations described above.

6.5.5 Radial profiles

The following radial profiles of NGC5055 have beam calculated according to the procedure described in section 5.10 from the primary beam corrected moment 0 maps.
Since the further reduction from moment maps to radial profiles limits on integration inside ellipses, the properties detected above translate to the profiles and base on the same reasons. `Clean` has higher values because of the low residuals in msclean that lead to lower emission in the restored image and get blanked more often. The relative differences, however, are enormous: up to 25% for natural and 40% for robust weighting with respect to `clean` are more than expected from the images (28). At least, figure 29 demonstrates that the qualitative difference in the radial profiles is small, too.

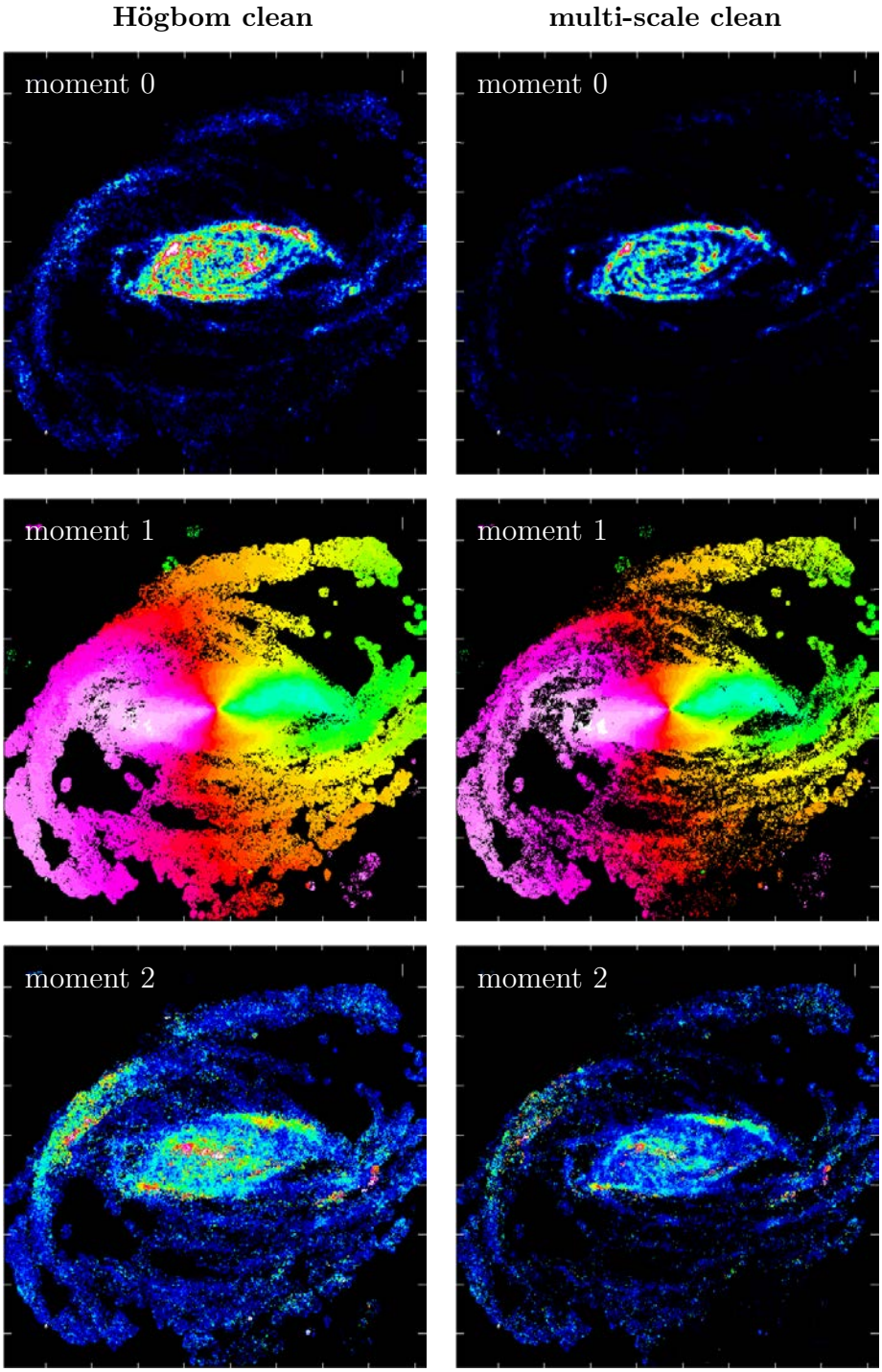

Figure 28: Comparison of `clean` and multi-scale clean for the natural moment maps of NGC5055. When msclean is used considerably more flux falls below the 3σ threshold and gets blanked resulting in clearer structures. The colors (blue over green and red to white) range from -0.02 to 0.2 Jy/beam km/s (moment 0), 0 to 700 km/s (moment 1) and 0 to 30 km/s (moment 2).

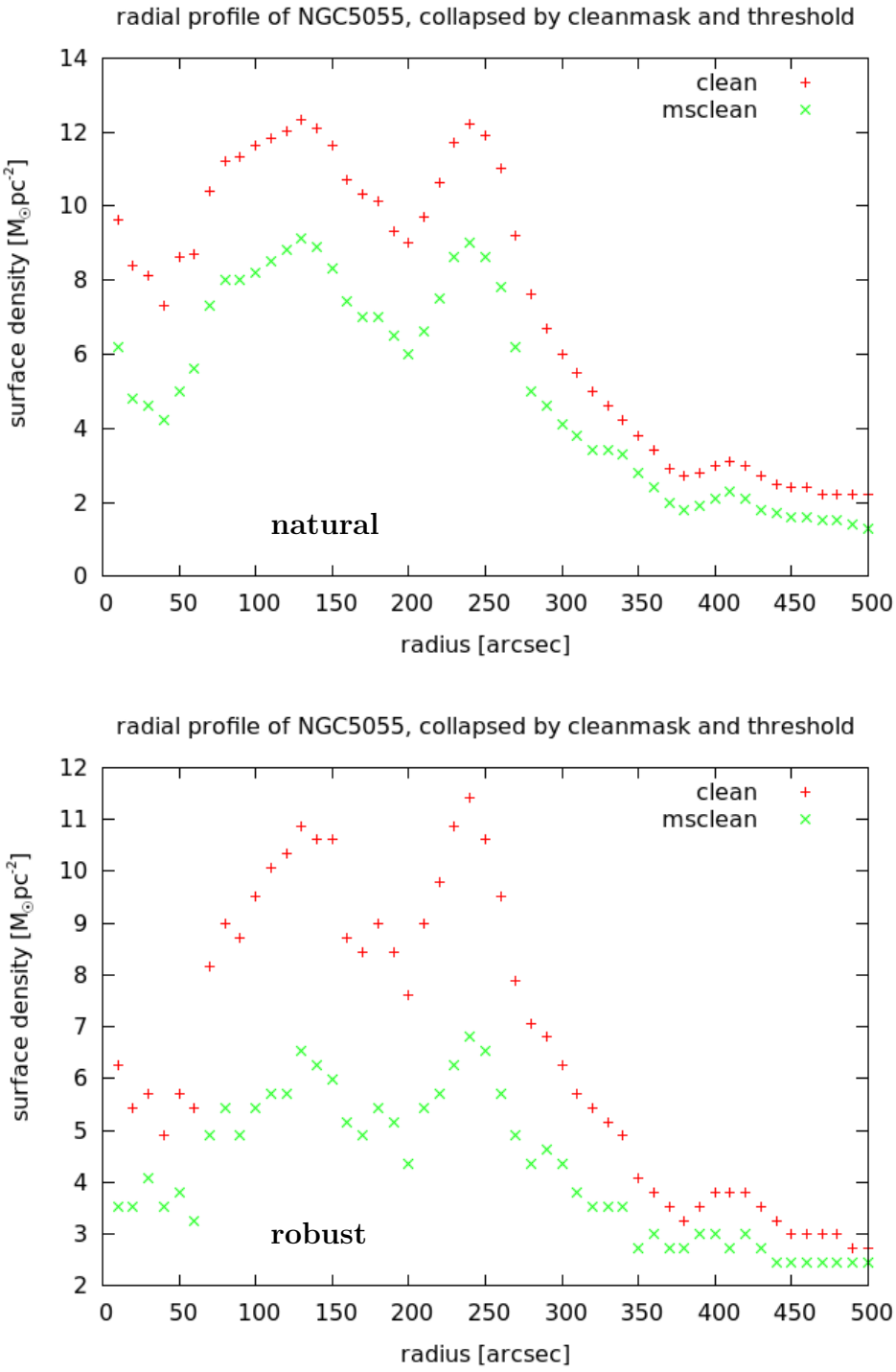

Figure 29: The radial profiles of NGC5055

6.5.6 Conclusion

When looking at the outputs after cleaning, multi-scale clean appears to produce better results already at first sight. A more detailed, but still visual analyses reveils msclean to model emission smoothly with uniform residuals. Högbom's ansatz of point sources cannot keep up when it comes to modeling extended emission. Measurements of flux density then approve the first impression of significantly lower residuals combined with more cleaned flux and therefore better cleaning. Apart from that, both methods obtain similar characteristics in further steps of processing. The greatest problem so far is whether rescaling must be applied to mscleaned cubes or not and how it should be done correctly.
The advantages in imaging are a better convergance behaviour, especially when cleaning to low thresholds that simply cannot be done in `CASA` with Högbom's algorithm or modifications of it.
On the theoretical side, it is reasonable to model emission of extended hydrogen clouds by extended sources.

6.6 Deep multi-scale cleaning

As could be seen in section 6.5.1, multi-scale clean allows deep cleaning down to a threshold of 1.5σ even for natural weighting. This removes more sidelobes in the restored image leaving only little effects and an image close to the theoretical clean image. In this process only minimum of residuals should remain superseding the need to rescale images in order to measure correct flux values.
As can be seen in figure 30, `CASA` had some problems in channel 69 to 72. These artefacts have no physical meaning but arise when images are opened with CASAviewer while the last channels are still being processed. For a basic analysis of deep cleans, this is irrelevant and can easily be corrected in later computations.
To get correct results when using no mask, the approach of section 5.6 was applied where an image double the size of desired one gets cleaned. In case of NGC5055 an image of $2048 \cdot 2048$ pixels had to be used that was clipped to the area formerly analysed for the `clean` - msclean comparison and in THINGS. `CASA`, however, is not able to clean it at once, so it had to be split up into two parts that got cleaned individually and concatenated afterwards. An problem of this procedure is getting two slightly differing clean beams that prevent `CASA` from calculating moment maps of the combined images. Unfortunately, the computation could not be repeated with predefined identical beam sizes because of the long duration of 3.5 weeks on a 64-core server. Therefore all further analysis must rely on two seperate files. The clean beams are $8.83'' \cdot 8.24''$ at a position angle of $-54.3°$ and $8.94'' \cdot 8.27''$ at $-43.0°$.
Figure 31 shows the resulting image (left), model (center) and residual (right) of channel 28 and 58 with velocities of 578.5 km/s and 423.9 km/s. The background around the galaxy is very flat without large scale leftovers as can be seen in figure 24 for `clean` and msclean at 2.5σ threshold. Hence, all visible sidelobes of the dirty beam got removed. Computerbased analysis will eventually still find structures, but on a very low level. The residual image confirms the remarkable good job multi-scale clean did as only in the areas with the highest cleaned flux, a faint shadow of the galaxy remains. The values are not significantly higher than in the surrounding noise, though, allowing the residuals to be described as flat and noise-like. Because of the low threshold, a large amount of pixel size noise gets cleaned and even larger regions up to $18''$ get cleaned. Setting a mask would prevent this, but holds the risk of neglecting faint, but real emission that is covered by sidelobes in the half-cleaned image of which the mask is made.
The greatest hope upon deep multi-scale cleaning was to get rid of the complex process of rescaling and keep only one data cube that is suitable for flux measurements of emission and maintains correct noise properties. Compared to unrescaled `clean`s or mscleans the residuals drop about one magnitude to $\sim 3.5 \cdot 10^{-5}$ Jy/beam when cleaned to 1.5σ. The restored image still contains a background of $\sim 3.2 \cdot 10^{-4}$ mJy which means even in emission free regions the residuals make up a maximum of $\sim$10% of the flux. This stands in strong contrast to `clean` and msclean at 2.5σ where the residuals make up the whole background except for very few noise peaks. Scaling 10% of the flux down changes the result little enough to safely neglect this effect and forget about rescaling. Especially as rescaling is ill-defined for multi-scale clean beam and hence introduces an error, too.

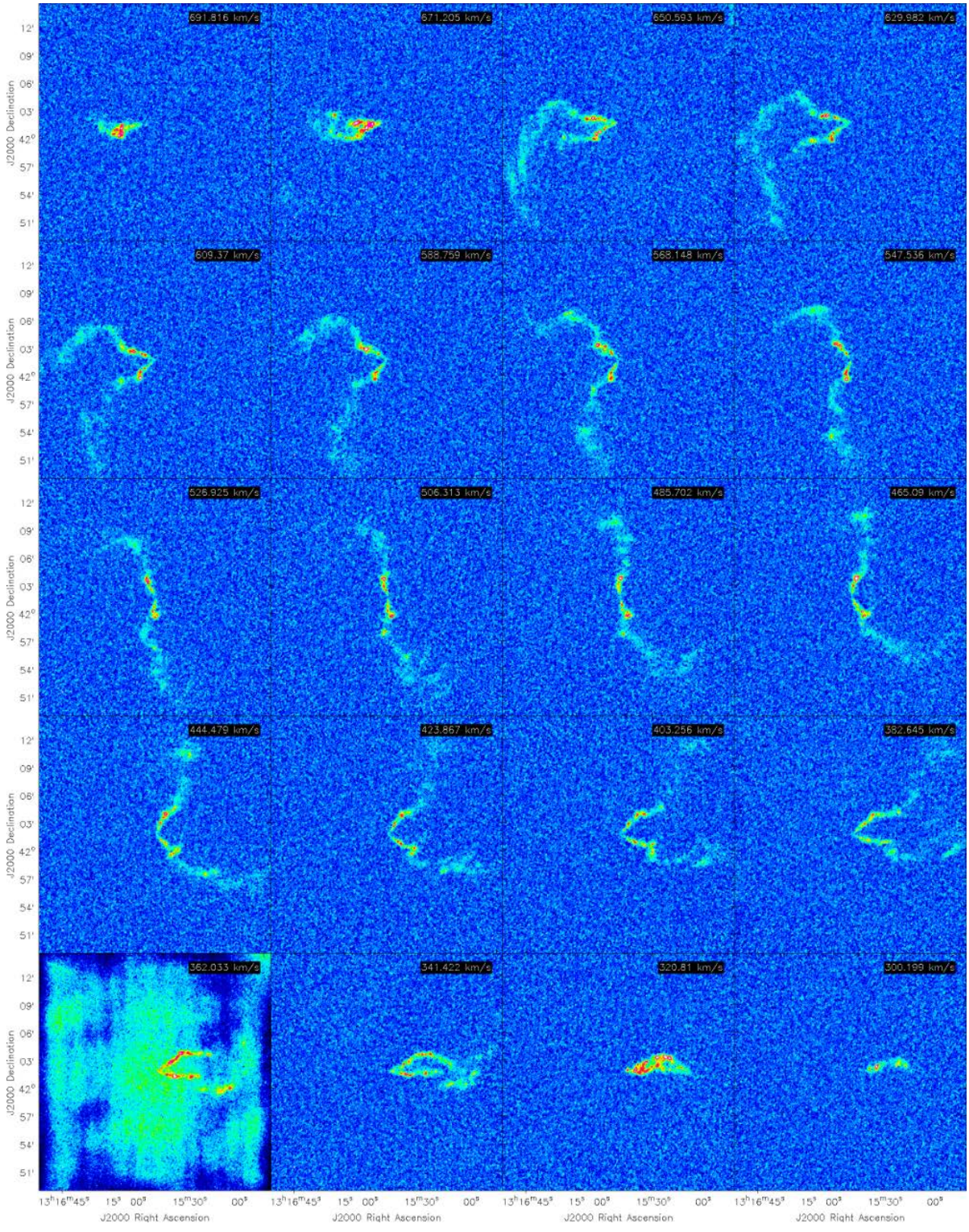

Figure 30: color range: -2 to 6 mJy/beam

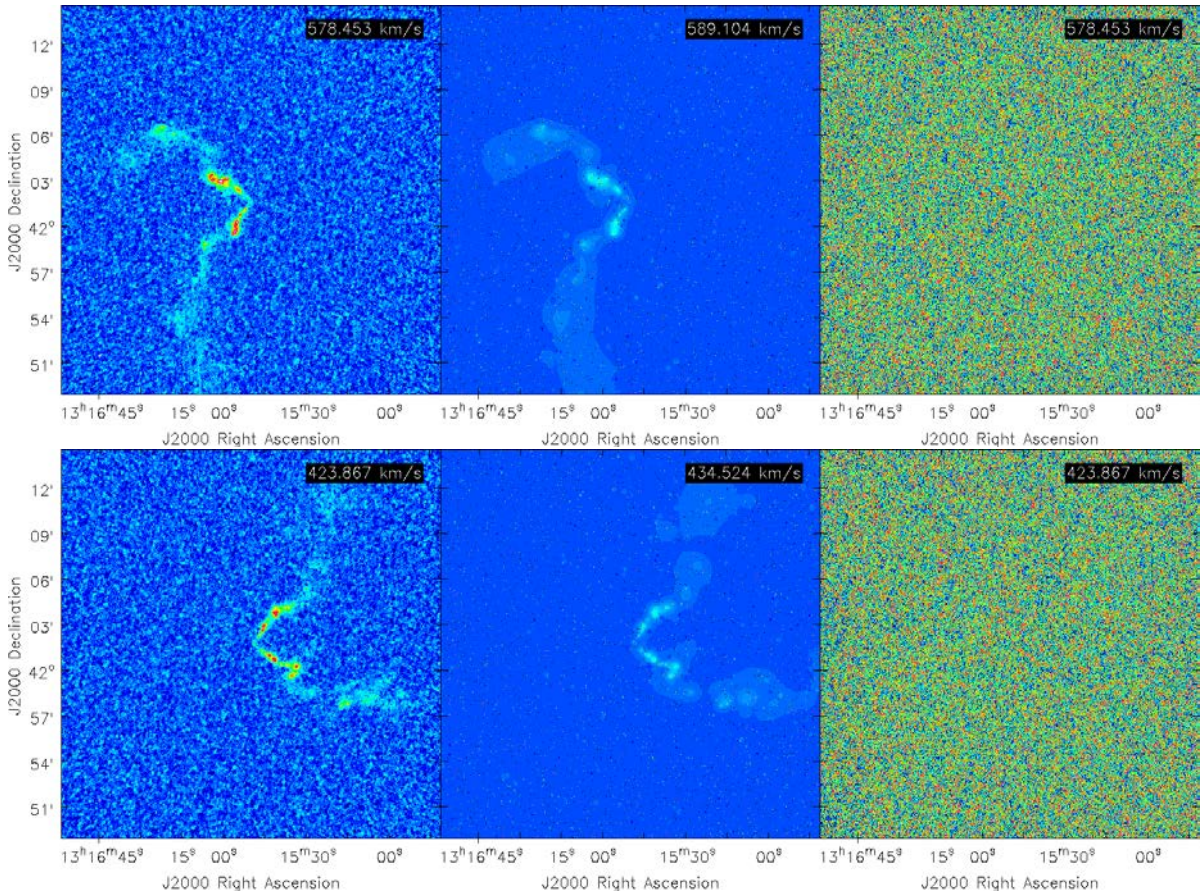

Figure 31: Deep cleaning of NGC5055 down to 1.5σ shows uniform, noise-like background in the restored images (left). The residual image (right) confirm this as only very little emission is left at the area with the highest cleaned flux. Due to the low threshold a considerable amount of noise gets cleaned, too, and added to the model image (center). The color ranges are -2 to 6 mJy/beam (restored image), -0.2 to 0.5 mJy/pixel (model) and -0.6 to 0.6 mJy/beam (residual).

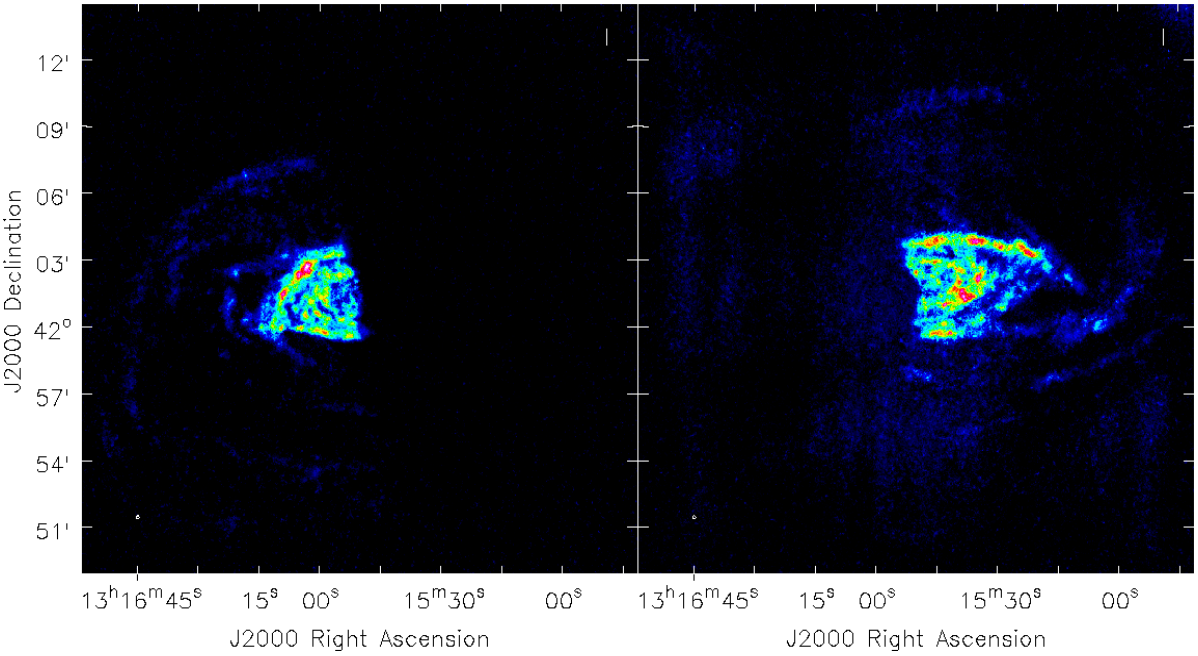

Figure 32: Because of the mentioned problems the natural moment maps are split into two files consisting of channel 0 to 39 (left) and channel 40 to 87 (right). The color is code identically from 0.004 to 0.2 Jy/beam km/s.

As the absolute value of the noise drops merely about 10%, the visible effect on moment maps is minor. Less noise decreases the threshold to only include real emission and some more faint structure should get discernible. The natural moment maps of figure 32 were produced with a threshold $3\sigma = 0.9\,\mathrm{mJy/beam\,km/s}$ which is $0.3\,\mathrm{mJy/beam\,km/s}$ less then for the respective `clean` map. The problem with two seperate files, however, prevent that enhancement to show.

Overall, deep multi-scale cleaning improves the images significantly and they approach the theoretical clean image very well. However, the best effect is to render rescaling useless and save one step of data reduction plus the effort of having to deal with two images. The corresponding disadvantages of the increased quality, long computation times even on fast machines and right now problems in `CASA`, will certainly diminish in the next years making multi-scale clean a seminal algorithm for future interferometric observation.

7 Data products

The following pages contain for each of NGC2403, NGC3184 and NGC5055 selected channel maps, moment maps, spectra and radial profiles based on multi-scale clean. All showns plots base on natural weighting and the used masks is displayed by a white contour in the channel maps. The mask are generally not very good as it is complicated and sometimes impossible to calculated connected mask regions without covering large areas of noise, too. Table 4 gives on overview of the parameters used in imaging.

name	image size [pixel]	pixel size [″]	number of channels	channel width [km/s]
NGC2403	2048	1.0	61	5.2
NGC3184	1024	1.5	72	2.6
NGC5055	1024	1.5	87	5.2

name	weighting	clean beam [″] major	clean beam [″] minor	noise [mJy/beam]	inclination [°]	position angle [°]
NGC2403	NA	7.97	7.09	0.38	63	124
	RO	4.65	4.06	0.45		
NGC3184	NA	7.30	6.65	0.36	16	179
	RO	5.04	4.85	0.40		
NGC5055	NA	8.83	8.24	0.36	59	102
	RO	5.46	4.90	0.41		

Table 4: Overview of the parameters used for cleaning

7.1 NGC2403

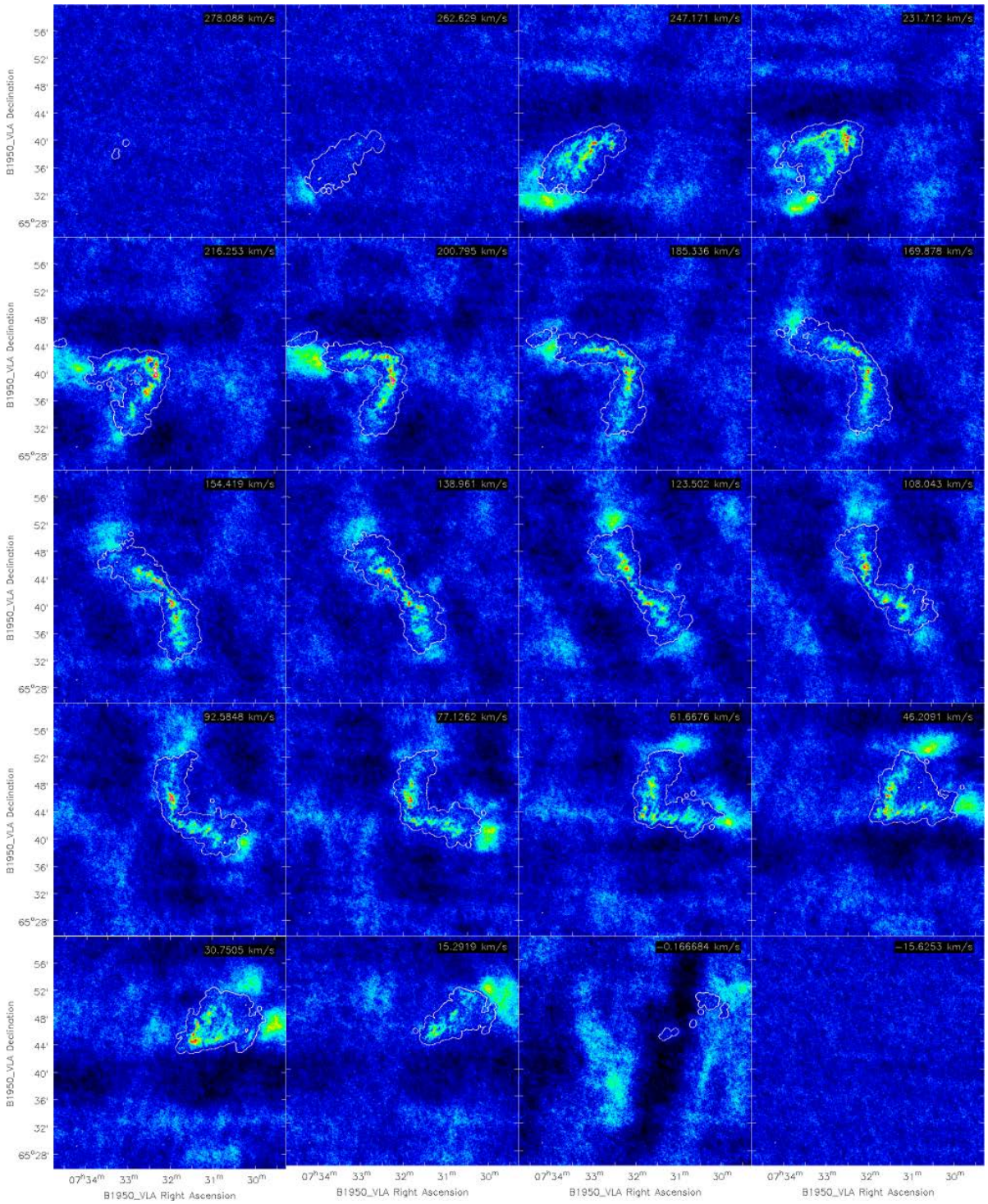

Figure 33: Channel maps of NGC2403 in natural weighting using multi-scale clean. Every third channel is displayed. Color range: -2 to 8 mJy/beam

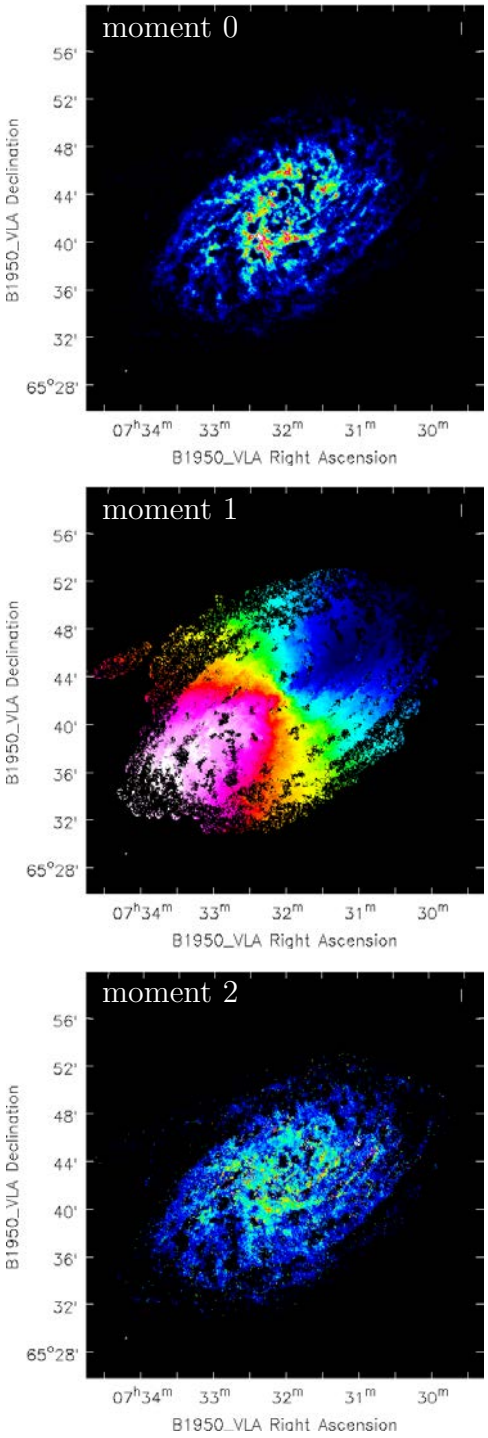

Figure 34: Moment 0, 1 and 2 calculated from the natural weighted, multi-scale cleaned cube of NGC2403. Color range: 0.006 to 0.02 Jy/beam km/s (moment 0), 0 to 250 km/s (moment 1) and 0 to 20 km/s (moment 2).

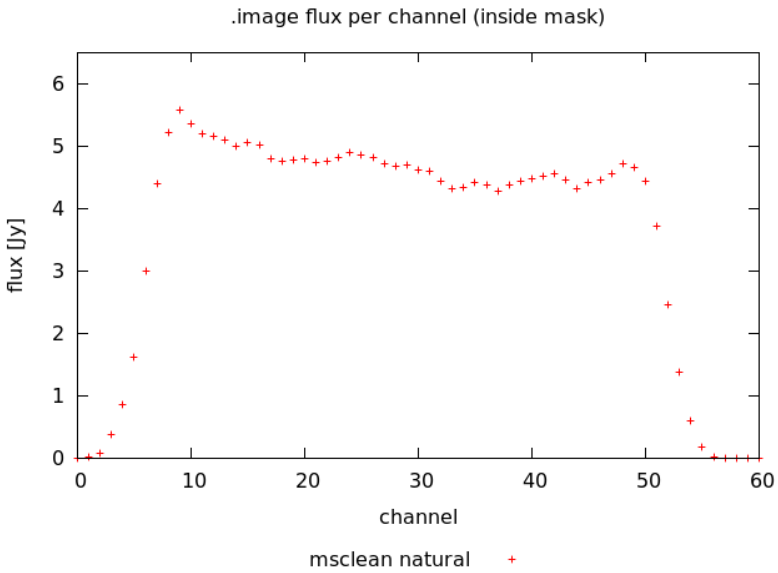

(a) natural

Figure 35: Spectrum of NGC2403 calculated from multi-scale cleaned data with natural.

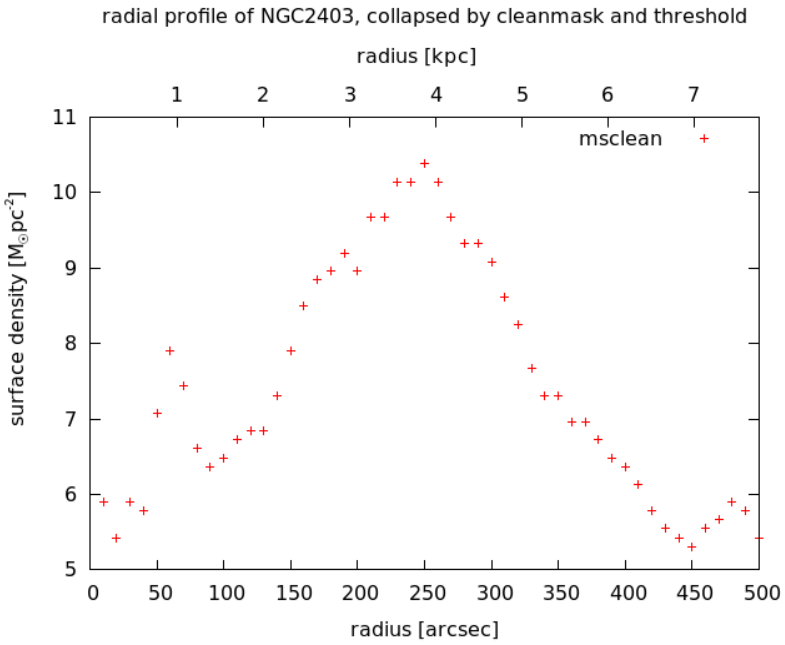

(a) natural

Figure 36: Radial profile of NGC2403 calculated from natural weighted, multi-scale cleaned.

7.2 NGC3184

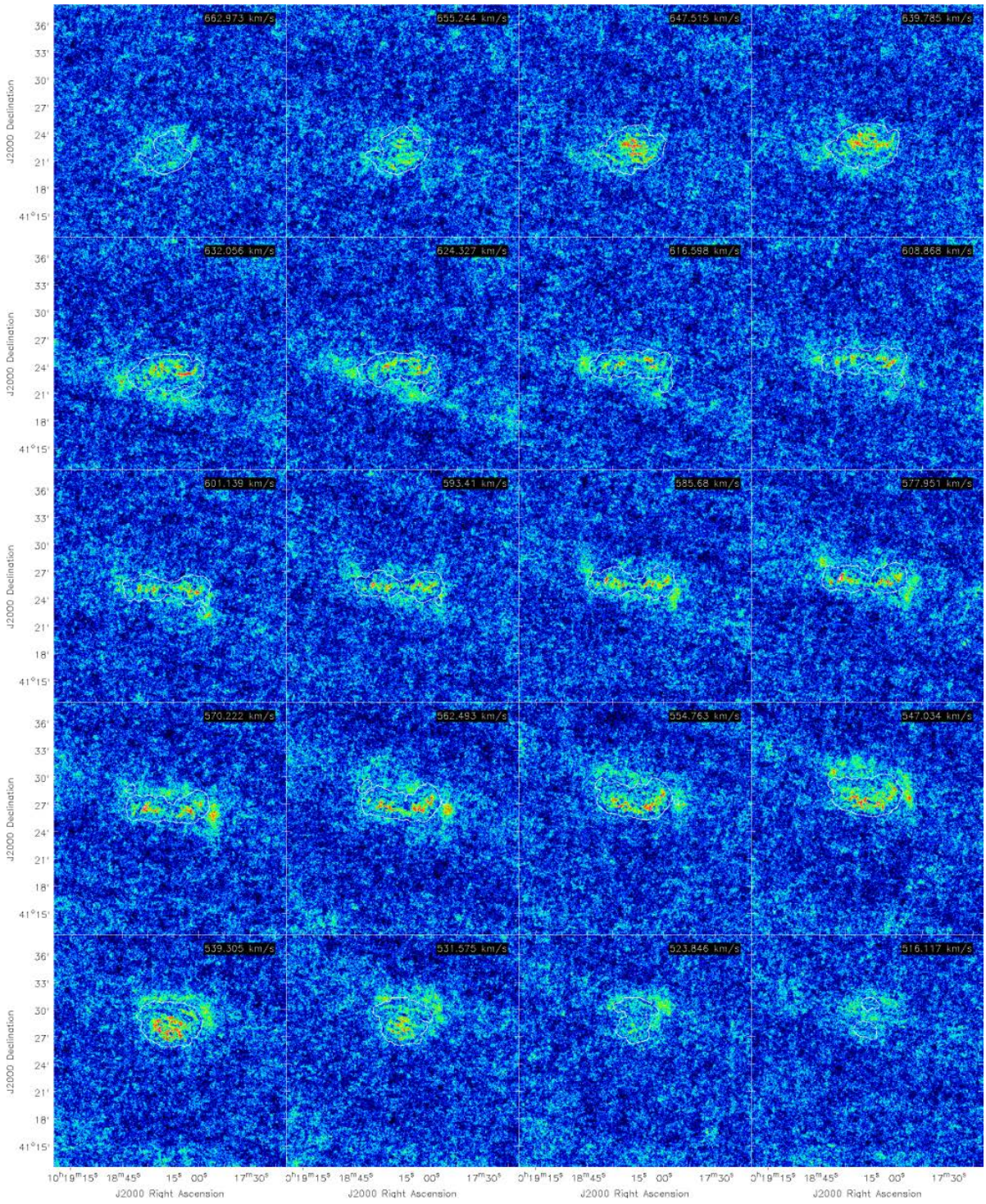

Figure 37: Channel maps of NGC3184 in natural weighting using multi-scale clean. Every third channel is displayed. Color range: -1 to 3 mJy/beam

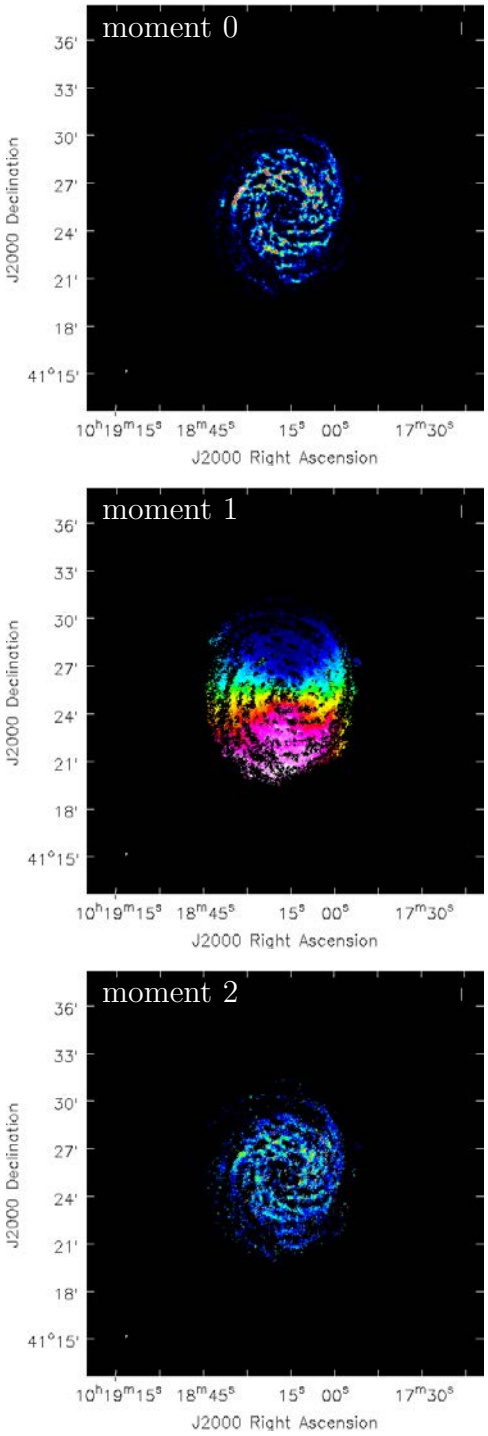

Figure 38: Moment 0, 1 and 2 calculated from the natural weighted, multi-scale cleaned cube of NGC3184. Color range: 0.002 to 0.06 Jy/beam km/s (moment 0), 520 to 660 km/s (moment 1) and 0 to 15 km/s (moment 2).

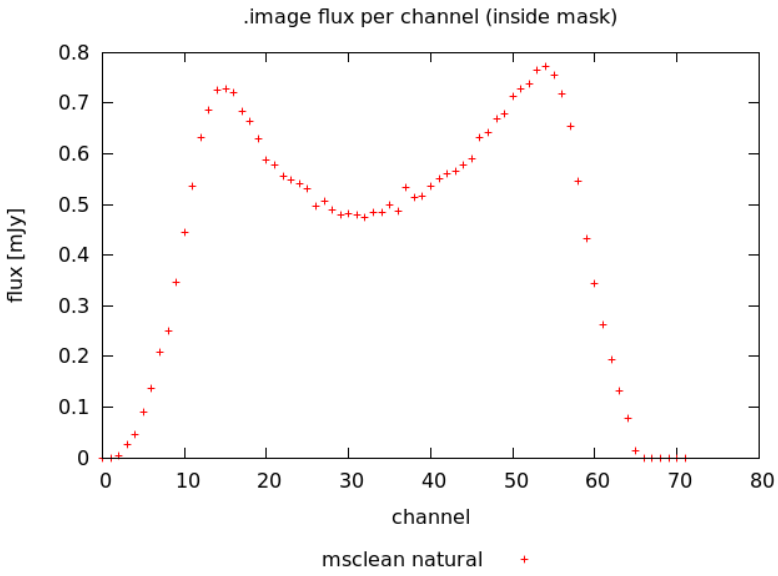

(a) natural

Figure 39: Spectrum of NGC3184 calculated from multi-scale cleaned data with natural.

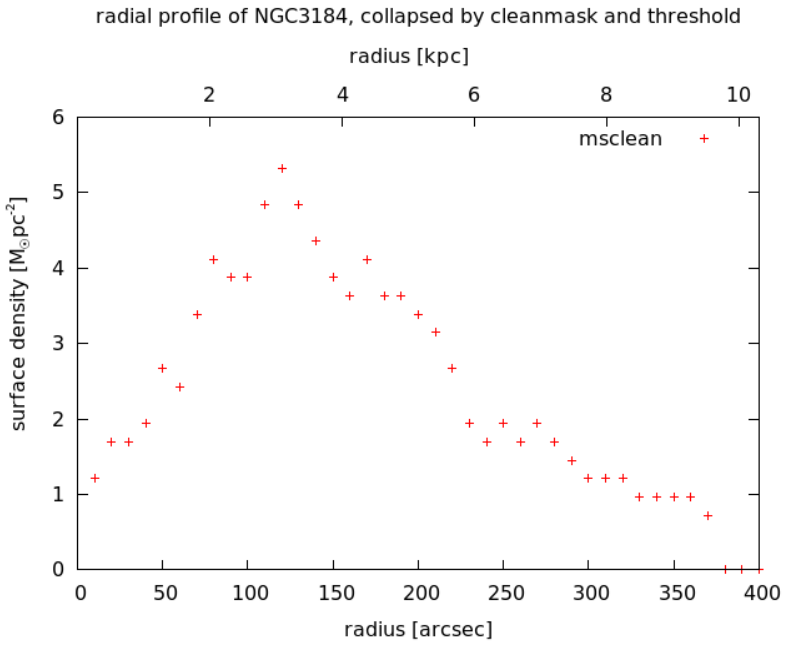

(a) natural

Figure 40: Radial profile of NGC3184 calculated from natural weighted, multi-scale cleaned.

7.3 NGC5055

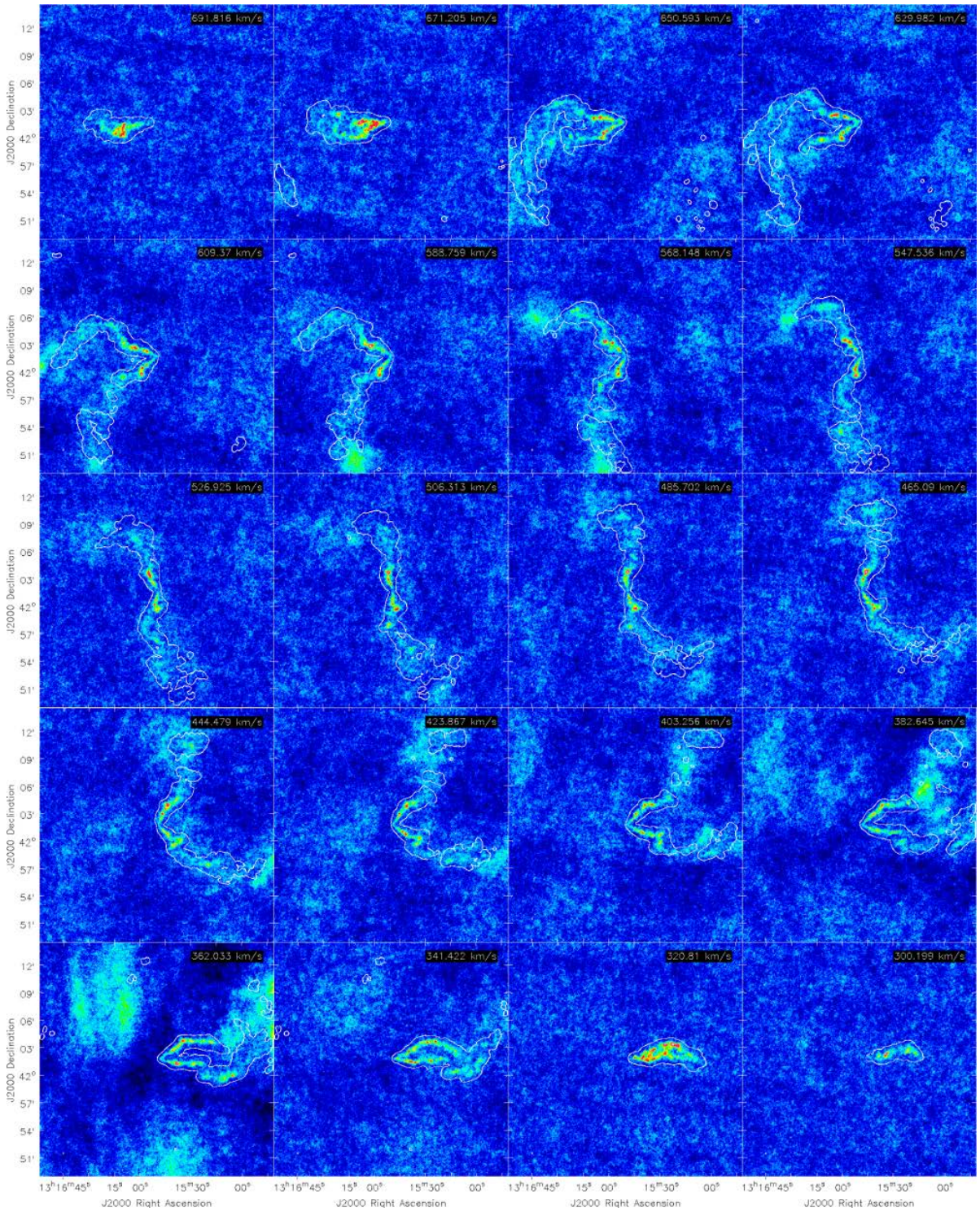

Figure 41: Channel maps of NGC5055 in natural weighting using multi-scale clean. Every third channel is displayed. Color range: -2 to 6 mJy/beam

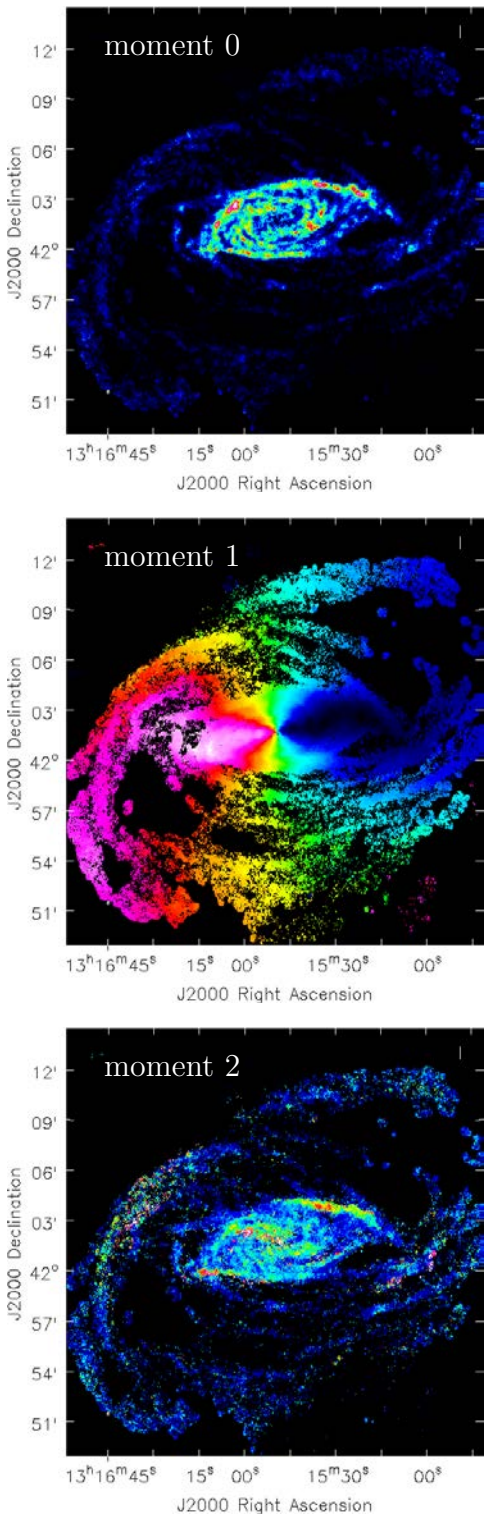

Figure 42: Moment 0, 1 and 2 calculated from the natural weighted, multi-scale cleaned cube of NGC5055. Color range: 0.006 to 0.2 Jy/beam km/s (moment 0), 300 to 700 km/s (moment 1) and 0 to 25 km/s (moment 2).

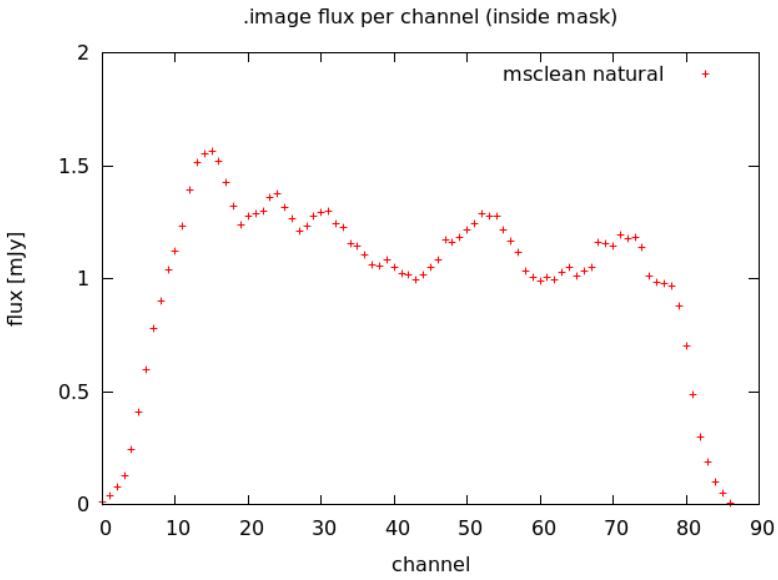

(a) natural

Figure 43: Spectrum of NGC5055 calculated from multi-scale cleaned data with natural.

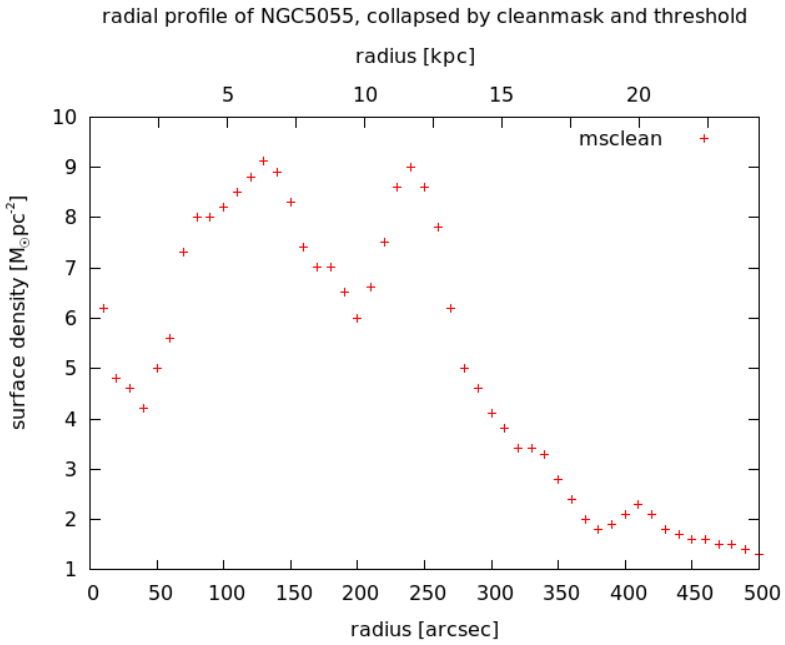

(a) natural

Figure 44: Radial profile of NGC5055 calculated from natural weighted, multi-scale cleaned.

8 Appendices

8.1 Appendix A: Residuals of different multi-scale cleans

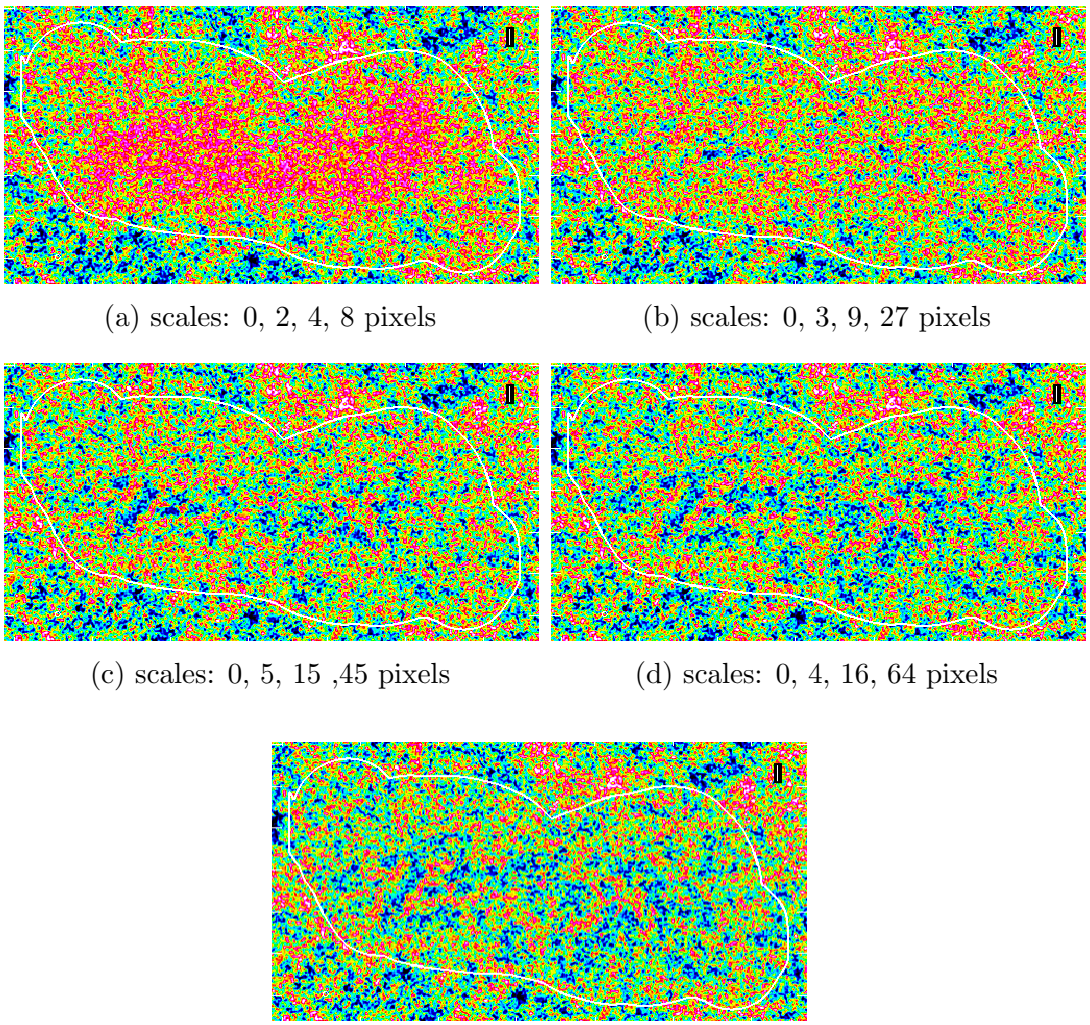

(a) scales: 0, 2, 4, 8 pixels

(b) scales: 0, 3, 9, 27 pixels

(c) scales: 0, 5, 15 ,45 pixels

(d) scales: 0, 4, 16, 64 pixels

(e) scales: 0, 3, 9, 27, 75 pixels

Figure 45: The residuals of mscleaned NGC3184 decrease remarkably with increasing size of the maximum scale. (Color range from -0.1 mJy/beam to 0.1 mJy/beam)

8.2 Appendix B: Further moment maps

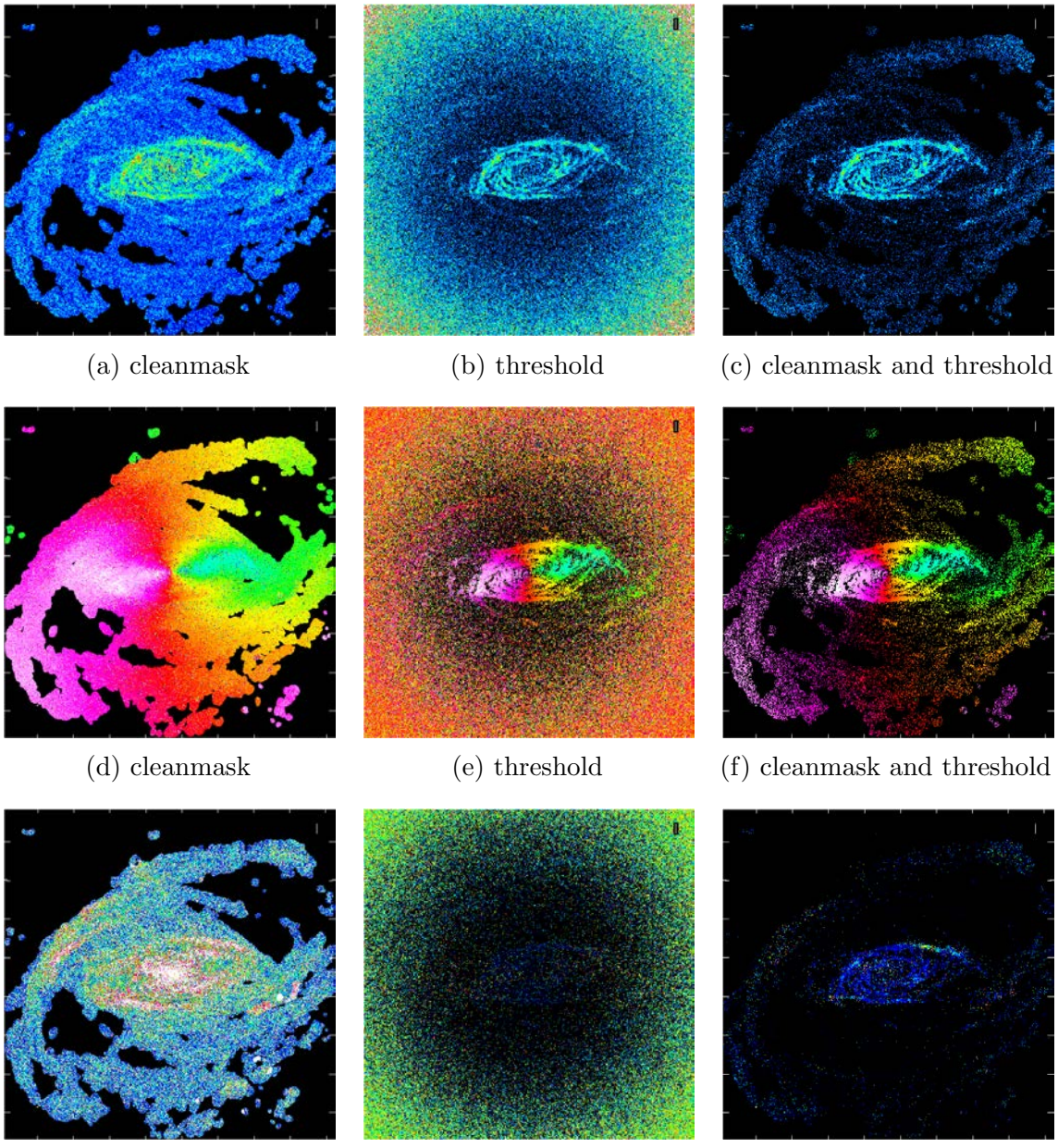

(a) cleanmask (b) threshold (c) cleanmask and threshold

(d) cleanmask (e) threshold (f) cleanmask and threshold

(g) cleanmask (h) threshold (i) cleanmask and threshold

Figure 46: NGC5055, multi-scale clean, robust, color ranges are given by -0.05 to 0.15 Jy/beam km/s (moment 0), 0 to 700 km/s (moment 1) and 0 to 30 km/s (moment 2).

8.3 Appendix C: Robust moment maps

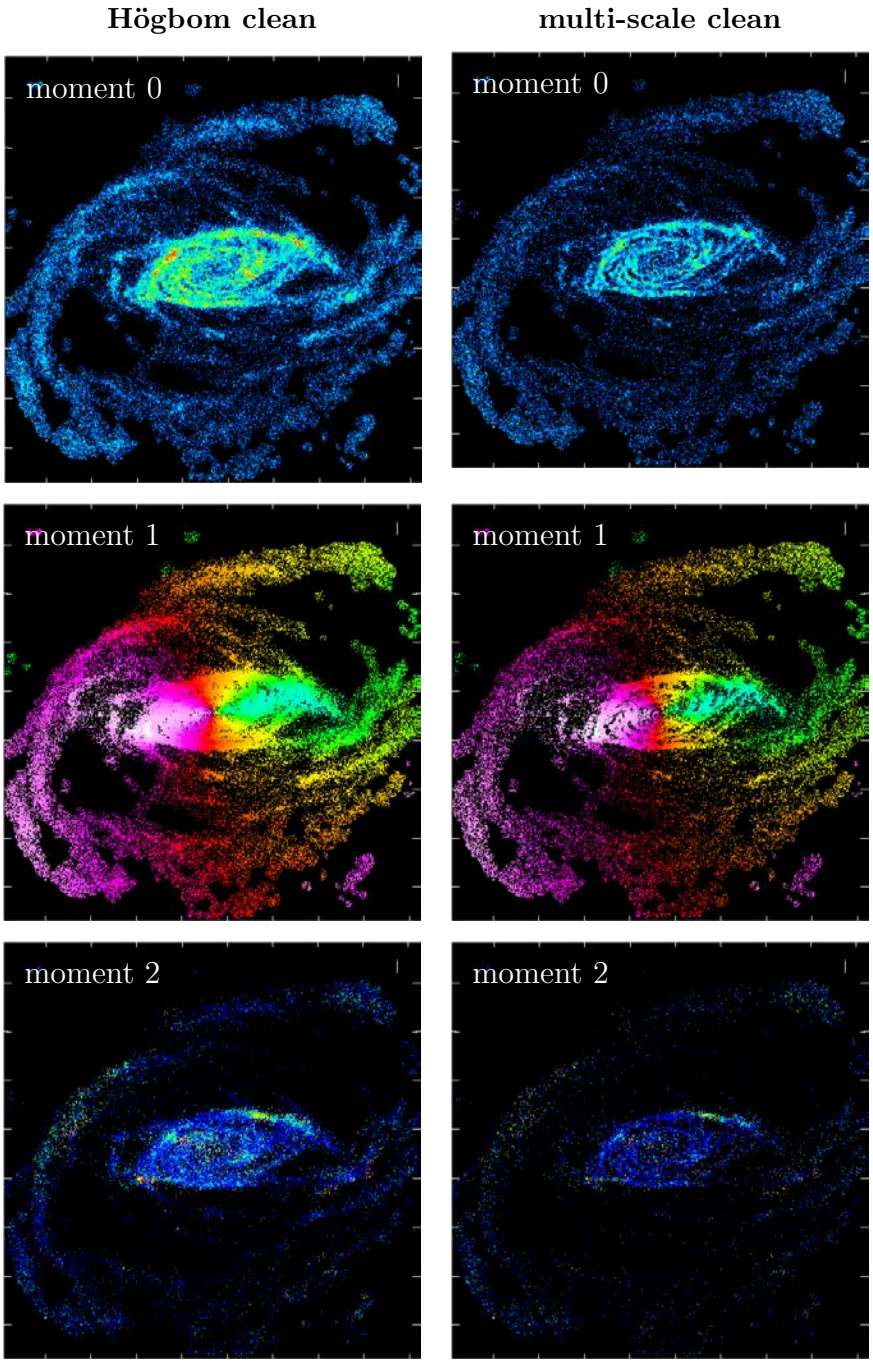

Figure 47: Comparison of `clean` and multi-scale clean for the robust moment maps of NGC5055. When msclean is used considerably more flux falls below the 3σ threshold and gets blanked resulting in clearer structures. The colors (blue over green and red to white) range from -0.02 to 0.2 Jy/beam km/s (moment 0), 0 to 700 km/s (moment 1) and 0 to 30 km/s (moment 2).

Bibliography

R.N. Bracewell. *The Fourier transform and its applications*. McGraw-Hill electrical and electronic engineering series. McGraw-Hill, 1978. URL `http://books.google.de/books?id=mu5QAAAAMAAJ`.

D. S. Briggs. *High Fidelity Deconvolution of Moderatly Resolved Sources*. PhD thesis, 1995.

B. G. Clark. An efficient implementation of the algorithm 'CLEAN'. *Astronomy and Astrophysics*, 89(3):377–388, September 1980.

T. J. Cornwell. Multi-scale CLEAN deconvolution of radio synthesis images. *IEEE Journal of Selected Topics in Signal Processing*, 2(5):793–801, October 2008. ISSN 1932-4553. doi: 10.1109/JSTSP.2008.2006388.

J. A. Högbom. Aperture Synthesis with a Non-Regular Distribution of Interferometer Baselines. *Astronomy and Astrophysics Supplement*, 15:417, 1974.

Adam K. Leroy, Fabian Walter, Elias Brinks, Frank Bigiel, W. J. G. de Blok, Barry Madore, and M. D. Thornley. The Star Formation Efficiency in Nearby Galaxies: Measuring Where Gas Forms Stars Effectively. Astron.J.136:2782-2845,2008, 12 2008.

J. Ott. Vorstoss in den unteren Massenbereich von Galaxien: Die irregulaeren Zwerggalaxien Holmberg I, Sextans A und M81 DW A. Master's thesis, 1999.

Planck Collaboration. Planck 2013 results. I. Overview of products and scientific results. 2013.

F. R. Schwab. Relaxing the isoplanatism assumption in self-calibration; applications to low-frequency radio interferometry. *Astronomical Journal*, 89:1076–1081, 1984.

G. B. Taylor, C. L. Carilli, and R. A. Perley. Synthesis Imaging in Radio Astronomy II. volume 180, 1999. URL `http://adsabs.harvard.edu/abs/1999ASPC..180.....T`.

A. R. Thompson. Fundamentals of Radio Interferometry. pages 11–36. Astronomical Society of the Pacific, Astronomical Society of the Pacific, 1999.

F. Walter, E. Brinks, W. J. G. de Blok, F. Bigiel, Jr. R. C. Kennicutt, M. D. Thornley, and A. K. Leroy. THINGS: The HI Nearby Galaxy Survey. *The Astronomical Journal*, 136(6), December 2008.

Declaration

Ich versichere, dass ich diese Arbeit selbstständig verfasst und keine anderen als die angegebenen Quellen und Hilfsmittel benutzt habe.
Heidelberg, den 12. August 2013,